Torstein Ingebrigtsen Bø

Scenario- and Optimization-Based Control of Marine Electric Power Systems

NTNU
Norwegian University of
Science and Technology

Summary

Diesel electric propulsion has become the industry standard for e.g., oil and gass vessels, cruise vessels, ferries, and vessels with dynamic positioning (DP) systems. Diesel engines are paired with generators to produce electric energy, which is used by electric motors for propulsion of the vessel, and also by other consumers, such as hotel loads, drilling drives, cranes, and heave compensators. This system is reliable and efficient due to the flexibility of the electric grid. DP is often used as a motivating example in this thesis. The thrusters of a vessel using DP is used to fix the position and heading of the vessel. The power plant is operated with redundancy, as a single fault should not lead to loss of position. However, this redundancy decreases the efficiency of the power plant. This thesis presents new ideas and results on how to increase the efficiency of a hybrid power plant with diesel generator sets and batteries while maintaining the required safety level.

A model of a marine vessel is presented in Chapter 2. This model includes the power plant, a hydrodynamic model, and control systems. The power plant includes generator sets, batteries, switchboards, thrusters, and hotel loads. Environmental loads are included in the hydrodynamic model, such as first and second order wave loads, mean and gusting wind, and ocean current, along with the hydrodynamic model of the vessel and the thrusters. The included control systems are a power management system, a DP-controller, thrust allocation, and low level controllers of producers and consumers. Earlier marine vessel simulators mainly focused on the hydrodynamic model or the power plant. However, the present model combines the three models, to investigate the complex integration and interaction effects between the models. These interaction effects are especially important when investigating the DP performance after faults in the power plant. Chapter 2 presents the models needed for this integration. Three simulation cases are presented, to shows that the simulator can capture the interaction effects.

A simulation-based dynamic consequence analysis is presented in Chap-

ter 3. The tool uses the simulator from Chapter 2 to simulate several possible worst case scenarios. This tool can be used by the operator to optimize the electric power plant configuration, and to show that no single failure lead to loss of position. The dynamic consequence analysis is necessary when stand-by generators are considered, as the vessel may lose position during the time from when the fault occurs until the plant fully recovers, even if the vessel maintains its position after recover.

A scenario-based model predictive controller (MPC) is presented in Chapter 4. This controller uses fault scenarios, internally, to constrain the nominal trajectory, which is an alternative to conventional static safety constraints. The control of generator set speed of a marine power plant is used as a case study. Simulations show that fault scenarios can replace static safety constraints by using this controller.

Chapter 5 presents a method to control peak-shaving. Peak-shaving by batteries is used to cancel out power fluctuations, which cause variations in the electric grid's frequency. However, the batteries may get too hot if power demand is too large. The proposed controller, based on a power spectrum analysis and MPC, reduces the power fluctuations as much as possible without letting the battery get too hot. Simulations using data generated by the simulator in Chapter 2 showed that the controller can achieve these objectives as long as the characteristics of the load does not change too rapidly.

Use of the vessel itself as energy storage during DP operation is explored in Chapter 6. A vessel oscillates about its mean position by reducing the thruster power when the total power demand of the vessel is high and increasing it during periods of low power consumption. An analytical formula for motion amplitude given by power amplitude is calculated in this chapter. The formula is compared with simulations, and the simulation results agreed with the formula. It is also shown that the resulting deviations in position from variations of several megawatts are no larger than typical position deviations from the dynamics of ocean waves and wind.

The proposed models and controllers are demonstrated through simulations using MATLAB/SIMULINK. The MPC-based controllers are implemented in ACADO.

Acknowledgments

cussions. I would like to give thanks to all of my fellow colleges at Department for Engineering Cybernetics, Department for Marine Technology, and AMOS for a good working and social environments in and outside the university.

I would like to express my gratitude to my climbing buddies, who have patiently listened, and giving me betas for climbs, life, and the PhD. I would also like to thank my friends and family for their support. Finally, I would like to give special thanks to my parents, Karl Ove Ingebrigtsen and Audhild Bø, for always being there for me and supporting my choices.

Trondheim, December 2015   Torstein Ingebrigtsen Bø

Contents

Abbreviations

BESS   Battery Energy Storage System
CO_2 Carbon dioxide
DP   Dynamic Positioning
FLR   Fast Load Reduction
MPC   Model Predictive Control
MVM   Mean Value Model
PMS   Power Management System
TA   Thrust Allocation

Chapter 1

Introduction

1.1 Background

The main motivation for this thesis is to reduce the environmental footprint of vessels with diesel electric propulsion. Global climate change may be one of the most important and challenging environmental problems of today (Pachauri et al.; 2014). It is estimated that total CO_2 emissions from the maritime sector in 2012 was 800 million tons (Marine Environment Protection Committee, IMO; 2014). No statistics are available on the emissions of diesel electric vessels, but the combined CO_2 emission of roll-on/roll-off vessels, ferries, and cruise vessels were 117 million tons in 2012. Therefore, reducing emissions from these vessels would be significant for the global environment. Reducing CO_2 emitted from marine vessels can be achieved by reducing the fuel consumption, which in addition lowers vessel operational cost. This is a good incentive for the vessel owner and renters to implement methods that reduce emissions.

The International Maritime Organization (IMO) sets limits on NO_X emissions through MARPOL Annex VI (Figure 1.1) (IMO; 2011). The Tier III requirements are now enforced within the emission control areas on all new vessels in operation and Tier II applies to all new vessels outside of these areas (Figure 1.2). Reducing NO_X can be achieved by better control of diesel engines; including new air paths, such as exhaust gas recirculation; or by adding exhaust gas treatment systems, such as selective catalytic reduction (SCR). As NO_X form at high temperatures, NO_X emissions often increase with a higher engine load. In contrast, SCR requires a minimum temperature to work and therefore, requires a medium or high engine load. For vessels operating between Norwegian harbors, the Business Sector's
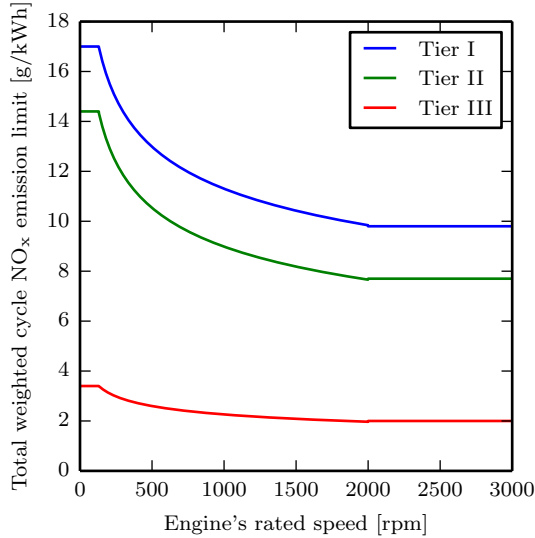
Figure 1.1: NO$_X$ limits given by the IMO Tier requirements. The Tier I, II, and III rules apply for all vessels constructed in 2000, 2011, and 2016 or later, respectively. However, the Tier III rules apply to vessels while operating in Emission Control Areas.

NO$_X$ Fund provides financial support to project reducing NO$_X$ emissions, such as installing an SCR or for consumption of urea used in SCRs.

MARPOL Annex VI also adds limits on SO$_X$ and particulate matter (PM). This sets limits on the sulfur content in the fuel. The exhaust gas treatment systems, such as scrubbers, can be used to reduce the SO$_X$ and PM emissions, and the sulfur content limits on the fuel can then be by-passed. The formation of PM increases when the air-to-fuel ratio is low (rich combustion), which may occur during torque load changes in the diesel engines (Guzzella and Onder; 2010). Therefore, smoother power consumption may reduce PM emissions. MARPOL Annex VI also sets emission limits for ozone-depleting substances and volatile organic compounds.

The Energy Efficiency Design Index (EEDI) is included in MARPOL Annex VI, which sets maximum CO$_2$ emission of a vessel based on average of emission of similar existing vessels. However, vessels with diesel electric propulsion are excluded from this requirement (Bazari and Longva; 2011).
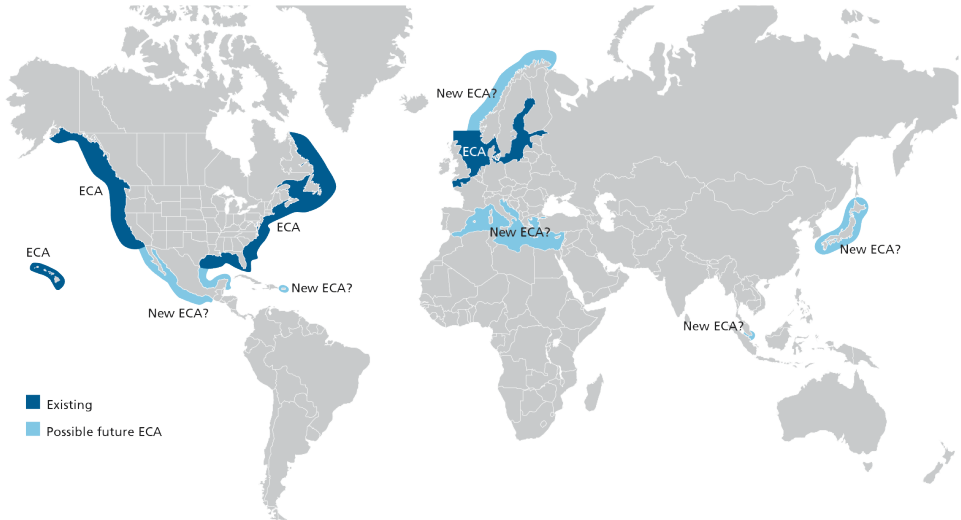
Figure 1.2: Emission control areas (ECA) for Tier III and possible future ECA as indicated by DNV GL. Note that the ECA in the North Sea and Baltic Sea are only regulating SO_X emissions. Courtesy: DNV GL.

1.1.1 Dynamic Positioning

In this study, vessels with dynamic positioning (DP) systems are used as an example, although many of the results are useful for other cases. The thrusters maintain the vessel's position and heading fixed during DP operation. The subsystems of a DP system are shown in Figure 1.3. The position measurement of the vessel is measured by e.g., GPS, taut-wire, or acoustics. An observer filter out the wave induced motion components and estimates a low frequency position and velocity from these measurements. The DP controller uses this estimate to determine the desired force and moments to control the vessel position. Thrust allocation converts this global force to local forces for each thruster. Then, the propulsion unit controls the thrusters to provide the desired thrust (Sørensen; 2011).

1.1.2 Diesel Electric Propulsion

Diesel electric propulsion has become the industry standard for e.g., oil and gass vessels, cruise vessels, ferries, and vessels with DP system. An example of a diesel electric power plant is given in Figure 1.4. The power plant consists of multiple pairs of diesel engines and electric generators (generator set). The generator sets deliver power to the propulsion units as well as other
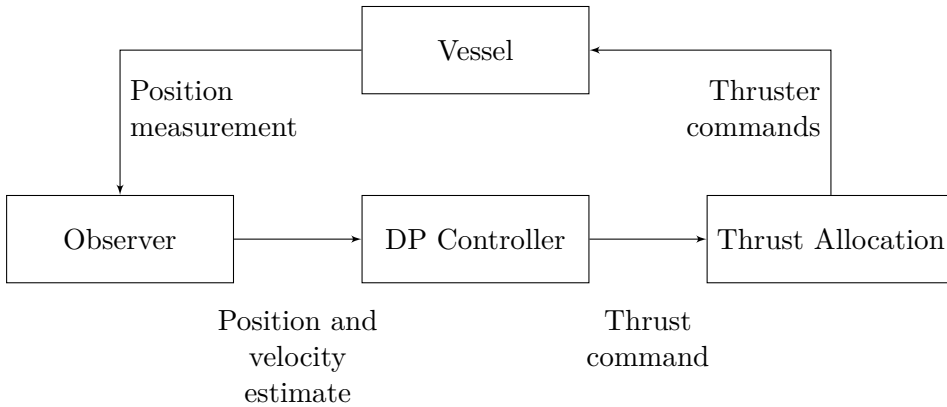
Figure 1.3: Systems included in dynamic positioning

consumers, such as hotel loads, drilling equipment, cranes, and auxiliary systems. One of the advantages of diesel electric propulsion is flexibility, because the power plant is easily reconfigured. This can be utilized to increase efficiency by running the optimal number of engines. Safety can be increased by increasing the redundancy and segregating the electric grid into independent grids where each grid can independently maintain the operation (Radan; 2008; Ådnanes; 2003).

Diesel electric propulsion is mainly used on vessels with changing power and/or redundancy requirement, because the additional equipment between the diesel engine and the propeller shaft decreases the efficiency during high-load conditions. *Vandal* was the first vessel with diesel electric propulsion, launched in 1903. The technology evolved further for submarines during World War I. However, for commercial vessels, the technology got traction with the demand from dynamic positioning of thrusters that are more responsive and the development of power electronics in the 1980s (Hansen and Wendt; 2015; Skjong, Rødskar, Molinas, Johansen and Cunningham; 2015).

For vessels with DP class 2 and 3, it is required that any single fault should not lead to loss of position (IMO; 1994). Redundancy in the power plant is used to fulfill this requirement. Figure 1.4 shows a single line diagram for a drilling vessel. In typical DP operations, the power plant is configured so that one switchboard could fail and the remaining switchboards are still able to keep the position of the vessel until the operation is terminated.
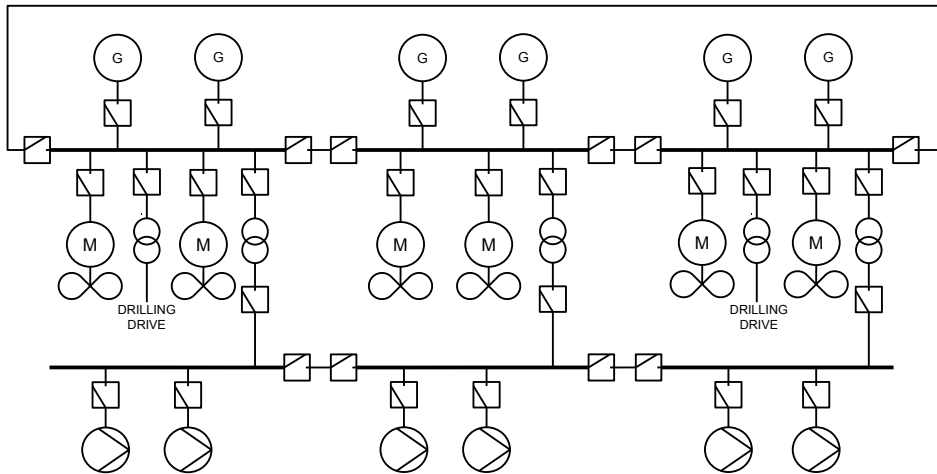
Figure 1.4: Single line diagram of a power plant on a drilling vessel.
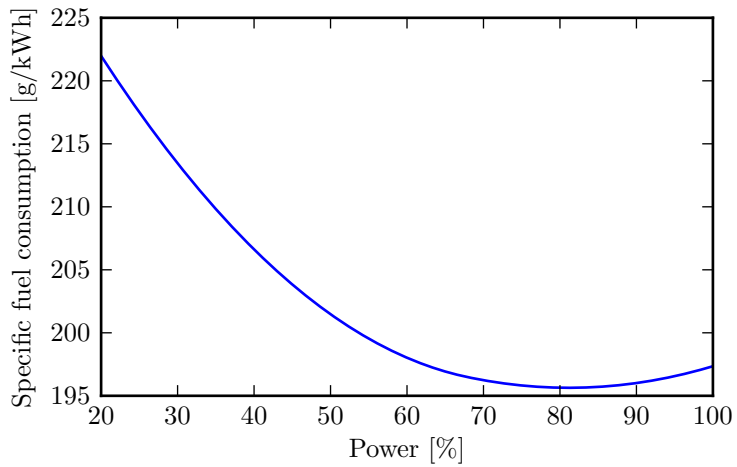
Figure 1.5: Specific fuel consumption of a typical marine diesel engine.
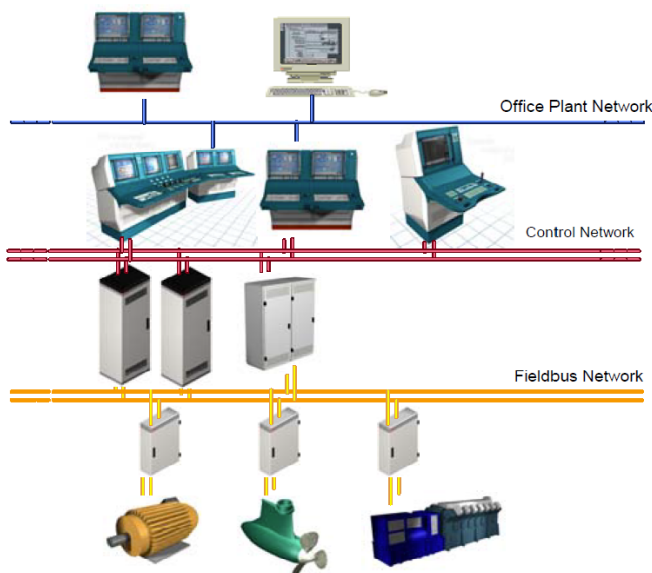
Figure 1.6: Hierarchy of control systems and networks for a typical marine power system. Courtesy: Sørensen (2013).

1.1.3 Marine Automation

One of the first examples of automation of marine engine room was the Haugvik-project. In this project the Norsk Hydro owned ammonia tanker M/T Haugvik was retrofitted with measurement and monitoring systems, so that the engine room could be monitored from the bridge. This was performed by Norges Skipsforskningsinstitutt (later MARINTEK) and Norsk Hydro. The motivation behind the project was to reduce the need of competent personnel, due to the lack of competent personnel in the industry and to lower the operational cost. The success of this project later led to the establishment of Norcontrol and the engine room zero notation (E0) by Veritas (later DNV GL) (Overbye; 1989).

A typical hierarchy in a marine automation system is presented in Figure 1.6. The local controllers are at the bottom level, which control the equipment, such as thrusters, drilling equipment, and HVAC. These low-level controllers communicate with high-level controllers via a redundant fieldbus network. The high-level controllers coordinates the low-level con-

trollers and may include dynamic positioning controllers and the power management system. Furthermore, these high-level control systems communicate with operation stations around the vessel through redundant Ethernet networks, often called A and B networks. A third Ethernet network, network C, is used for non-essential communications, such as administration and printing. This network may also have an onshore connection through satellite communication, so that the vessel can be optimized from onshore. This hierarchy is useful for several reasons. One reason is the segregation of more critical communication from less critical communication. This hierarchy also separates the time scales, as the fastest control actions are done by the local controllers, while high-level controller do the slower coordination (Sørensen; 2013).

A power management system (PMS) is used for coordinated control of the electric grid. Its main tasks are to make sure that sufficient power is available and to prevent blackouts in case of faults. The PMS is often the most interconnected system on a marine vessel, because it must communicate with all main power consumers, producers, and distributors. The two layer architecture is also used for control of marine power plants, with the low-level controllers, such as switchboards, governors, and breakers, and a high-level controller, PMS. The low-level controllers protect the equipments, while the PMS takes charge of the coordination, to prevent blackouts and optimization of the plant (Ådnanes; 2003).

The switchboards control the power plant at the lowest level. It includes protection systems, such as under/over frequency protection, reverse power of generators, and short circuit relays. In addition, the switchboards calculate active and reactive power, frequency, and voltage, and these signals are then sent to the PMS field station. The breakers includes protection relays with varying delays depending on their position in the power plant. This is timed carefully such that faulty equipment is disconnected and no other equipment is affected. Frequency drives may implement fast phase back system (FPBS), also known as frequency guard (May; 2003). This reduces power consumption of the frequency drives if the frequency is too low, and eventually cuts the power if the frequency decreases low enough. Governors on the generator sets controls the generator sets throttle, to control the electrical frequency and load sharing among the generator set. An automatic voltage regulator in the generator is used to control voltage and reactive load sharing; this is accomplished by changing the field current. These systems are implemented such that an operator can control the plant locally and turn off the PMS to control the plant manually. For example,

new generators can be connected by activating the synchronizer, and the generator can be manually connected when it is in sync (Ådnanes; 2003).

The PMS is implemented through field stations to control the plant and operating stations for human machine interface. As the loss of a field station should not be the worst case failure on a DP vessel, there is one field station per switchboard or one per generator set. Their physical location in a DP 3 vessel is also important, because they should be segregated in case of fire and flooding. The field stations communicate with low-level controllers through the field bus network, or directly over hard-wired signals. Hard-wired signals are often used when frequent data updates are needed, such as to determine breaker status, as an opening of a breaker may require immediate coordinated control by the PMS. Two CPUs and a master/slave architecture is typical used in field stations, where the slave is ready to immediately take over control if the master CPU fails (May; 2003).

The operator station is used as the human-machine interface. Multiple operator stations are placed around the vessel, such as one to monitor the power plant from the DP control station, and another for control of the power plant by the engineer. They communicate with the field station through the A and B network.

These are functions typically implemented on a PMS (May and Foss; 2000):

Power available: The vessel should have sufficient available power at all times. However, sometimes there are not enough power, this may occur due to the connection of large loads or disconnection of producers. The frequency will begin to drop if this situation is not handled correctly, which will give blackout. Thus, a power available signal is used. The available power of the producers is summed and allocated to the main consumers by priority. The reaction time is typically within tenths of a second. In addition, the PMS accepts or rejects connections from large power consumers when required, based on available power.

Fast load reduction: FLR is used in addition to power available. The FLR sets power limitations on the frequency drives of propulsion motors or other motors with frequency drives. These frequency drives react within milliseconds due to the fast power electronics. Therefore, FLR is often used for fault events, such as the loss of generator set or opening of bus-tie breakers. The FLR is triggered by hard-wired signals and reduces power consumption within tens of milliseconds.

Load shedding: Load shedding is used in extreme cases, when FLR and power available are insufficient. Consumers are disconnected completely from the grid to reduce power consumption. However, this is a drastic method, because it often takes much effort and time to restart systems.

Ramp control: Ramps are often used to constrain power increases of consumers, so that large load steps on the generators are avoided. In some cases, these ramps are dynamically set by the PMS depending on operation and configuration of the vessel.

Automatic start and stop of generator set: Generator sets may be automatically started and connected by the PMS when power demand increases. This is often performed using start tables. A new generator set is connected if the power demand increases above a threshold for a certain length of time. Similarly, generators can be disconnected if the power demand decreases below a threshold for a certain time. Generators are often automatically started and connected in cases of severe faults.

Automatic monitoring: The PMS can check health of the system and react if the system is unhealthy. This is needed as some faults escalate very quickly. An example is a fault in the governor. If the governor gives full power, the corresponding generator set will take additional load. The other generator sets may then go into reverse power and trip. Then, the bus is left with only the unhealthy generator set, and the future of the plant is uncertain. This may happen within tens of seconds, which is faster than a human can detect, identify, and react to the fault. In this case, the PMS should detect and identify the fault and disconnect the generator set before the other generator sets trip on reverse power.

Blackout Recovery: The worst case scenario occurs sometimes, and the power system blacks out. In such cases, the power system must be recovered carefully. This is often performed by a preprogrammed sequence, so that the most important equipment is connected first.

Logging: The PMS is also used for logging; the operator uses this option to optimize the configuration and fault diagnostics.

The PMS is usually operated by the machine room operator who communicates with the bridge, so that the power plant is correctly configured.

For example, the bridge may tell the machine room operator that a new operation requiring more power will be started soon. Then, the PMS operator may start and connect additional generator sets and give their acceptance for the operation to start. The maintenance of diesel engines is typically scheduled by the running hour of the engine, which is the number of hours the engine has been running. Therefore, the operator select engines for stand-by so that the desired share of running hours is achieved. Although a load-dependent start is often activated, load-dependent stop is typically disabled. The operators often prefer to control this function themselves, so that the engines are not shut down at wrong time and to optimize the individual share of running hours. However, this can be performed automatically, and is often implemented with mode control. The configuration is achieved automatically by selecting the vessel mode (e.g., transit, stand-by, or drilling). The power available is presented for the operator at some operation station, such as DP and drilling operation station, to indicate the general status of the power plant.

1.1.4   Model Predictive Control

Several methods based on model predictive control (MPC) will be described in this study. MPC includes a model of the controlled plant. The future trajectory of the controlled states is predicted and optimized with respect to a cost function and constraints. This optimization gives an optimal control sequence. The first input in this sequence is applied, at the next update time instant the trajectory and control sequence are optimized, and the first input of this control sequence is applied. This process is repeated continuously (Maciejowski; 2002).

MPC is in use for DP in Kongsberg Maritimes greenDP system (Kongsberg Maritime; n.d.). The advertisement for this system claims that the fuel consumption is reduced by approximately 20%, and power fluctuations are reduced by 50–80%. In this case, the vessel is controlled to move within a region, instead of being controlled to a set point. This approach gives a smoother thrust and small disturbances can be neglected.

MPC has had the largest impact in refining, petrochemical, and other chemical factories, with more than 2,500 applications in these sectors and in total more than 4,500 applications were collected by Qin and Badgwell (2003). MPC is most attractive for plants with multiple coupled inputs and outputs. The hierarchy typically used to control a plant with MPCs consist of three levels, a plant controller, high-level MPC controllers, and low-level controllers. A static plant level optimizer calculates set-points for

the MPC. The MPC is then used for the transition between the set-points, and to keep the plant at the set-points. The MPC provides the set-points for local controllers of low-level equipment, such as pumps, valves, and motor drives. It is also common for the plant optimizer to produce a range instead of set-points for the output variables of the plant, such as in the greenDP. The disadvantage of MPC is the need of a good model of the plant, which are needed for accurate predictions, and computational complexity, which challenges reliable real-time implementations.

MPC has already been proposed for marine power systems and can be used to control power generation, e.g., Hansen et al. (1998); Paran et al. (2015); Veksler et al. (2013). It has also been suggested to use MPC for the coordinated control of producers and consumers, e.g., Park et al. (2015); Stone et al. (2015); Veksler et al. (2012b). MPC can control active filters to reduce harmonic distortion, e.g., Skjong, Molinas and Johansen (2015); Skjong, Molinas, Johansen and Volden (2015); Skjong, Ochoa-Gimenez, Molinas and Johansen (2015).

1.2 Current Trends

Many initiatives have been implemented in the last few years to reduce marine power plants emissions, e.g., Hansen et al. (2011); Mathiesen et al. (2012); Myklebust and Ådnanes (n.d.); Veksler et al. (2013). New classification rules allows startup of stand-by diesel engines and thrusters after a failure e.g., DNV (2015, Part 6 Chapter 26 Section 2) and ABS (2014, Section 8), and to operate with closed bus-ties; however, this challenges redundancy (DNV GL; 2015a). Moreover, the number of diesel engines running can be reduced, which will increase efficiency and reduce maintenance.

The combination of diesel electric and diesel mechanic propulsion has also been suggested (Myklebust and Ådnanes; n.d.). Methods for reducing load variations have been presented, such as batteries (Kim et al.; 2015), super-capacitors (Chen et al.; 2010), feed-forward control of generators, and load compensation using thrusters (Mathiesen et al.; 2012).

Battery and power electronics have been developed rapidly and several vendors invests in the development of batteries for marine vessels (ABB; n.d.; Martini; 2015; Valmot; 2014) and DNV GL allow the use of batteries during DP operation from January 1, 2016 (DNV GL; 2015b, Part 6 Chapter 3). Batteries are being used as the main power supply for a ferry (Martini; 2015). The maritime battery forum (Norwegian forum by DNV GL) reported that 26 vessels are using batteries among their member organiza-

tions (Opsand; 2015). Some advantages of batteries include:

- Peak-shaving, using the batteries (or super-capacitors) to reduce power fluctuations. This may reduce wear and tear on the diesel engines, increase efficiency, and batteries make it easier to synchronize new generators into the grid.

- Stand-by emergency power/uninterruptible power supply. Today the number of diesel engines has been set such that there is sufficient power available if a fault occurs, which gives a low utilization of the diesel engines. Currently, two generator sets are used in cases when only one is required during fault-free operation. Thus, if one generator fails, the other can maintain power production. However, if batteries are being used, one generator set can run, and the battery can take the full load until a new generator set is connected to the grid or the operation is terminated.

- A battery can be used to run the diesel engines at optimal load. First, the diesel engines can run at the optimal utilization and charge a battery with the excess power. Then, when the battery is fully charged, the diesel engine can be turned off. The battery will then supply the needed power, until the diesel engine is turned on again when the battery charge is depleted. This requires many charging/discharging cycles, which destroys the battery in the end. Therefore, the economics of this method should be studied to check if the reduction in fuel consumption pays off the extra wear and tear on the battery.

Direct current (DC) distribution should not be ignored when evaluating the future of diesel electric propulsion (Hansen and Wendt; 2015). DC allows the use of variable speed engines, which can increase efficiency. Figure 1.7 shows the specific fuel consumption for a variable speed engine. Note that the optimal speed of the engine varies with power. Other advantages of DC include simplified connection of DC power sources, no frequency limits on the generators (or electric grid), and no reactive power. However, some challenges exist considering high power use cases and short circuits.

Many new combinations of systems (or so-called hybrid concepts,) will soon be available in which the best of several systems are combined, such as diesel electric and batteries, AC and DC, and diesel-electric and mechanic. Even more complex systems will be developed than those available today. The needs for better verification (e.g., HIL (Johansen and Sørensen; 2009)), decision support, and autonomous control systems will increase.
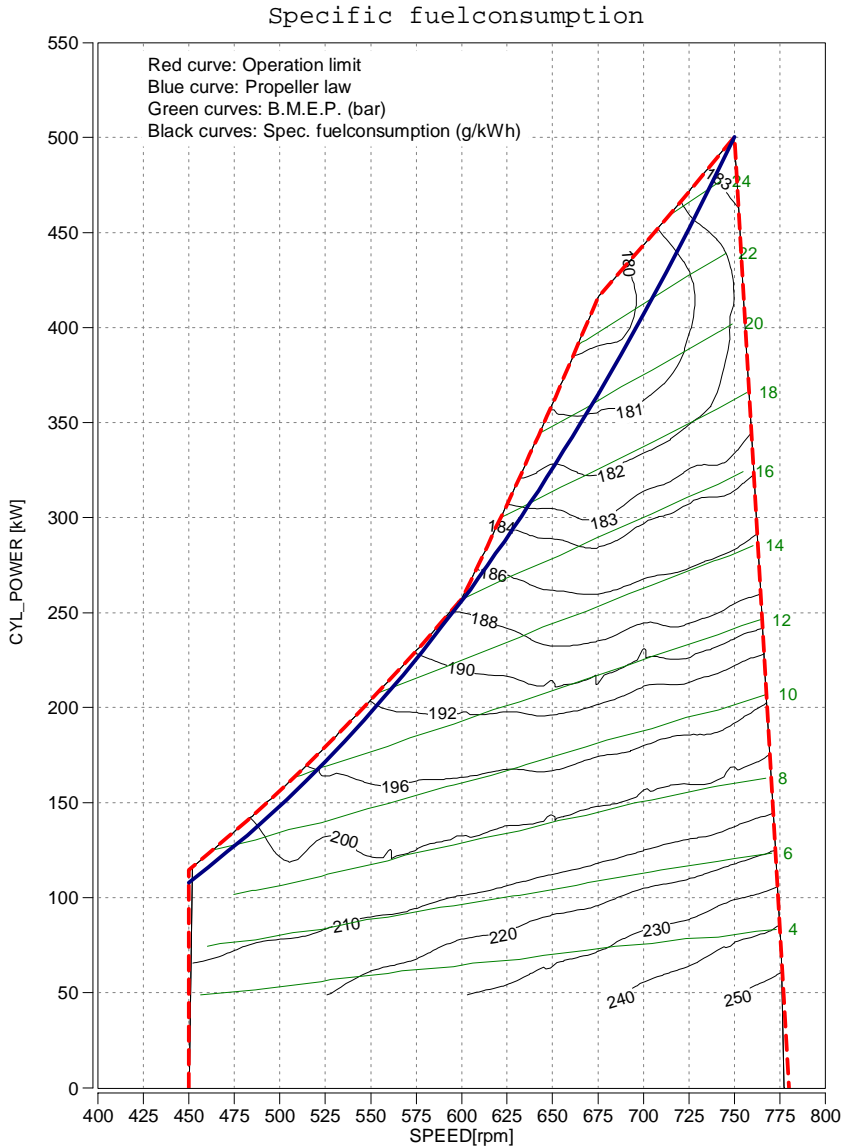
Figure 1.7: Specific fuel consumption of a typical marine variable speed diesel engine. Note that the contour lines for specific fuel consumption are not equidistant. Courtesy: Rolls-Royce.

Use of energy storage to optimize a power system was commercialized by the automotive industry in 1996 with the Toyota Prius (Ehsani et al.; 2009). A marine power plant has many similar challenges as a hybrid electric vehicle (HEV).

- Power demand varies, in the short-term, e.g., urban driving or load fluctuations from thrusters in harsh weather, and in the long-term, in slow traffic vs. highway or stand-by operation vs. transit.

- Future perspective of zero-emission zones for cars in cities and for marine vessels in harbor.

- The control of charging and discharging of energy storage is challenging for a hybrid car and a marine vessel, as future power demand is highly uncertain.

However, more flexibility and higher safety and reliability are required onboard a marine vessel than a HEV. A marine vessel has multiple power producers that can be turned on or off. In addition, a marine power plant controls its power consumers by constraining their demand; however, this may be a possible for autonomous cars in the future as well.

There is an increasing trend towards plug-in hybrid electric vehicles (PHEV) (Wirasingha and Emadi; 2011). With the increase of the battery size, the similarities between energy management for marine vehicles and those for automotive vehicles have become stronger. Different control strategies have been suggested to manage energy in a PHEV, including rulebased, fuzzy logic, and optimization-based control (Wirasingha and Emadi; 2011).

On-shore power grids are often considered stiff, which means that a change in power for a typically sized consumer or producer in the grid will result in a small or no change in the voltage and frequency of the grid. In contrast, marine power grids are considered weak. As consumers and producers can be the same size, a change in the consumed power can result in large changes in voltage and frequency. However, the increased renewable energy penetration in on-shore grids has produced some of the challenges of marine power plants for onshore power grids. Weisser and Garcia (2005) noted that a wind penetration level of $\geq 40\%$ is not recorded in autonomous medium-scale power grids, as higher penetration decreases power quality below the desired level. Holttinen et al. (2011) and Eriksen and Orths (2008) presented some challenges regarding increased penetration of wind power. These problems typically arise when the level of penetration

increases above 10–20%. The reserve requirement increases with increased wind penetration. The grid is also dependent on the interconnection among grids to balance power. This is the case in Denmark, which is dependent on balancing power from neighboring countries. Hydropower plants can be used for energy storage, which is much cheaper than batteries using today's technology. Improved wind forecast would improve scheduling, which would provide better predictions of future power production. The domestic grid must also be reinforced so that geographical imbalances can be handled. Power consumers can also be used to balance power, by controlling electric water boilers, charging electric vehicles, and cooling houses (Hovgaard et al.; 2013). These methods are strongly related to methods suggested for marine power plants. The interconnection among grids and reinforced grids are related to closed bus-tie operations, using hydropower for energy storage is equivalent to using batteries, and better control of consumers is also implemented on marine vessels.

1.3   Motivation

The flexibility of a vessel with DP and diesel electric propulsion gives a large opportunity to optimize the plant for reduction of environmental emissions. However, the system is highly complex, interconnected, and dynamic, due to the interactions between the environment and the propulsion, power and control systems. In addition, many operational objectives are conflicting, such as safety requirements and minimization of fuel consumption. As a greater number of diesel engines typically gives a safer vessel, but also increased fuel consumption.

Therefore, a large effort was put into the establishment of the system simulator. The simulator was needed for the further development and testing of new high-level control strategies. A large portion of the time spent on the PhD was used on this development, due to the complexity caused by the number of components, where appropriate models was selected and implemented to achieve the desired compatibility, fidelity, and computation performance.

Optimization-based control techniques are ideal for control of these systems. Control objectives can be reformulated to constraints and cost functions, and be handled explicitly. One of the constraints is that any single fault should not lead to loss of position. Scenarios can be used to model such constraints. The vessel can optimize its nominal performance using one or several predicted scenarios. Then, multiple scenarios modeling multiple

different faults can be used to ensure the plant's safety.

There are many ways to reduce greenhouse gas emissions from vessels including:

optimize the operation e.g., better tuning of controllers, new control strategies, and coordinated control,

optimize the configuration e.g., turning on or off generator sets, connecting switchboards,

optimize equipment e.g., proper dimension of needed power ratings, increasing the efficiency of thruster drives, and adding

new equipment e.g., batteries, capacitors, active filters, and DC distribution systems.

All of these methods above will be utilized in this thesis, except optimizing the equipment. The focus is to reduce the number of running generator sets. Marine diesel engines are typically operated at 20–50% of rated power; however, their optimum is about 80% (Figure 1.5). In addition, some NO_X reduction systems do not operate if the exhaust gas is too cold; therefore, a high engine utilization is required to achieve a high enough exhaust gas temperature. There are many reasons to run at low power, including:

Unclear situation: The operator of the vessel must be sure that the vessel is safe. However, the operator may not know the current safety status of the vessel. A situation in which the vessel is running with an unnecessary high safety level can be avoided by providing more relevant information about the vessel's safety status to the operator. Some operators override the automatic control system that starts and stops the generators because they do not trust or understand the control system.

Frequency variations: The varying electric power demands of a marine vessel may be a reason to increase the number of diesel engines. Although the mean power consumption is low, the power variations may cause undesirable large frequency variations. The resulting varying frequency makes it difficult to synchronize and connect additional generator sets, and increase the wear and tear on the diesel engines from thermal and mechanical stress. Consequently, the rotational inertia of the plant increases by committing additional generator sets, which reduces frequency fluctuations. Moreover, the fuel consumption curves

for diesel engines are given under static load conditions and underestimate fuel consumption during fluctuating load conditions.

Economy: It is common for some types of vessels for the renter to pay for the fuel of the vessel. Therefore, the vessel owner and operator of the vessel do not have an incentive to reduce fuel consumption. However, the vessel owner pays for maintenance of the engine, which often follows the running hours of the engines. Therefore, maintenance is reduced by reducing the number of running engines, which reduces costs for the vessel owner. However, the cost of interrupting or aborting an operation due to a fault in the power plant is typically much higher than the possible cost reduction by optimizing the plant. Therefore, it may be a large economic risk to reduce redundancy for a more efficient but less robust power plant.

The topics of this thesis are investigating methods for better configurations and safer control. Better configurations can be achieved by modeling (Chapter 2), which can be used to design better vessels, and a better decision support system (Chapter 3) so that the operator can make better decisions. The power fluctuations problem can be handled with better control of the generator sets (Chapter 4), and use of batteries or thrusters for peak shaving (Chapters 5 and 6). The performance of a given power plant configuration will increase using these methods (less fuel consumption, less wear and tear, and easier synchronization). In addition, these control methods may make previously unsafe configurations safe.

1.4   Publications

The following publication are the basis of the thesis:

- Bø, T. I. and Johansen, T. A. (2013). Scenario-based fault-tolerant model predictive control for diesel-electric marine power plant, *MTS/ IEEE Oceans*, Bergen, Norway.

- Bø, T. I., Johansen, T. A. and Mathiesen, E. (2013). Unit Commitment of Generator Sets During Dynamic Positioning Operation Based on Consequence Simulation, Proc. 9th IFAC Conf. Control Applications in Marine Systems.

- Bø, T. I. and Johansen, T. A. (2014). Dynamic safety constraints by scenario based economic model predictive control, *Proc. IFAC World Congress*, Cape Town, South Africa, pp. 9412–9418.

- Bø, T. I., Johansen, T. A., Dahl, A. R., Miyazaki, M. R., Pedersen, E., Rokseth, B., Skjetne, R., Sørensen, A. J., Thorat, L., Utne, I. B. et al. (2015). Real-time marine vessel and power plant simulation, Proceedings of the ASME 34th International Conference on Ocean, Offshore and Engineering, OMAE 2015.

- Bø, T. I., Johansen, T. A., Sørensen, A. J. and Mathiesen, E. Dynamic Consequence Analysis of Marine Electric Power Plant in Dynamic Positioning. Submitted for publication

- Bø, T. I. and Johansen, T. A. Dynamic safety constraints by scenario-based economic model predictive control. Submitted for publication.

- Bø, T. I. and Johansen, T. A. Battery Peak-Shaving Control in Electric Marine Power Plant using Nonlinear Model Predictive Control. Submitted for publication.

- Bø, T. I., Dahl, A. R., Johansen, T. A., Mathiesen, E., Miyazaki, M. R., Pedersen, E., Skjetne, R., Sørensen, A. J., Thorat, L. and Yum, K. K. (2015). Marine vessel and power plant system simulator. *Access, IEEE* **3**: 2065–2079

- Johansen, T. A., Bø, T. I., Mathiesen, E., Veksler, A. and Sørensen, A. J. (2014). Dynamic positioning system as dynamic energy storage on dieselelectric. doi: 10.1109/ACCESS.2015.2496122 ships, *Power Systems, IEEE Transactions on* **29**(6): 3086–3091.

1.5   Structure of the Thesis and Main Contributions

The thesis is a collection of papers, which makes the chapters self-contained. However, the model used in Chapter 2 was used for the simulations in several other chapters.

Chapter 2: This chapter presents a marine vessel system simulator. The simulator includes marine power, DP, and control systems. The main contribution is the presentation of the models required for the system simulator. The motivation behind the simulator was the need for a simulator that could model the interaction effects between the DP system and the electrical system under nominal conditions and when faults occur. More knowledge of the current safety margin can

be found by using a simulator which can simulate faults in the electric system, how they are handled, and how they affect the stationkeeping performance. The simulator allows new methods to be tested and verified including interaction effects. In addition, the simulator includes interaction effects between the DP system and the electric system, such as power fluctuations generated by wave induced motion. This can be used to optimize power producers with load time series from the simulator.

Chapter 3: The simulator was used for development of the simulation-based consequence analysis. The main contribution of this chapter is the analysis method. The analysis was performed by establishing all possible worst case scenarios, and simulating them to verify that the vessel could maintain its position during the worst case scenario. The method was compared with the conventional static method. A drilling rig was used in the simulation study with several fault scenarios and grid configurations. Different recovery methods were used in the simulation study to show different transient performance.

Chapter 4: A scenario-based MPC was presented in this chapter. The controller used fault and nominal scenarios internally. The fault scenarios are used to constrain the nominal scenario, so that the plant can be maintained within the constraints after a fault scenario occurs. This transfers the safety requirements, given by the fault scenarios, from safety constraints on a nominal trajectory to safety constraints on fault trajectories, which is the main contribution of the chapter. As it may be difficult to find static constraints for the nominal trajectory, this increases the room for optimization, which may make increase the plant's performance.

The MPC controller is applied on a marine power plant. One of the reasons to use many diesel engines is to provide sufficient rotating inertia to withstand a loss of a generator. Lossing a generator increases the load on the remaining generator sets and the frequency will decrease due to rate constraints on the diesel engine's torque. This scenario will lead to a blackout due to under-frequency if the safety margin is too small or the load is not sufficiently reduced. Therefore, loss of a generator set was used as the fault scenario in the case study, where the set-point of the governor is adjusted by the MPC.

The safety margin is dynamic, which allows the electric frequency to vary within a safe range, instead of fixing it to a nominal frequency.

This may increase the safety margin in some cases, so that the configuration is safe in cases where it is unsafe with conventional control methods.

Chapter 5: Batteries are useful for peak shaving to reduce load fluctuations. The diesel engines will produce a slowly varying load, and the batteries will handle load fluctuations. Batteries get hot if the electric power is too high; therefore, power is constrained by the battery temperature. This chapter presents a controller that uses a combination of spectrum and statistical analyses with MPC to control the peak shaving, so that the load fluctuations are canceled by the batteries. However, when the batteries get hot, the most important frequencies in the load fluctuation are canceled.

Chapter 6: A formula for calculating the position variation given by the power fluctuation was presented in this chapter. As inertia of a marine vessel is large, kinetic energy is also large, even at low velocities. Large power fluctuations are canceled out by the thrusters if the vessel is allowed to oscillate around the desired position. The loss is also small when a sufficiently large mean force (e.g., wind or current) is applied to the vessel. This method allows the vessel to use extra thrust when the electric power demand is small, and the vessel will then move toward the mean force. The thrust can be decreased during periods of high power demand, and the mean force will move the vessel back to its original position. The mass of the vessel is used as an energy storage device to reduce variations in electric power, which is an alternative to using batteries, flywheels, or a super-capacitor for peak shaving.

Chapter 7: Concluding remarks and future perspectives are presented in the last chapter.

Chapter 2

Marine Vessel and Power Plant System Simulator

This chapter is based on Bø et al. (2015).

2.1 Introduction

2.1.1 Shipboard Electrical System

The onboard electric power system is crucial for most modern marine vessels conducting advanced operations. Diesel-electric propulsion is common in offshore oil and gas vessels and cruise/passenger ships with dynamic positioning (DP).

The ability to conduct stationkeeping and maneuvering subject to current, waves, and wind loads depends on the power plant capacity. Insufficient power may result in decreased DP performance and loss of position. More severely, a total loss of electric power, known as a blackout, results in loss of control of the vessel.

Redundancy in power capacity, distribution, and in the number of generating units is one possible alleviation of the risk of power system faults. However, redundancy is costly. Economical expenses are significant, both in terms of investment in equipment, which most of the time is not strictly necessary, and in terms of machine running hours leading to more frequent maintenance, and increased emissions and fuel consumption.

The mentioned concerns motive the development of new power plant control strategies and the introduction of new power sources. Such steps are not trivial, due to the complex and strongly interconnected nature of

onboard marine power plants, and the weak grid, i.e., sensitive to changes both in produced and consumed power. Numerical simulation is a valuable tool for investigating such effects at all stages of design, implementation, and operation.

2.1.2   Previous Work

A number of marine power plant simulation solutions exist. The intended use ranges from commercial to academic, and the content from a few state equations to complete software suites. A selection follows:

Marine Cybernetics' CyberSea technology platform encompasses models of hydrodynamics, electro-mechanics, and sensors (Marine Cybernetics; n.d.). It is used for independent hardware-in-the-loop (HIL) testing (Johansen and Sørensen; 2009) and dynamic capability analysis (DynCap) (Pivano et al.; 2014).

U.S. Office of Naval Research's Electric Ship Research and Development Consortium studies include both real-time HIL simulators (Ren et al.; 2005), models of higher fidelity (Steurer et al.; 2007), and extension to hybrid plants (Xie et al.; 2009).

Marine Systems Simulator (MSS) (MSS; 2010) library and simulator for MATLAB/Simulink is a 2004 merge of (Perez et al.; 2006, Section 1): marine GNC toolbox (Fossen; 2002), MCSim (Sørensen et al.; 2003), and DCMV (Perez and Blanke; 2003). It has vessel dynamics, environmental (wave, surface current, and wind) loads, and advanced thruster models.

DNV GL's Sesame Marine DNV GL (n.d.) risk management software includes Marintek's SImulation of Marine Operations (SIMO) motion and stationkeeping simulator. The system is capable of modeling multibody systems and flexible systems.

Italian Integrated Power Plant Ship Simulator includes an integrated power system model implemented in the Simulink environment (Bosich et al.; 2012).

NTNU models include thruster power consumption (Hansen et al.; 2001) and power management system functions (Radan; 2008).

NTNU bond graph model library Pedersen and Pedersen (2012) includes a vessel model. The library is also verified through full-scale experiments.

Some solutions mainly focus on the electrical system without concern for the actual DP performance and related consumption, while others do the opposite.

2.1.3 Design of System Simulators

The simulator presented in this chapter is a system simulator. This means that the purpose is to model interactions between each of the subsystems of the complete system, and it should be flexible, so that many different cases can be studied. A modular design achieves this.

The use cases of the simulator will determine the dynamics that we need to model and parameterize. The difference in magnitude of the smallest and the largest timescale of the dynamics in such a multi-physics simulator may be in order of decades. It is therefore essential to decide the important timescales for the particular study.

The smallest timescale of the vessel is, in the electric system, in the order of milliseconds. In the other end, quasistatic studies such as effects of wear and tear, are in the order of months and years. For simulating short-circuit, the fast dynamics must be modeled, while the effects of the environment, and wear and tear, can be assumed constant. On the other hand, the electric system can be assumed to be in steady state when simulating DP operation, as the timescales of the electric system are much smaller than the timescale of the vessel motion. Figure 2.1 lists the time scale of the simulator components. For certain components model reductions should not take place, as discussed in respective sections later.

The complexity of a system simulator grows with the number of components and the fidelity level. By increasing the fidelity level, more parameters with higher order model structure, and a more thorough verification and validation are required. In addition the computational speed will typically be reduced. For studies where high fidelity level is required, not all the submodels need to be of high fidelity, as long as the model reduction is done properly and with care. By using a modular design, it is easy to use low fidelity models to identify where higher fidelity is required. These models can then be replaced with high fidelity models.

Verification and validation is challenging for system simulators due to the high complexity. Each submodel can be verified by itself, but this
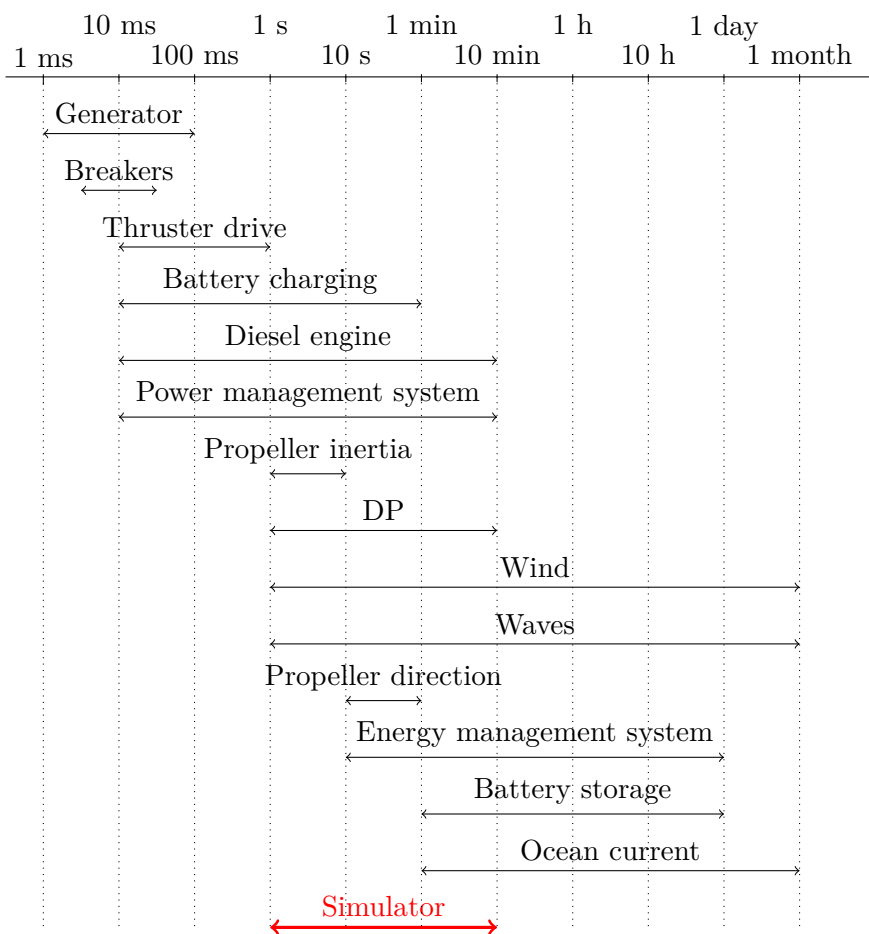
Figure 2.1: List of components in the simulator and their time scales.

does not verify their integration. Small scale or full scale tests can be used for verification, but this is costly and time consuming. In many cases experiences from a set of trained operators are the most practical way of verifying expected system-level performance.

2.1.4   Use Cases

The simulator has been used in several studies considering DP with diesel-electric propulsion and consumers such as hotel loads and motors for drilling, compressors, and pumps.

A selection of typical use cases follows:

Realistic power consumption profile: Since the DP controller and thruster models are interconnected with the power plant, the power load fluctuations are represented in a realistic way. The interaction between the many control subsystems, such as PMS, thrust allocation, thruster torque, or speed control, is included (Bø and Johansen; 2013). The simulator can therefore be used to generate time series for later use in isolated subsystem simulation (e.g., diesel engine simulation).

Fault consequence analysis: The plant behavior in the event of an electrical fault, such as the loss of a genset, can be simulated (Bø et al.; 2013). The resulting DP performance is then also available. This may improve the conventional capability analysis, which is calculated assuming that the propulsion system is in steady-state. Indeed, transients during plant reconfiguration can be critical (Pivano et al.; 2014).

Operation optimization: The detailed level of modeling includes many states for each submodule, for instance temperature and power output. Based on these, operation may be optimized with regards to emissions, maintenance, or fuel consumption.

Concept evaluation: Submodules representing new subsystems such as energy storage device (ESD), can be interfaced to the simulator. This allows investigation of new power sources and their effect on the overall control and performance of the plant.

It must be stressed that the simulator is not limited to diesel-electric propulsion, nor DP operations.

2.1.5 Contribution

This chapter focuses on the models and methods needed for an integrated simulator of the electric power system together with the vessel motion including the DP system. Secondly, some new models are established and verified to achieve the desired fidelity level and performance. Most of the models are verified models from literature. The scope of the simulator runs from high-level control systems, such as the positioning system and power management system (PMS), to high-fidelity models of power generators, storage, and consumers, such as gensets, batteries, and thrusters, respectively. The accuracy of the simulator is only verified qualitatively due to the complexity of the system. Quantitative verification of the plant is research still to be done and is considered outside the scope of this chapter.

2.1.6 Overview of the Chapter

This chapter consists of three sections, the model is presented in Section 2.2, the new models are verified in Section 2.3, and simulations are shown in Section 2.4. The modeling section starts with an overview of the simulator, followed by details of the power management system. The electrical components are then presented, with the switchboard and generator. Next, two models of diesel engines are presented, followed by the thruster models. Last is a presentation of the hydrodynamic model of the vessel, the environmental forces and the DP control system. In Section 2.3, verification of the electric bus model and simplified diesel-engine model are presented. Section 2.4 presents a simulation of a drilling rig in DP operation, then simulation of a fault is shown, before a simulation with batteries is presented.

2.2 Modeling

2.2.1 Simulator Overview

The main assumptions of the simulator are:

Steady-state electric system: It is assumed that the electrical system is in steady state, this is done to obtain real-time capabilities. The simulator captures dynamics with time scale down to 1 second. However, the dynamics of the electric system are often in milliseconds and are therefore assumed to be in steady state, as illustrated in Figure 2.1. This is verified in Section 2.3.1. The simulated electrical variables are frequency, voltage, active power, and reactive power. It is therefore

possible to simulate faults, such as under/over-frequency, slowly developing under/over voltage fault, and reverse power. However, it is not able to simulate phase imbalance, transient voltage faults, short-circuit, and harmonic distortion.

Mean-value engine model: The diesel engines are modeled by mean-value engine models. This means that most of the components in the diesel engine system are mathematically modeled based on the physical laws. However, the in-cylinder process is simplified so that it gives only a cycle average output such as average shaft torque, and mass and energy flow of the combustion gas.

Power management system: The objective of the PMS is to make sure that the power plant is safe and efficient. More details are given in Section 2.2.2.

Protection relays: Protection relays are not modeled, as breakers can be tripped by a timer. This means that some custom protection relays need to be implemented to simulate a partial blackout. Alternatively, post-processing can be used to detect when breakers should be opened.

Fixed pitch, variable speed thrusters: The thrusters are assumed to be fixed pitch propellers, with the possibility to run with variable speed. Thrusters that can rotate in any direction, azimuth thrusters, and fixed direction thrusters (e.g., tunnel thrusters) can be simulated.

An object-oriented modeling structure has been used to model the marine power plant. This means that each block in the simulator represents a physical component in the vessel, and further subsystem blocks represent internal physical components of the larger system.

The top level view of the model is illustrated by an example in Figure 2.2. This view represents the information flow for motion control of the vessel. A DP controller has been used in the presented case. Alternatively, the setpoints of the thrusters can be given manually during transit, maneuvering, or other operations without DP control.

For this case, the view contains:

1. Observer; estimates the position and velocity of the vessel from measurements.

2. DP control system; calculates a desired thrust command.
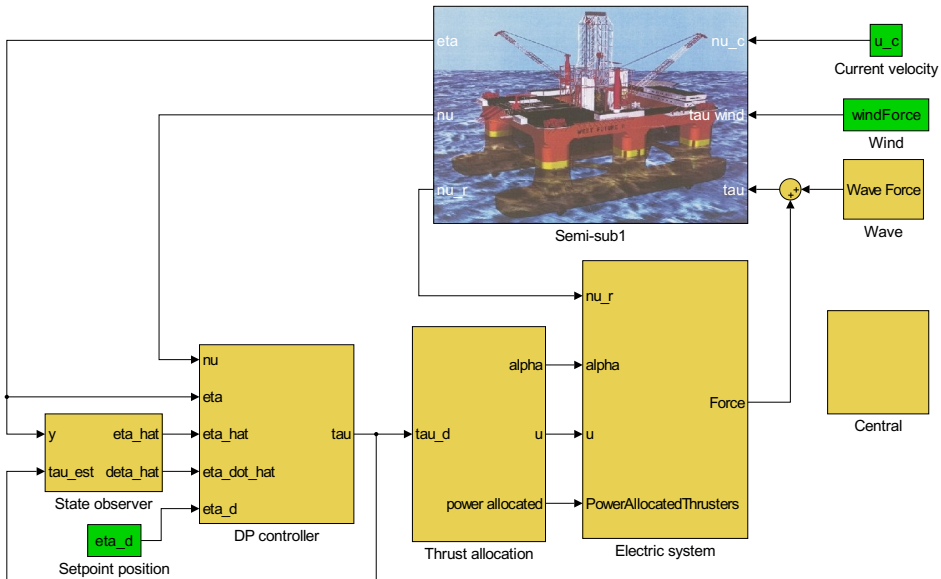
Figure 2.2: Example of top level view, including the vessel model, observer, DP controller, thrust allocation, and the electrical system. The electrical system is further presented in Figure 2.3. The central block is used for common calculations.

3. Thrust allocation (TA); converts the desired thrust command for the vessel to thrust commands for each thruster.

4. Electric system with thruster model; converts the thrust command to actual thrust, and electric power consumption.

5. Environmental model; generates realistic loads for the environment.

6. Vessel model; calculates the motions of the vessel given the thruster and environmental loads.

7. Central; this block is used for common calculations.

The electric power plant is modeled inside the electric system block. An example of a power plant is shown in Figure 2.3 and consists of:

1. Generator set; consisting of a prime mover (e.g., diesel engine), a generator, a speed governor, and an automatic voltage regulator (AVR).

2. Thruster drives; consisting of a frequency converter, an electric motor, a propeller, and controller.
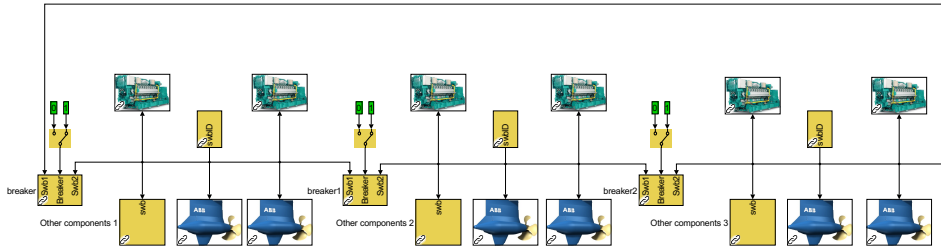
Figure 2.3: Example of power plant view, including the bus-tie breakers, thrusters, generator sets, and other loads block. This power plant is used for simulation of drilling rig in Section 2.4.

3. Other components; this can be hotel and drilling loads, which are modeled as time series of power consumption. However, this block may also be used for energy storage, such as batteries with a frequency converter. The load is then negative when the block delivers power and positive when it consumes power.

4. Switchboards; connecting loads and producers.

5. Breakers; connecting and disconnecting components.

Simulink was chosen in order to extend the MSS toolbox (Perez et al.; 2006) to include better thruster models and an electric power plant. The downside by choosing Simulink is the modeling of interconnections. The system is hard to divide into levels as required by the subsystem architecture of Simulink. We chose to use the top level model view for the vessel control. The electric power plant is a subsystem in this view and it is made to mimic a single line diagram. The stiff solver ode15s is used as numerical solver in the case study, since the local controllers give a stiff model.

Some first order lowpass filters are used to avoid algebraic loops, where the time constant of the filters are chosen to be smaller than the fastest dynamics of the relevant models. This is needed since we ignore some fast dynamics. The filters can therefore be seen as simplified models of the ignored dynamics. One example is the power available signal. An algebraic loop occurs since the power available is dependent on the power consumption, while the power available also constrains the power consumption. This is solved by adding a lowpass filter on the power available signal, which is faster than the time scale of the consumers. Alternatively, one may use dis-

crete time and a delay for these signals, but this reduces the performance of the chosen implicit ode solver.

2.2.2   Power Management System

The objective of the PMS is to make sure there is always enough power available, to prevent blackout. If a blackout occurs, the power should be restored as fast as possible. The PMS starts additional generators when the excessive power capacity of the connected producers is too low. In addition, the PMS allocates power to the different consumers, by first summing the current power capacity of the producers, and then sharing this among the consumers based on their desired power consumption and priority. This signal, called *power available*, is sent to some consumers, stating the maximum power limit for the specific load. Load shedding (disconnection of consumers) is done in extreme cases, when power reduction must be done immediately (e.g., close to under-frequency).

Fast load reduction is an alternative method to reduce the power consumption quickly. It reduces the load of the thruster drives, since they can change the power consumption quickly due to the frequency converters. Shortly after the fault is cleared or the capacity is increased, the drives can increase their loads. This is in contrast to load shedding where the consumers often needs to be restarted after being disconnected.

The PMS can also adjust the droop and isochronous load sharing parameters to adjust the load sharing. This is done during progressive loading after connection of generator sets. Progressive loading is implemented to ensure that the power generation of the new producer is slowly increased from no load to desired load sharing.

The PMS algorithm is implemented in C++ as an S-function block and can easily be configured to different power plants. The object-oriented focus of the simulator is kept in the PMS implementation, so that new functionalities, such as automatic start and stop, can easily be added.

2.2.3   Bus Voltage Calculation

The voltage of the bus is needed to calculate the load sharing of the generators. The generators are connected in parallel as shown in Figure 2.4a. The loads are assumed to be independent of the bus voltage, their active and reactive power are therefore given. Thévenin equivalent circuit, as shown in Figure 2.4b, of the connected generator sets is used to calculate the bus
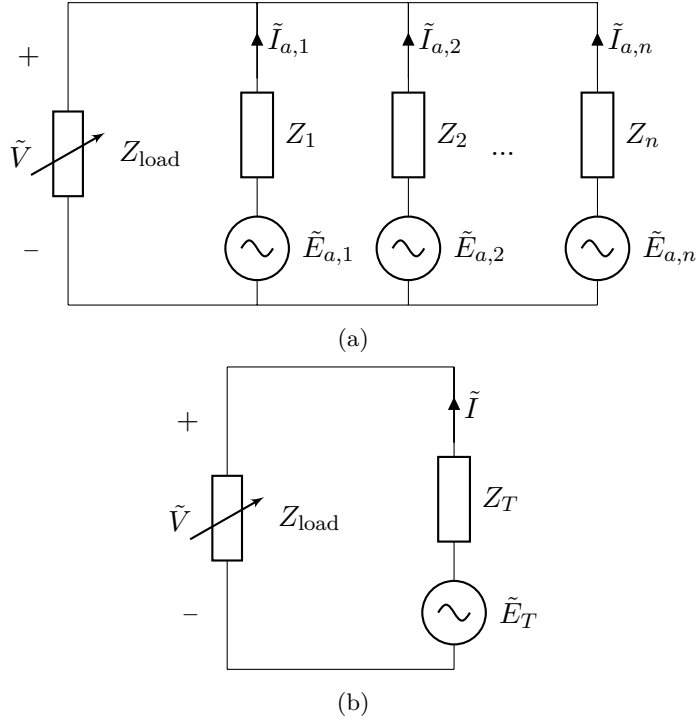
Figure 2.4: (a) Circuit diagram of bus with one load with the impedance Z_{load} and n generators. (b) Thévenin equivalent circuit of (a).

voltage. This circuit is closed by the loads, which have a known power consumption but unknown impedance.

The resulting power on the bus is then given as

$$P_{\mathrm{bus}} + jQ_{\mathrm{bus}} = 3\tilde{V}\tilde{I}^* = 3\tilde{V}\frac{\tilde{E}_T^* - \tilde{V}^*}{Z_T^*}, \tag{2.1}$$

where P_{bus} and Q_{bus} are the active and reactive power of the loads, $\tilde{V}$ is the line-to-neutral bus voltage, $\tilde{I}$ is the current, $\tilde{E}_T$ is the Thévenin equivalent voltage, and Z_T is the Thévenin equivalent impedance. Equation (2.1) has either two solutions, one solution, or no solution. For the case where there exists two solutions, the solution with the largest absolute value for the bus voltage is used. The largest voltage yields a high resistance of the load, and a low current, hence low internal loss. The lower voltage solution gives a resistance smaller than the Thévenin equivalent resistance, which is unphysical. This yields a high current, with very high internal loss since

most of the voltage drop occurs over the internal impedance.

During simulations it may occur that there exists no valid solution. This may happen when the load increases rapidly (a load is connected) or the Thévenin equivalent voltage of the generator decreases rapidly (fault in AVR or disconnection of a generator). In such cases, the voltage is set to a low value. This gives an incorrect load sharing, but the AVR will increase the voltage quickly. During the verification study in Section 2.3.1, a valid solution of the bus voltage was regained within 0.1 millisecond. This is permissible since the time is very short compared to the time scale of the mechanical system. A lowpass filter must therefore be added when simulating voltage protection relays.

2.2.4 Generator

In marine power plants, synchronous generators are typically used to produce power. As mentioned earlier, the generator is assumed to be in steady state and with balanced phases. The electrical torque is

$$\tau_e = \frac{p + p_{\text{loss}}}{\omega} = \frac{p}{\omega} + \frac{r(p^2 + q^2)}{\omega v^2}, \tag{2.2}$$

where p and p_{loss} are the active power generated and power loss in the generator, r is the resistance in the stator windings, q is the reactive power, and v is the terminal voltage. The terminal line-to-neutral voltage is given as (Krause et al.; 2013):

$$\tilde{V}_a = -Z\tilde{I}_a + \tilde{E}_a, \tag{2.3}$$

where Z is the internal impedance of the generator set, $\tilde{I}_a$ is the current through phase a and $\tilde{E}_a$ is the induced line-to-neutral voltage for phase a.

It is assumed that the magnitude of $\tilde{E}_a$ is perfectly controlled by the AVR or at least the dynamics are much faster than the dynamics of the mechanical system. This is verified in Section 2.3.1. The per phase angle of $\tilde{E}_a$ is

$$\angle\tilde{E}_a = \frac{\theta N_{\text{poles}}}{2}, \tag{2.4}$$

where θ is the mechanical angle and N_{poles} is the number of poles of the generator. Parameters are found from (Krause et al.; 2013).

The AVR regulates the terminal voltage by manipulating the induced voltage. In this simulator, we use a droop controller to determine the setpoint, based on the reactive power of the generator set. This takes care of the reactive load sharing. The generators deliver equal amount of reactive power if they have equal voltage droop curves.

2.2.5 Diesel Engine

The dynamics of the diesel engine are the slowest dynamics of a diesel electric power plant. Most modern diesel engines are turbocharged to provide increased power density. When a turbocharged diesel engine needs to increase its delivered power, more air is required into the cylinders to avoid incomplete combustion and visible smoke in the exhaust. However, the response of the air system is slow, due to the rotating inertia of the turbocharger and the large air and exhaust receiver volumes. This gives rise to the *turbo-lag*. In addition, increasing the fuel injection rises the temperature in the cylinder.

Constraints are, therefore, added to the engine control output by the engine manufacturer to ensure that the fuel injection is not changed too quickly. This is done to avoid that the engine is damaged by a rapid change of temperature, and that the air pressure in the inlet manifold is large enough to allow for complete combustion. These constraints are in some cases conservative, and the air dynamics may be neglected since the engine will always run with complete combustion due to these constraints.

Transients of the diesel engines can be grouped into three categories (Benajes et al.; 2002). The first is energy transfer delay which happens due to signal delay, preset valve closure or injection timing. The time scale of such phenomena is in milliseconds. In simulation, this can only be seen by detailed modeling of the cylinder process and the fuel injection system. Secondly, the already mentioned air dynamics are the most interesting physics in this kind of application. The typical transient time scale of the air dynamics is in seconds. Lastly, the thermal transients are caused by the thermal inertia of the system, which may have time scale of tens of minutes.

Mean Value Model

The main purpose of the diesel engine simulation model is to capture the air dynamics including pressure before the engine cylinder which can be related to the charge air available for combustion. In the mean value engine model, most of the physics in the engine system components are captured except for the in-cylinder process, i.e., the thermodynamic cycle. The main components included in the model are an engine cylinder block, a turbocharger, a charge air cooler, an air receiver, and an exhaust receiver. The implemented mean value engine model is based on the models presented in Chow and Wyszynski (1999); Guzzella and Onder (2010); Heywood (1988); Pedersen and Engja (2000); Yum and Pedersen (2013); Zacharias (1967).

The engine system including a turbocharging system is inherently a thermodynamic process with gas mixture as medium. Therefore, main variables of the system are pressure, p; temperature, T; and fuel-air equivalent ratio, F. Also flow variables, such as mass flow of gas, $\dot{m}$; enthalpy flow or rate of change in internal energy, $\dot{E}$; and mass flow of burned fuel, $\dot{m}_\mathrm{b}$, are necessary to describe the dynamics of the system.

A filling and emptying method (Chow and Wyszynski; 1999) is used to construct the thermodynamic process model of the system. In this approach, the target model is constructed by placing control volumes in a series as configured in the real system and putting a flow restriction between adjacent control volumes. It is assumed that the thermodynamic states, such as pressure and temperature, are uniform within a control volume and that there is no accumulation of mass in the flow restriction. Then, all the components fall into two categories: a thermodynamic control volume or a flow restriction. Generally, pipes, receivers, and cylinders are thermodynamic control volumes; whereas any valve, port, compressor, turbine, and heat exchangers are considered as flow restrictions.

Thermal control volumes determine the thermodynamic states of the system. They consist of two parts. The first one is a flow junction where mass conservation and the first law of thermodynamics are implemented. The second part is the flow accumulation where the net rate of change in mass and energy are integrated. The integrated values are the mass, m_cv; the internal energy, U_cv; and the mass of burned fuel within the control volume, m_f; which are states of the system. Pressure and temperature are derived from a table of thermodynamic properties, such as the JANAF table (Chase; 1998), and by using the equation of state (i.e. ideal gas law). In order to achieve faster simulations, a semi-empirical formula for thermodynamic properties found in Zacharias (1967) is used in place of the table.

A flow restriction, placed between two control volumes, determines the flow rate of mass and energy between them. The flow rate depends on pressure and temperature of the adjacent control volumes. In many cases, the equations of the equivalent ideal flow for compressible gas is used for this purpose. The equation used for the model assumes an isentropic process across the restriction (Heywood; 1988). Therefore, any forms of energy gain or loss should be accounted for to satisfy the conservation laws.

In case of a compressor and a turbine, the model requires a performance data map from measurement or a manufacturer. The map represents the relationship between the pressure ratio across the device and rotating speed of the rotor, ω_TC; versus the corrected mass flow, $\dot{m}_\mathrm{corr,TC}$; and the isen-

tropic efficiency of the process, η_{TC}. Having acquired the mass flow and the efficiency, the energy flow in and out can be calculated assuming an isentropic process. Then the torque for each turbomachine can be calculated as

$$\tau = \frac{\dot{m}\Delta h}{\omega_{\mathrm{TC}}} \tag{2.5}$$

where, $\dot{m}$ and Δh are actual mass flow and change in enthalpy across the machine. A dynamic equation is used for the mechanical rotation of the turbocharger.

$$J\dot{\omega} = \tau_{\mathrm{turb}} - \tau_{\mathrm{comp}}, \tag{2.6}$$

where τ_{turb} and τ_{comp} are the torque by the turbine and compressor, J is the rotational inertia of the turbocharger, and ω is the angular velocity of the turbocharger.

The whole engine block, including intake and exhaust valves, fuel injection system, cylinders, and pistons is simplified to a single flow restriction model. In this model, the input is the pressure, p_{AR}; and temperature of the air receiver, T_{AR}; the engine speed, ω_{eng}; and the fuel rack position, u. Mass flow through this restriction model can be determined given a known volumetric efficiency of the process, η_{vol}.

$$
\begin{aligned}
\dot{m}_{\mathrm{in}} &= \eta_{\mathrm{vol}}\left(p_{\mathrm{AR}}\right)\rho_{\mathrm{AR}}V_d\frac{\omega_{\mathrm{eng}}}{n_s\pi}, \\
\dot{m}_{\mathrm{out}} &= \dot{m}_{\mathrm{in}} + \dot{m}_b, \\
\dot{m}_b &= m_{f,\mathrm{max}}u\frac{\omega_{\mathrm{eng}}}{n_s\pi},
\end{aligned}
\tag{2.7}
$$

where ρ_{AR} is the density of the gas in the air receiver, V_d is the displacement volume, n_s is the number of stroke of the engine cycle, $\dot{m}_b$ is the burned fuel mass flow, and $m_{f,\mathrm{max}}$ is the maximum amount of fuel injected per cycle. Energy flow in and out of the cylinder is calculated by

$$
\begin{aligned}
\dot{E}_{\mathrm{in}} &= \dot{m}_{\mathrm{in}}h_{\mathrm{AR}}\left(p_{\mathrm{AR}}, T_{\mathrm{AR}}\right), \\
\dot{E}_{\mathrm{out}} &= \dot{E}_{\mathrm{in}} + \dot{m}_{b,\mathrm{out}}\mathrm{LHV}\left(1 - C_{HT} - \frac{1}{\mathrm{LHV}\cdot\mathrm{SFC}}\right),
\end{aligned}
\tag{2.8}
$$

where h_{AR} is the enthalpy of air from the air receiver volume, LHV is low heating value of the fuel, C_{HT} is the heat transfer ratio, and SFC is the specific fuel consumption. The torque output of the engine is

$$\tau_e = \frac{\dot{m}_{b,\mathrm{out}}}{\omega_{\mathrm{eng}}\cdot\mathrm{SFC}}. \tag{2.9}$$
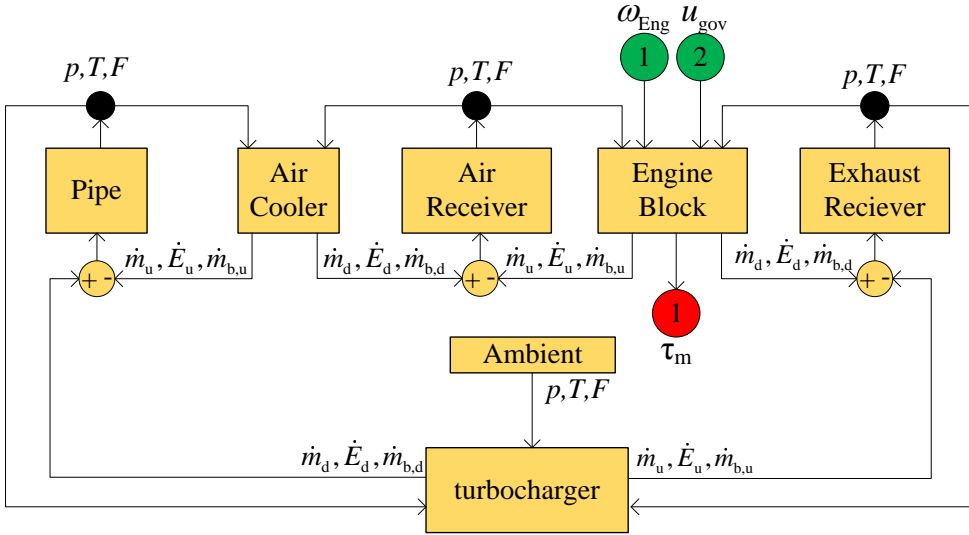
Figure 2.5: Mean value engine system model scheme, including a turbocharger, a charge air cooler and incylinder process.

The overall mean value engine system model is presented in Figure 2.5. Both compressor and turbine model require ambient pressure and temperature as boundary conditions for the system. The input to the overall model is fuel rack position and engine speed; the output is pressure and temperature of the air receiver, volumetric efficiency, and torque. The first three outputs are used in order to calculate the mass trapped in the cylinder per cycle, which is further used to calculate the maximum allowable injected fuel amount according to given fuel-air equivalent limit. This functionality is termed as smoke limiter, which ensures that the charge in the cylinder is lean enough to avoid visible smoke during rapid power output increase.

A short-coming of such a model is that it requires extensive parameter identification in order to achieve reasonable accuracy. However, a well-defined engine model can be used for different cases if the main physical variables are converted into per unit values. This may cause inaccurate response characteristics since machines at various power range should have somewhat different time scales. The step load response characteristics of a genset can be used to calibrate the overall model including the governor to match the given characteristics. Such characteristics can be found in the manufacturer's documentation, e.g. MAN Engines and Systems (2013).

Rate Constrained Model

A simplified model can be used for engines where the fuel rate is constrained such that the combustion is complete. In Section 2.3.3, simulations show that this is the case for maritime engines due to the conservative rate constraints set by the engine manufacturers. A simplified model that ignores the air dynamics and requires only one parameter is

$$\tau_m = k_u u, \tag{2.10}$$

where τ_m is the torque output of the diesel engine, and k_u is the gain from fuel rate to mechanical torque.

Shaft Speed Dynamics

The engine shaft speed dynamics is given by

$$\dot{\theta} = \omega \omega_b, \tag{2.11}$$

$$\dot{\omega} = \frac{1}{2H} \left(-D_f \omega + \tau_m - \tau_e \right), \tag{2.12}$$

where θ is the mechanical angle, ω is the per unit mechanical angular velocity, ω_b is the base mechanical angular velocity, and the windage friction constant is denoted D_f. This is derived by the swing equation and assuming linear damping. H is defined as

$$H = \frac{1}{2} \frac{J\omega_b^2}{P_b}, \tag{2.13}$$

where J is the rotational inertia of the generator set and P_b is the base power of the generator set (Krause et al.; 2013).

Governor

The two engine models use the same governor, which is based on droop control (Woodward; 2004). The commanded fuel index is then calculated by a PID controller with back calculation to avoid wind-up of the integrator term. The derivative of the frequency is calculated by using the *dirty derivative*.

$$\omega_{\text{ref}} = \omega_{\text{NL}} - K_{\text{droop}}p, \tag{2.14}$$

$$u = K_p(\omega_{\text{ref}} - \omega) + K_i\xi - K_d\hat{\omega}, \tag{2.15}$$

$$\dot{\xi} = \omega_{\text{ref}} - \omega + K_b(u_{\text{saturated}} - u), \tag{2.16}$$

$$\dot{\hat{\omega}} = N(\omega - \hat{\omega}), \tag{2.17}$$

where the K_d, K_i, K_p, and K_b are the nonnegative derivative, integration, proportional, and back-calculation gain. The per unit produced generator power is denoted p. The symbols ω_{ref}, ω_{NL}, and $\hat{\omega}$ are the reference frequency, setpoint no-load frequency, and estimated time derivative of the frequency.

For the rate constrained model, an additional constraint on the fuel index is needed to avoid too large temperature variations in the cylinder and sooting due to too little air for complete combustion. This constraint is predefined and, therefore, static. In the case study, the engine is allowed to increase the fuel index with 20% of the rated output and then increase the fuel index with $8.1\%/s$. This is found by tuning the engine model response to fit recovery time and frequency drop in MAN Engines and Systems (2013).

For the mean value model, a smoke limiter constrains the governor's command. The amount of air available for a cycle is

$$m_{\mathrm{air}} = \eta_{\mathrm{vol}} \frac{p_{\mathrm{AR}} V_d}{R T_{\mathrm{AR}}}, \tag{2.18}$$

where η_{vol} is the volumetric efficiency, p_{AR} and T_{AR} are the pressure and temperature at an air receiver, R is the specific gas constant and V_d is the displacement volume of a cylinder. Given the maximum fuel-air equivalent ratio, $F_{\max}$, the maximum fuel index, $u_{\max}$, is given by

$$u_{\max} = m_{\mathrm{air}} \frac{F_{\max} f_s}{m_{\mathrm{f,inj}}}, \tag{2.19}$$

where f_s is the stoichiometric fuel-air ratio and $m_{\mathrm{f,inj}}$ is the amount of maximum fuel injection per cycle. In the case study, $F_{\max}$ is chosen as 1 in order to give a reasonable engine response.

2.2.6   Energy Storage Devices

ESDs include batteries, capacitors, fuel cells, or any other device capable of providing and consuming power on demand. They are accounted for by the PMS as available power reserve, and depending on the control strategy adopted by the PMS, it might substitute a fast load reduction strategy. The inner dynamics in the energy storage devices are disregarded, since it is assumed that its dynamics are much faster than the remaining components.

All components included here are simplified, since the losses are modeled using an efficiency table. This method makes it simple to include and model more components with data provided by the manufacturers.

2.2.7 Thrusters

The thrusters are modeled as propellers which are driven by electrical motors. The propellers are assumed to be fixed pitch, while the speed is variable. No thruster-thruster or thruster-hull interaction losses are included. It is assumed that the torque of the electrical motor is perfectly controlled. A frequency converter is often used to control the motor. The time scale of the dynamics of the frequency converter is much faster than the dynamics of the mechanical part of the thruster drives, and it is therefore neglected. A speed controller is used to control the thrust. The open water characteristics are used to calculate the desired shaft speed, from the requested thrust. The thrust is given by (Sørensen; 2013)

$$T_a = \text{sign}(n) K_T \rho D^4 n^2, \tag{2.20}$$

where K_T is the thrust coefficient found from open water tests, ρ is the density of water, D is the propeller diameter, and n is the shaft speed. This gives the desired shaft speed

$$n_d = \text{sign}(T_d)\sqrt{\frac{|T_d|}{K_T \rho D^4}}. \tag{2.21}$$

The desired thrust signal must be smoothed since the desired thrust is typically calculated at 1 Hz. Large power fluctuation will occur at each thruster command update instant if this is not done. A second order filter is therefore used for this task.

The four-quadrant model of the propeller presented in Smogeli (2006), is used to calculate the actual thrust and torque of the thruster. The benefit of this model is that it models *wind milling* (i.e., shaft speed and torque have different signs). The advance velocity of the propeller is assumed to be equal to the relative velocity of the vessel. This means that wave-propeller interaction due to vessel motion is included, but wave-propeller interaction due to wave-induced particle motion is not included (Sørensen and Smogeli; 2009).

This model was first presented by Miniovich (1960). The thrust and torque coefficients are defined as

$$C_T = \frac{T_a}{\frac{1}{2}\pi R^2 \rho V_{0.7}^2}, \tag{2.22}$$

$$C_Q = \frac{Q_a}{\frac{1}{2}\pi R^3 \rho V_{0.7}^2}, \tag{2.23}$$

where T_a is the thrust, R is the radius of the propeller, and Q_a is the propeller torque. $V_{0.7}$ is the undisturbed incident velocity to the propeller blade at radius $0.7R$ and is defined as

$$V_{0.7} = \sqrt{V_a + (0.7\omega R)^2}, \tag{2.24}$$

where ω is the angular velocity of the propeller shaft.

The angle of attack of the propeller at $0.7R$, β, is defined as

$$\beta = \arctan\left(\frac{V_a}{0.7\omega R}\right). \tag{2.25}$$

To estimate C_T and C_Q, a Fourier approximation as a function of β is used, with parameters from Smogeli (2006).

The power consumption of the thrusters are typically reduced after a fault by the fast load reduction. This is done by limiting the torque of the electrical motor driving the propeller. In practice, this is done by the frequency converter.

The thrust allocation needs an estimate of the power consumption of the thrusters. The four-quadrant model is not suitable for this purpose, as the advance velocity is not available for the thrust allocation. The power consumption by the electric thruster is therefore approximated by

$$p = k|f|^{1.5}, \tag{2.26}$$

where f is the thrust amplitude, and k is a constant which can be found from bollard pull test results or open water tests (Sørensen; 2013, Chapter 9). Due to the approximation, the actual and approximated power consumption may be different.

2.2.8 Other Components

The last model in the electrical power simulator is a block named *other loads*. It represents loads that do not directly influence the propulsion system and are modeled as time series of desired and actual power consumption. The load is divided into two parts: high and low priority loads. Both send a desired power consumption to the PMS. The PMS will then allocate power available back to these loads. The PMS will first allocate power to the high priority loads, which may be an emergency system. The thrusters will then get allocated the remaining power, before the low priority loads get the last remaining available power. The actual consumed power is set equal to the allocated power available.

2.2.9   Vessel, Environment, Observer, and DP Controller

Models from the MCSim toolbox and MSS toolbox (Perez et al.; 2006) are used to model the vessel. In the simulation cases we have chosen models suitable for DP operations. The MSS toolbox contains multiple vessel models, and the model should be chosen depending on the simulation case.

MCSim is a high fidelity vessel model for low speed simulations, which includes wave frequency motions and low frequency motions. The low frequency motions includes forces from slowly varying current, second order wave drift, mean wind, and wind gust, in addition to hydrodynamic and thruster forces from the vessel. Wave frequency motion is found by motion transfer functions. MCSim uses transfer functions which can be found from WAMIT (Lee; 1995).

The state observer is a passive observer based on Fossen and Strand (1999), and the DP controller is implemented as a PID controller.

The fastest time scales of the vessel motion dynamics is the time scale of the wind gust, around 1 seconds. The slowest time scale is the change of the environmental condition, this is in the order of tens of minutes to hours or days. The environment is set constant, except for a slowly varying ocean current. Simulations are usually done using a shorter time horizon than the time scale of the change of environment condition. In such cases, the environment can be assumed to be constant during the simulation period.

2.3   Verification

Most of the models used in this simulator are well known models, which are already verified. However, the electric model, the rate constrained diesel engine model, and the parameters of the mean value diesel engine model needs to be verified.

2.3.1   Electric Model

A generator model based on flux linkages is used to verify the electric model (Krause et al.; 2013, Section 5.11). Parameters for the model are found in Krause et al. (2013, Table 5.10-1) and the simulations are done with two generators connected to the same load. The generator sets are operated with similar diesel engines, AVR, and governors for both models and generator sets.

For the steady-state model, the load is set to consume a constant power. The load of the flux-linkage model is set by a resistance, which gives the

desired power consumption when the voltage is at the rated value.

In Figure 2.6, the power, voltage, and frequency of the generators are plotted for a step increase of the load from 20% to 70%. Note that the simulated power of the steady-state model fits the power consumption of the flux-linkage model. A drop in the power of the flux-linkage occurs since the resistance of the load is suddenly increased, which also gives a voltage drop. The small difference afterward is mainly due to the different models of the load. The frequency is perfectly modeled, as expected since the power response is close for the two models. However, the voltage is not as well aligned during the first tenth of a second. Both models are able to capture a drop in voltage. However, while the timescale of the drop is consistent between the model (few milliseconds), the magnitude is inconsistent (6.3% for steady-state model and 71% for the flux-linkage model). There are also some sub-transients which are not captured by the steady-state model.

In order to model the voltage accurately, a high fidelity model of the load is also needed. This may be difficult for a marine vessel consisting of many different consumers where each consumer needs to be modeled.

2.3.2   Diesel Engine Model

A good diesel engine model should be able to predict fuel consumption as well as the engine dynamics in terms of speed under transient loads. It is crucial to get a correct fuel consumption curve because the model uses a prescribed cycle efficiency curve rather than actual cycle calculation in the cylinders. Such a curve can be obtained by fitting to the given fuel consumption data available for the engine.

However, the dynamic response of the engine arises from a combination of effects from multiple submodels of the system. The mean value model used in the simulator alone has about 50 parameters, of which some are arrays. Finding proper parameters and tuning the model can be a cumbersome process, even if the performance data of the engine is available. In order to ease the configuration process, one can use a well verified simulation model and normalize the output. However, the timescale of the engine dynamics may differ. Therefore, such a model should be re-tuned to match the dynamics of the engine of interest.

This can be done by tuning a limited number of parameters which have major influence on the engine response to the load changes. In this chapter, the gains for the governor controller, the inertia of turbocharger, the inertia of generator set, and the maximum fuel-air ratio are chosen as tuning parameters. The response curve from the load acceptance test of a specific
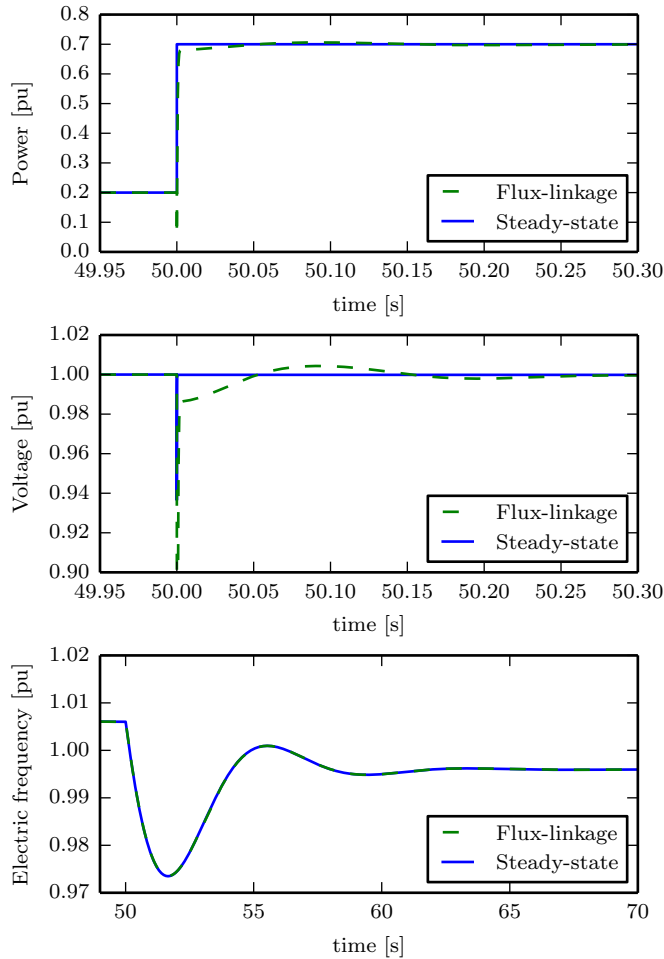
Figure 2.6: Simulation of a step increase of the load from 20% to 70% of the rated values. The simulations are done with the models described in Section 2.2.4 (steady-state) and models presented in Krause et al. (2013, Section 5.11) (flux-linkage). Upper: power of generators. Middle: terminal voltage of generators. Lower: electric frequency of generators, note the difference in the time scale.
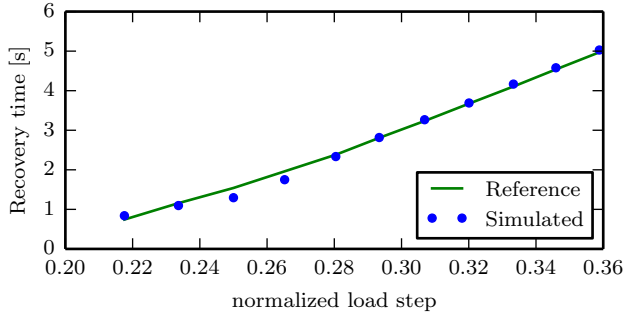
Figure 2.7: Dynamic response fitting of diesel engine.

engine was used as reference. Then, simulation and optimization are used to curve-fit the simulated response with the reference data.

The mean value model used in this chapter is a generic model for a medium speed four-stroke engine with a reasonable set of parameters. The reference engine is MAN 16V32/44CR which has power rating of 9.6 MW. The reference response curve for frequency recovery time and the frequency recovery time vs. step load amplitude plot are used to fit the engine response of the model to the measured value (MAN Engines and Systems; 2013). Frequency recovery time is defined as the time interval from the frequency deviates from the steady state band until it again enters the band according to ISO 8528-5. Such a band is assumed to be 1%, and the result of fitting is shown in the Figure 2.7.

2.3.3   Rate Constrained Diesel Engine Model

As mentioned in Section 2.2.5, diesel engine manufacturers constrain the rate of change of the throttle position. However, a smoke limiter will assure that the throttle position is limited such that complete combustion and maximum torque is achieved.

In Figure 2.8, the earlier presented generator set is subjected to a load step from 20% active power to 60%. The figure shows the responses of the throttle position with and without the smoke limiter and the rate constraint of the manufacturer activated. The constraints are also included, showing the smoke limiter level and the rate constraint. It is clear that the rate constraint from the manufacture are always lower than the smoke limiter. The smoke limiter can therefore be neglected. It should be noted that this result is only valid for this engine.
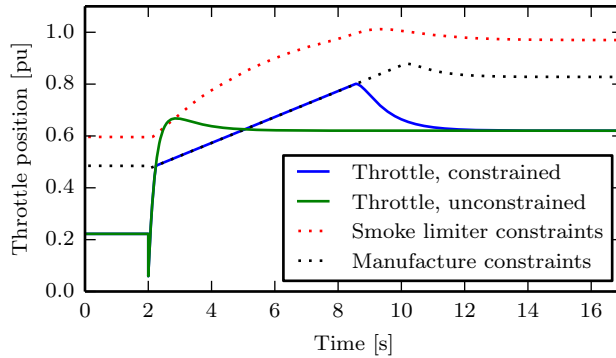
Figure 2.8: Throttle response of a load step, with and without constraints. The dotted lines represent the rate constraint of the manufacturer and the throttle constraint of the smoke limiter.

2.4 Case Study

Three cases are analyzed, where the objective is to illustrate simulations that are only possible through a multi-domain simulator. It is noteworthy that the focus is in the qualitative analysis, but not on quantitative analysis, since the overall simulator is not quantitatively verified.

A drilling rig is used to illustrate the simulator capabilities, not only for fault scenarios but normal operations as well. The electrical system is shown in Figure 2.3. The rig has three switchboards, which are connected in a ring configuration. Two generator sets are connected to each switchboard. The rated outputs of the diesel engines are 9.1 MW. In addition, two thrusters are connected to each switchboard with a rated output of 4.2 MW and a rated thrust of 506 kN. The thrusters' position are shown in Table 2.1. The rig pontoon length is 84.6 m, with total mass of 27×10^6 kg. The dynamic model is assuming low speed, as well as current is considered as a component of the vessel total speed, instead of a force. More details about the vessel can be found in MSS (2010).

Besides the drilling rig, a hybrid supply vessel was modeled to verify the influence of energy storage devices on the vessel electrical stability. The electrical system is shown in Figure 2.9, where a battery pack, a 2.2 MW generator, and a 3.3 MW generator are connected to each power bus. The thruster characteristics are described in Table 2.2. The vessel length is 80 m, with total mass of 6.2×10^6 kg.

Table 2.1: Thruster position on the drilling rig hull

Thruster	Thruster type	X Position [m]	Y position [m]
1	Azimuth	-35	-27
2	Azimuth	-35	27
3	Azimuth	0	-27
4	Azimuth	0	27
5	Azimuth	35	-27
6	Azimuth	35	27
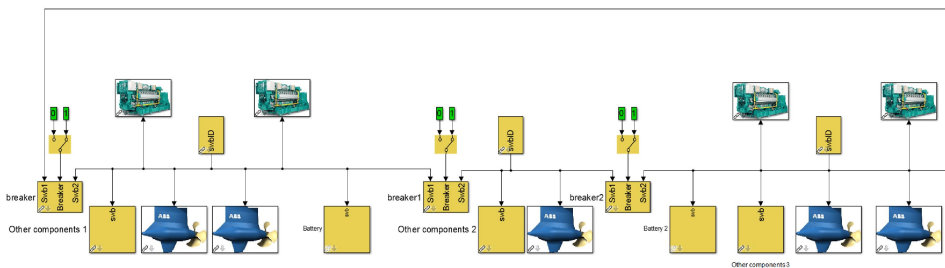
Figure 2.9: Power plant view of hybrid supply vessel used in simulations.

Table 2.2: Thruster position and size on the supply vessel

Thruster	Type	X Position [m]	Y position [m]	Max Power [MW]
1	Azimuth	-30	-5	2.7
2	Azimuth	-30	5	2.7
3	Tunnel	24	0	1.5
4	Tunnel	27	0	0.85
5	Tunnel	30	0	1.5

A summary of the simulated environmental conditions is shown in Table 2.3. Wind, wave, and current direction in all simulation cases are always from north to south, the JONSWAP wave spectrum (Hasselmann et al.; 1973) and the NORSOK wind spectrum are used (Sørensen; 2013).

Table 2.3: Environmental condition summary for the simulation cases

Simulation case	H_s [m]	T_p [s]	V_w [m/s]	V_c [m/s]
2.4.1	5	8.5	14	1
2.4.2	5	7	14	.3
2.4.3	4	7.7	12	1

2.4.1 DP Operation Scenario

The first case study shows a typical DP operation. The goal is to demonstrate the load fluctuation due to the DP system's reaction to environmental forces and the power generated by the power producers. The position and heading setpoints are fixed at the origin. The buses are connected in a ring configuration, with all bus-tie breakers closed.

Figure 2.10 shows the vessel surge position and electric bus frequency for the simulated case. Notice that the simulator is able to capture different time scales and time constants in the vessel positioning and the generator power. A power variation of same time scale as the wave frequency is clearly visible. In addition, the change of thruster setpoint gives ripples at 1 Hz.

2.4.2 Bus Opening Scenario

During a DP operation, it is possible that one bus is isolated from the remaining grid due to a pre-fault detection, reverse power flow, etc. In this case, the interaction between the electrical system and the DP system is exemplified. Even though the maximum generated capability and thruster forces are unaltered, there is an instantaneous power surge in the buses due to the reconfiguration.

In the simulation, the vessel is in DP operation and heading north, with closed bus-tie and five generator sets running (two connected to each of the first two switchboards and one to the third switchboard). Switchboard 3 is separated from the other two switchboards, by opening the breakers connected to Switchboard 3 at $t = 200$ s. The power consumption is constrained by the fast load reduction, due to the increased load.

Figure 2.11 shows the power bus reconfiguration effect on the dynamical positioning system. It is noticeable that when the power plant is reconfigured, the DP system positioning is influenced due to load reduction. This scenario can only be simulated with an integrated simulator, since the in-
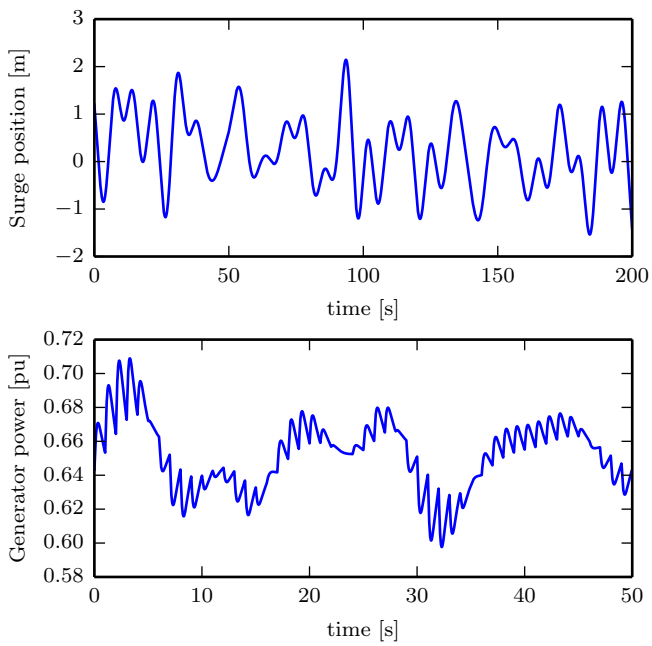
Figure 2.10: Results from simulation of drilling with DP, presented in Section 2.4.1. Upper: surge position of the vessel. Lower: power produced by generators connected to the main bus in per unit.
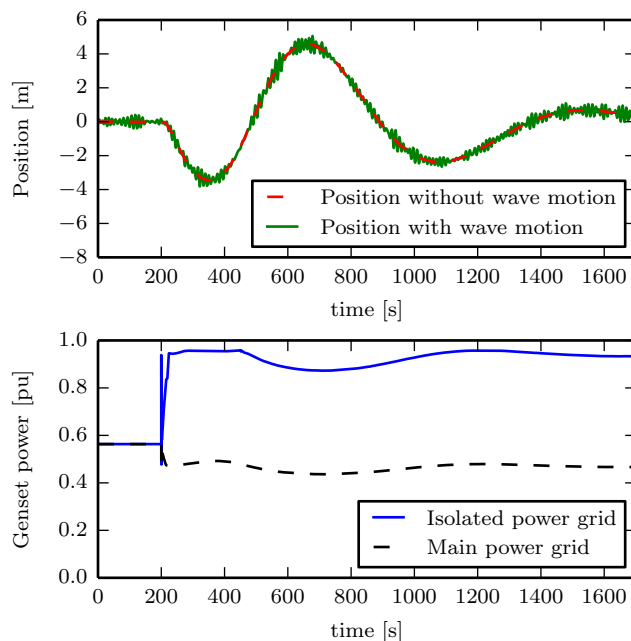
Figure 2.11: Results of the simulation case presented in Section 2.4.2. The drilling vessel is in DP operation with closed bus-tie breakers. After 200 seconds the bus-tie breakers connected to Switchboard 3 is opened. Upper: Position deviation from the setpoint. The green solid line is the position deviation, while the red dashed line is the position deviation without the wave motion. Lower: power consumption for each bus. The blue solid line is the generator power at the isolated power grid (Swb. 3). The black dashed line is the generator power at main power grid (Swb. 1 and 2).

terdependency in the positioning system and electrical system is the factor leading to the positioning transient.

Both the vessel positioning and the filtered position (estimated by the state estimator) are presented in Figure 2.11, since the wave frequency motion makes it harder to observe the mentioned effect.

2.4.3 Energy Storage Devices

The last case demonstrates how the addition of an energy storage device will increase overall safety, mostly due to the fact that the extra power injection in the bus will limit the frequency drop by the generator. The system presented here uses the supply vessel presented in Section 2.4. All four generators and five thrusters are initially connected. An ESD is connected to the power system. After 1 second, one of the generators is abruptly disconnected from the power grid, generating a power surge for the remaining three generators. The ESD is controlled in frequency droop mode, but it will be connected only when the frequency drops below 98.5%.

The results from this scenario are shown in Figure 2.12. The vessel position is virtually the same for both simulation cases, the main difference is that the frequency drop is much smaller in the case with ESD. It is known, that protection systems like load reduction and shedding will be activated when the frequency drops below 2% to 3%, possibly deactivating large power consumers, such as thrusters, drilling system, etc. If the frequency drops even further, it could lead to partial or even total blackout.

From the maintenance point of view, with smoother generator load variation, the wear and tear will be reduced, improving the generator working conditions and reducing maintenance costs.

This simulation shows that the simulator allows investigating the vessel and ESD dynamical behavior during a fault, in which the frequency drop is the main concern. The ESD is able to bound the frequency drop to a safe margin, potentially preventing a larger scale fault.

Other operation strategies may be implemented for the ESD, such as peak shaving, on-off operations, etc., if the simulator is properly set up.

2.5 Conclusion

In this chapter, a simulator for marine vessels electric propulsion is presented. The main contribution is the presentation and verification of the needed models for the integration of power plant simulation and vessel mo-
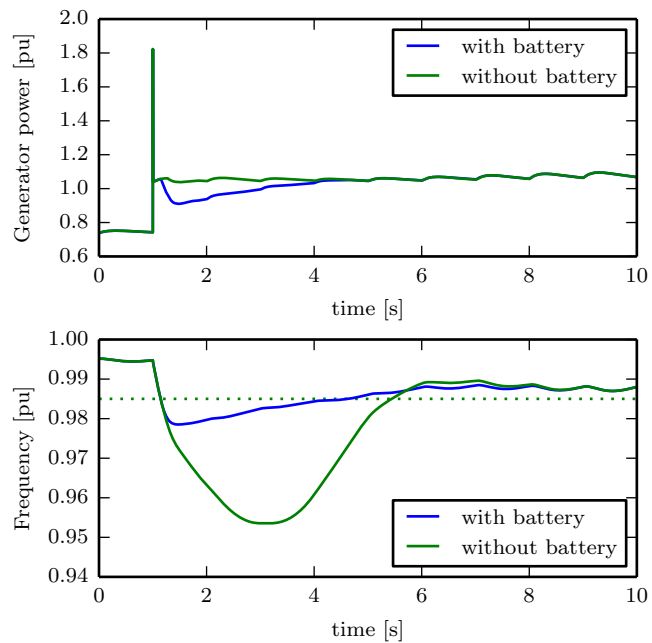
Figure 2.12: Results from presented in Section 2.4.3. After 1 second one out of four generator is disconnected. Upper: generator power, with and without battery. Lower: electric frequency of the main bus, with and without battery.

tion simulation. In addition to demonstrations of the integrated simulator, enabling qualitative analysis of cases that cannot be described with several decoupled simulators. Detailed models of the vessel, propeller, thruster drives, generator sets, and controllers are included in the system simulator, in addition to interaction effects between the components. A module based platform is presented, where models of different fidelity can be chosen. Due to the modularity, the simulator can be reconfigured to different vessels with electric propulsion, and different operations can be simulated. Simulink was used to implement the simulator. The case studies presented in the chapter show some capabilities of the simulator. More detailed simulations of, for instance, fault scenarios contribute to increased knowledge about the behavior of the electrical system, control systems, and safety functions. This may lead to more reliable vessels and safer operations in the future.

Chapter 3

Dynamic Consequence Analysis of Marine Electric Power Plant in Dynamic Positioning

This chapter is based on Bø et al. (n.d.).

Introduction

Dynamic positioning (DP) systems are used for stationkeeping of marine vessels. The general safety requirement for classes 2 and 3 is that any single fault should not propagate into a loss of position (IMO; 1994). This is enabled by redundancy, which means that if one redundancy group fails, remaining redundancy-groups have sufficient capacity to maintain station-keeping.

An online consequence analysis is required for DP vessels of classes 2 and 3 (IMO; 1994, Section 3.2.4.2). The IMO rules state that: "This analysis should verify that the thrusters remaining in operation after the worst case failure can generate the same resultant thruster force and moment as required before the failure." An alarm should be raised if this verification is negative. Another tool is DP capability plots, which are used to determine the environmental limits of an operation. These plots show the maximum static or quasi-static wind, current, and wave loads in which the vessel can maintain its position, for all headings and different configura-

tions (e.g., worst-case, nominal case). Specifications of this plot are given in IMCA (2000). Drift-off analysis is used during drilling operations to determine when to initiate the disconnection of the riser from the vessel to avoid damage to the riser (ISO; 2009). Because, disconnection process of a riser during a drift-off is time consuming (e.g., in case of a blackout), a watch circle is set such that there is sufficient time to safely disconnect the riser if the process is started when the vessel passes the watch circle.

A power management system (PMS) is used for controlling the electrical power system. The main task of the PMS is to ensure the sufficient availability of power. In addition, the PMS coordinates fault recovery and typically optimizes the efficiency of a power plant. In the case of a major fault, loads must be quickly reduced to prevent the occurrence of under-frequency, because it takes time for diesel engines to increase their produced power. The PMS sends a *power available* signal to main consumers to ensure that only available power is used. This is the maximum allowed power for each consumer. It is calculated by acquiring the available power production level of each generator set and then allocating it to consumers based on their priority. *Fast load reduction* may be used when sudden load reduction is required (e.g., loss of producers), which sends a request to thruster drives to reduce their power. This proceeds as thruster drives can quickly reduce power consumption. Later, the available power of thrusters is increased back to normal.

In Pivano et al. (2014), a simulation-based consequence analysis is proposed. Notably, conventional DP capability analysis is non-conservative compared with time-domain analysis. Moreover, power constraints and transient recovery after faults are not considered in their analysis. A transient study was also performed, which showed that position excursion may be larger than acceptable during the transient recovery after a fault.

Recently, it has been proposed by the DNV GL DYNPOS-ER class notation that standby generators can be included in a consequence analysis (DNV; 2015, Part 6 Chapter 26 Section 2). Other class societies have similar class notations, e.g., ABS (2014, Section 8). Because the connection of generators can be blocked by hidden faults, it is conservatively assumed that one of the standby generators cannot connect because of a hidden fault. This provides the opportunity to run relatively few generator sets, which increases the efficiency of a plant. Typically, a marine diesel engine is at its highest efficiency when it delivers about 80% of its rated power. However, it is reported that during DP operations, diesel engines often deliver less than 50% and even down to 10% of the rated power. Moreover, during low-load

conditions, other problems occur, such as sooting, increased maintenance because of extra running hours, and inefficiency of some NO_X reduction systems at low temperatures (Realfsen; 2009).

The analysis proposed in this chapter can also be used as a decision-support tool for the optimal configuration of a vessel. Several configurations can be simulated to evaluate the safety and performance of each configuration. Today, an automatic start and stop table is typically used for commitment of generators on marine vessels (Ådnanes; 2003). Generator sets are started if the power demand is above a threshold for a certain duration of time, vice versa for disconnection. An optimized load-dependent start table was derived in Radan et al. (2005), where the table was optimized with respect to fuel consumption and constrained by a safety requirement, so that disconnection of a generator will not lead to blackout. Algorithms to optimize the load-dependent start and stop tables are also presented in Radan et al. (2006), based on the probability for each operational mode of the vessel. One of the problems with a start and stop table is its independence of operation. For diving and drilling vessels, the safety and redundancy requirements are much higher during operation than during transit. However, when using a start and stop table both operations will typically have the same configuration when the power demand is similar, even though this is not optimal. Therefore, some vessels have different start/stop tables for each mode and also a minimum number of generator sets for some modes to handle changing requirements. It is also common to override the automatic system by committing generators manually. For onshore and island power grids, multiple studies have looked into unit commitment, e.g., Contaxis and Kabouris (1991); Dillon et al. (1978); Dokopoulos and Saramourtsis (1996); Juste et al. (1999); Lowery (1966); Senjyu and Shimabukuro (2003).

The main contribution of this chapter is the development of a consequence analysis based on dynamic simulation of the transient recovery after a fault. The analysis is carried out by dynamic time-domain simulation of the vessel and its DP system for possible worst single failures. The simulations include power constraints and ramp constraints on the thrusters. This tool can also be used as a decision-support system for configuration of the power plant and selection of recovery-methods.

The chapter is divided into two sections. The method is presented in the first section and the second section presents a case study considering a drilling rig. The first section starts with an overview of the method followed by a presentation of the simulator. In Section 3.1.3, the fault models are presented, followed by acceptance criterion and environmental models. The
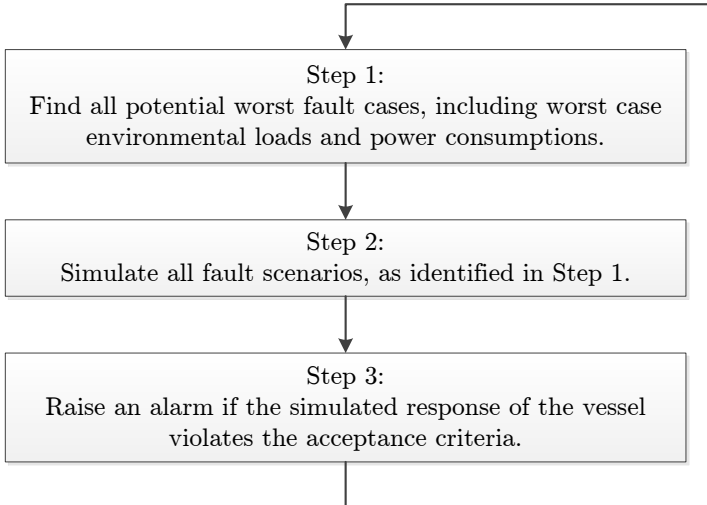
Figure 3.1: Steps in the dynamic consequence analysis.

second section starts with a presentation of the case plant, and results of the simulations are presented. Two different recovery-methods are used for this case study, in addition to several configurations of the power plant. The results of the simulations are discussed further in Section 3.2.3, before conclusions are drawn.

3.1 Method Overview

3.1.1 Method Overview

The problem to be solved is to verify that the vessel can maintain its position during the worst single fault. The analysis should capture the transient DP performance after the fault occurs and until the vessel is fully reconfigured, as the vessel may lose position during this period. We suggest the procedure shown in Figure 3.1 for this analysis. The analysis can be extended by repeating these steps for a number of alternative power plant configurations in order to compare and choose an efficient configuration.

3.1.2 Simulator

A dynamic simulator of the electric power plant and marine vessel is used. The simulator in this study should be regarded as an example implementation. Details of the simulator are given in Bø et al. (2015). We are mainly interested in the response of the DP-system due to faults in the power system. Hence, the implemented models are chosen to represent the DP-system as realistically as possible, with its algorithms, tuning, and constraints. The power system is included as it constrains the DP-system during fault recovery. The main components of the simulator are:

Vessel: A 6 DOF model is used to describe the motion of the vessel. The motion is divided into low-frequency motion and first-order wave frequency motion. The low-frequency motion includes non-linear drag, second-order mean and slowly varying wave, current, wind, and thruster loads. The first-order wave frequency motion is calculated from the wave spectrum and response amplitude operator (RAO) of the vessel.

Environmental Load: The wave spectrum used in this study is JON-SWAP with a narrow banded directional spectrum, although any other wave spectrum could be used. This is used to generate discrete waves, which are used to calculate the second-order wave loads. The wind and current are modeled with constant speed and direction. The choice of environmental conditions is further discussed in Section 3.1.5.

Dynamic Positioning System: The DP controller is implemented as a PID-controller. The position and velocity are given directly from the low-frequency motion of the vessel, assuming an accurate heading and position reference system. This is discussed further in Section 3.1.5.

Thrust Allocation: The DP controller calculates a total thrust command for the vessel, the thrust allocation (TA) then allocates a thrust command for each thruster. This is an optimization problem, constrained by the available power.

Power Management System: A PMS is included to simulate the control of power generation and distribution. It includes power available allocation and fast load reduction.

Thrusters: The thruster model includes models of the motor drive, electric motor, propeller, and the local thruster controller. A four-quadrant model is used to calculate the thrust and torque on the propeller. The

power consumption of the thrusters can be constrained by the PMS and the thrust allocation, this limits the power of the electric thruster motor.

Electric System: The electric system is assumed to be in steady state, as the mechanical systems in a diesel-electric propulsion system are much slower than the electric system. The modeled variables are frequency, voltage, active power, and reactive power. This allows us to simulate the power flow and power constraints. However, fast dynamics, such as short-circuit and harmonic distortions, are not included in the model. Some protection relays are included in the model, such as under/over-frequency protection and reverse-power protection. However, as fast dynamics are not modeled, protection relays based on voltage measurements are not included.

Generator Set: The generator set consists of a diesel engine and a synchronous generator. The fuel injection of the diesel engine is constrained by a rate constraint. This engine protection is typically used to avoid large thermal stress. The fuel consumption is calculated by a Willans approximation (Guzzella and Onder; 2010). All other fuel dynamics are ignored in this study, due to the conservative rate constraint. A governor is used to control the load sharing and speed of the engine. Typically, the governors use droop or isochronous control for the load sharing. An automatic voltage regulator is used to control the voltage and reactive power sharing.

Electric Loads: Loads other than thrusters and heave compensators are modeled as a time-series. These may be hotel loads, auxiliary loads, drilling drives, and cranes. These loads are prioritized, either above or below thruster loads in the PMS. Low-priority loads are reduced if the available power is not sufficient. However, high-priority loads will only be reduced if it is not sufficient to reduce both low-priority loads and thruster loads.

Heave compensators: Heave compensators are included in the model. The electric power consumption is proportional to the heave velocity when the velocity is positive, and zero when the velocity is negative. They may be assigned high-priority in the PMS.

A marine vessel simulator consists of hundreds of parameters and states that need to be initialized. These should be found automatically and may

come directly from the status of the vessel. In addition, some values must be predicted, such as the electric power consumption and environmental conditions. As the power constraint on the thrusters is indirectly dependent on the power consumption of the other consumers, it is important that the predicted mean and variation of the power consumption are not underestimated. The power consumption of all electric loads, except thrusters and heave compensators, can be recorded and used as the load case in the simulation. However, a safety-factor may be used to include uncertainties of the future load.

The simulator must be able to run much faster than real-time to be able to return results that are not outdated before they are completed, because of this the consequence analysis should be performed online as the operation and environment may be constantly changing. Several simulations can run in parallel to increase the performance, since the scenarios are independent of each other.

The simulations are started with the vessel's systems in a steady state. This is to make sure that the controllers, such as the I-term in the DP's PID-controller, have settled.

3.1.3   Fault Modeling

The simulated cases should include all potential worst-case scenarios based on faults in the power plant and thruster system, and may be identified by a report of the DP system's failure mode and effects analysis (FMEA) (DNV; 2012) or hardware-in-the-loop testing (Altosole et al.; 2009; Johansen and Sørensen; 2009). This could, for example, be faults such as loss of switchboard, loss of bus segment, loss of thruster, loss of generator set, fault in governor, frozen command signal, or equipment delivering maximum capacity when this is not desired (e.g., full thrust in drive-off). Incidents reports reveal that other causes, independent of the power plant, are as important, such as human error, faults in the reference system, and faults in the DP control systems (IMCA; 1995–2011; Kristiansen; 2014). Subsystem faults, such as faults in the auxiliary systems, are not considered when selecting fault scenarios, but the worst-case consequence of such faults should be considered, for example, shut down of a diesel engines due to faults in the auxiliary systems.

Only single faults are considered, and it is assumed that all protection systems are handling the fault as designed. Therefore, common mode and software faults are ignored in this study, as common mode faults should be detected by FMEA during the design of the system. HIL-testing can also

be used to detect common mode and software faults (Altosole et al.; 2009; Johansen and Sørensen; 2009).

3.1.4 Acceptance Evaluation

The method's third step is to evaluate the response of the simulated fault scenarios. An acceptance requirement can be that the vessel's position and heading error should be kept within the error tolerance. Other requirements may be more relevant in some cases, such as the riser angles for drilling vessels.

To evaluate the fuel consumption of the configurations, the simulation is carried out using the most recently recorded environmental conditions and power consumption.

3.1.5 Environment Modeling

The simulation of environmental disturbances is crucial for consequence analysis. It is hard to find the actual worst-case environment, as there are many random variables. For example, the wind gust can be strong and the waves can come in groups.

Therefore, each fault case can be simulated several times using different realizations of the environmental load. However, this is computationally expensive. It is assumed that the vessel's position in DP can be described as first-order wave frequency motion superimposed onto the low-frequency motion. Therefore, the consequence analysis considers only the low-frequency motion and the wave frequency motion is included in the positional error tolerance. This is done by determining the maximum expected wave frequency motion and subtracting it from the acceptance range. The variance of the position is (from linear theory and variance of a signal given by its power spectrum):

$$\sigma_i^2(\theta) = \int_{\omega=0}^{\infty} S(\omega) \text{RAO}_i^2(\omega, \theta) \mathrm{d}\omega \tag{3.1}$$

where $i = 1, 2, \ldots, 6$, θ is the angle between the heading of the vessel and the direction of the wave, $S(\cdot)$ is the wave spectrum, ω is the wave frequency, and $RAO(\cdot)$ is the position response amplitude operator for the vessel's wave frequency motion. It is assumed that the wave frequency vessel position is normal distributed, which is given by assuming normal distributed wave

elevation (Faltinsen; 1990) and the vessel motion response to be linear. This gives the expected maximum position error:

$$\eta_{i,max} = \sigma_i F^{-1}(1 - \varepsilon/2) \tag{3.2}$$

where $i = 1, 2, \ldots, 6$, ε is the probability quantile, $F^{-1}(\cdot)$ is the inverse normal cumulative probability function. Note that this procedure must be employed for surge, sway, and yaw, for all headings within the accepted range. This is an approximation as any correlation between surge, sway, and yaw is neglected.

The significant wave height, mean wind speed, and current velocity are increased by a safety-factor to include the uncertainty of the predicted environmental disturbance. The sea state can be estimated from the motion of the vessel (e.g., (Pascoal et al.; 2007)) or from weather forecasts, and can be configured automatically. The wind velocity is measured directly, so that the time average of the velocity can be used. Some DP algorithms estimate an ocean current velocity, which can be used for future simulation. However, the estimated velocity includes other effects, such as thruster loss and modeling error, and should be used with care.

3.2 Simulation Study

An implementation of the proposed method (Section 3.1) is used in this section. Several operational philosophies exist for control of marine electric power plant, and the response of the vessel is highly dependent on these philosophies. Results for two different fault recovery-methods are presented in this study. These should be seen as use cases of the dynamic consequence analysis, and are presented to illustrate the importance of some dynamic effects that are included in this analysis, but not in static analysis. Several configurations are also simulated to show that the method can be used to choose the optimal power plant configuration.

3.2.1 Case Plant

The simulated vessel is a drilling rig. The power and thruster system is shown in Figure 3.2 and consists of six diesel generator sets of 9.1 MW and six thrusters of 5 MW. Three 11 kV high-voltage AC switchboards are used to distribute the power, these are connected together in a ring topology. Details of the model are given in Bø et al. (2015). A drilling operation in DP is simulated, with a 2.1 m significant wave height, a mean wind speed
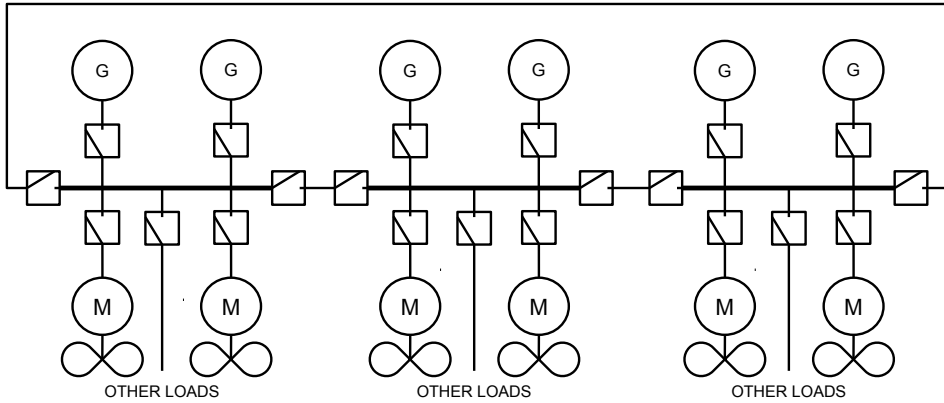
Figure 3.2: The propulsion system of the case study plant.

of 7.94 m/s, and a mean current of 0.68 m/s. Further, the equipment is referred to by their placement in Figure 3.2, the numbering goes from left to right. An environment safety-factor of 1.1 is used during the fault scenario simulations. This gives a significant wave height of 2.3 m, an 8.7 m/s mean wind speed, and a mean current of 0.75 m/s. The wave, wind, and current forces have the same direction, and the angle between the vessel's heading and the environment forces is 10° (head sea). The resulting thrust on each thruster is approximately 43 % of the rated thrust.

Drilling drives are simulated as pulse loads of 1.6 MW on Switchboards 1 and 3 for 1 minute, repeating every 3 minutes. Low-priority loads of 1 MW on each switchboard represent non-essential drilling equipment, which can be reduced in the case of a fault. Also, 1 MW high-priority loads are attached to each switchboard. Heave-compensators connected to Switchboards 1 and 3 are included in the model and the gain from the heave velocity to the power consumption is 1 MW s/m. The acceptance criterion is that the vessel should not move more than 3 meters or 5° away from the set-point. The safety-factor for the loads is 1.1 and the high pulse of the drilling drives are simulated to start when the faults occurs.

For this case the wave frequency motion has a standard deviation of 0.51 m; the maximum wave frequency motion is then 1.18 m and 0.01° when using a probability threshold of 98%. The small heading change occurs since the rig is symmetric, the waves are coming close to head-on, and the directional spectrum of the waves is narrow banded. Consequently, the low-frequency motion must be within 1.82 m and 4.99°.

Table 3.1: Alternative configurations. A dash — and a vertical bar | are used to denote when switchboards are connected or disconnected via a closed or open bus tie-breaker, respectively.

Configuration	# connected gensets per swb.			Swb. groups				
	1	2	3					
1	1	1	1	1	—	2	—	3
2	2	1	1	1	|	2	—	3
3	2	1	1	1	—	2	—	3
4	2	2	1	1	|	2	—	3
5	2	2	1	1	—	2	—	3
6	2	2	2	1	|	2	|	3
7	2	2	2	1	—	2	—	3

The configurations tested are shown in Table 3.1. Many more configurations are possible, e.g., open bus tie-breakers and one generator set per switchboard. However, these were chosen as they give sufficient power and represent a broad spectrum of configurations.

The following fault cases are simulated:

1. Loss of a generator set: a generator set is disconnected. Stand-by generator sets, if any, are connected after 45 seconds.

2. Loss of a thruster: Thruster 1 (left most) is disconnected.

3. Loss of a switchboard: both generators and all loads connected to Switchboard 1 (left most) are disconnected. Stand-by generator sets are connected to the healthy switchboards after 45 seconds.

4. Thruster full thrust: the thrust of Thruster 1 (left most) is fixed at full thrust. The thruster is disconnected after two minutes.

For Cases 1, 2, and 4 the PMS is configured to only reduce thruster loads. This is an example of an operational philosophy used to avoid frequent minor faults influencing the operation. During Case 3, it is simulated that the bus tie-breakers (directly or indirectly) connected to the faulty switchboard are opened. This strategy is typically used to avoid propagation of faults from one switchboard to the others. These faults are considered as possible worst-case scenarios for this simulated vessel. Note that Cases 1, 2, and 3 are possible drift-off cases, while Case 4 is a possible drive-off case.

The generators are running in droop mode with equal settings. This gives equal load sharing among the generators connected in each group. A fast phase back system (FPBS) is implemented on the thrusters based on May (2003). The load reduction is initiated when the frequency falls below 95% of the rated frequency, the power is reduced linearly, and fully reduced at 92.5%.

Two fault recovery-methods are simulated. In Recovery A, fast load reduction and power available signal are used to make sure that the vessel is able to avoid under-frequency due to overload. In Recovery B, these methods are deactivated. Then, the power plant can use the rotating energy of the generator set during this recovery, and load reduction is only initiated through FPBS. This gives less of a safety-margin against under-frequency, which increases the risk of blackout. Many other fault recovery-methods exist, such as power limit ramps on consumers instead of available power, and the selection of bus tie-breakers to open when the switchboards fails.

3.2.2   Simulation Results

Results from nominal and fault simulations are shown in Table 3.2. The *loss of position distance* is the maximum distance from the reference point to the low-frequency position of the vessel during the simulation.

Recovery A: Power Available

For Recovery A, Configurations 2, 4, 6, and 7 are accepted, while the others fail due to loss of position during the transient recovery after a fault. Configuration 2 may be preferred as it gives the lowest fuel consumption.

The position and heading error is shown in Figure 3.3, for Configurations 2 and 3 after the loss of Switchboard 1. For Configuration 2, the bus tie-breaker between Switchboards 2 and 3 is closed after the fault, while it opens for Configuration 3 (since it is indirectly connected to the faulty switchboard). A large transient position error occurs for Configuration 3 after the fault, although both configurations are able to stabilize the vessel to the reference after the fault. This is a case where a transient simulation is necessary to determine the safety of the configuration. The reason for the difference between the configurations is that the available power of a generator set is dependent on the load of the generator. Therefore, the available power for the thrusters will differ, as seen in Figure 3.5. When using closed bus-tie and equal droop settings, all the generators produce equal amounts of power before the fault. For Configuration 3 (closed bus) this means that

Table 3.2: Results from scenario simulations.

Configuration		1	2	3	4	5	6	7
Loss of position distance, Recovery A [m]	Loss of genset	**11.4**	0.4	2.8	0.4	1.2	0.4	0.6
	Loss of thruster	0.2	0.2	0.2	0.2	0.2	0.2	0.2
	Loss of switchboard	2.0	**0.7**	4.6	**0.7**	5.3	**0.7**	**0.7**
	Thruster, full thrust	0.5	0.6	0.5	0.6	0.5	0.6	0.6
Loss of position distance, Recovery B [m]	Loss of genset	**2.7**	0.0	0.0	0.0	0.0	0.0	0.0
	Loss of thruster	0.2	0.2	0.2	0.2	0.2	0.2	0.2
	Loss of switchboard	0.8	**0.7**	**0.9**	**0.7**	**1.3**	**0.7**	**0.7**
	Thruster, full thrust	0.6	0.6	0.6	0.6	0.6	0.6	0.6
	Fuel consumption [t/h]	2.45	2.61	2.60	2.76	2.76	2.93	2.93
	Fuel consumption increase [%]	-6.0	0.0	-0.3	5.9	5.9	12.5	12.4
Frequency variations [%]	Maximum deviation	0.94	1.13	0.96	1.13	0.96	1.13	0.97
	Standard deviation	0.18	0.14	0.13	0.13	0.11	0.13	0.09
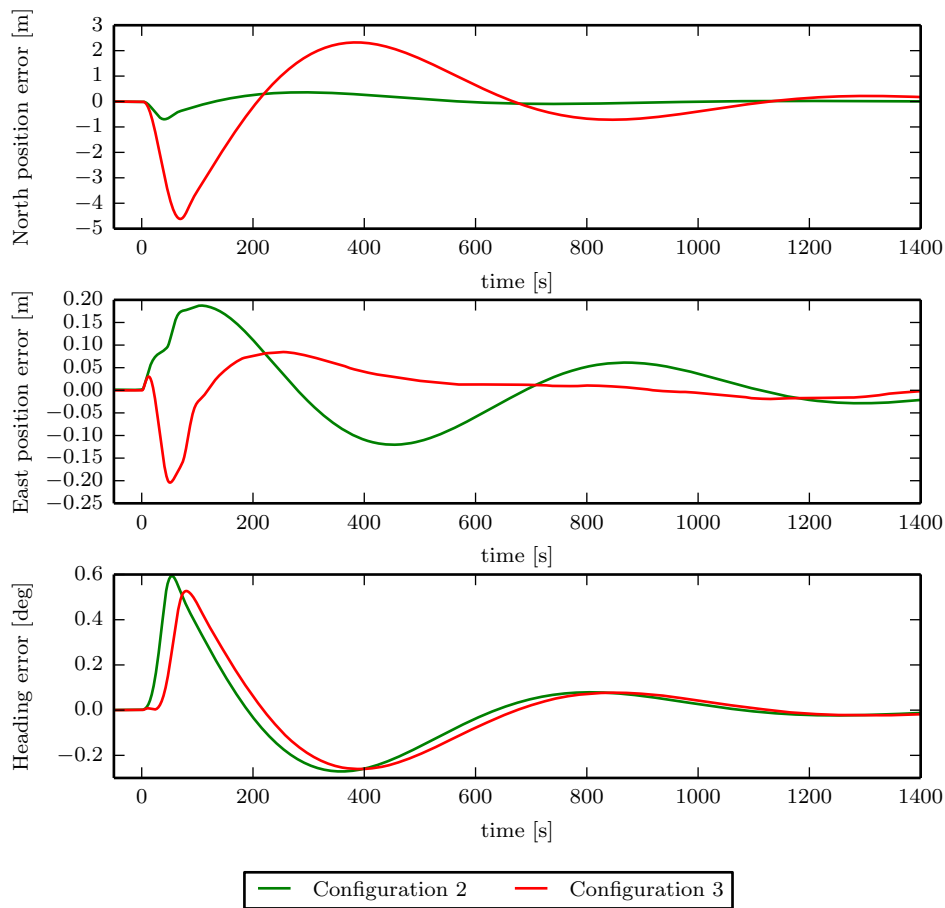
Figure 3.3: Position and heading error after loss of switchboard for Configuration 2 and 3, Recovery A. The fault occurs at $t = 0$.
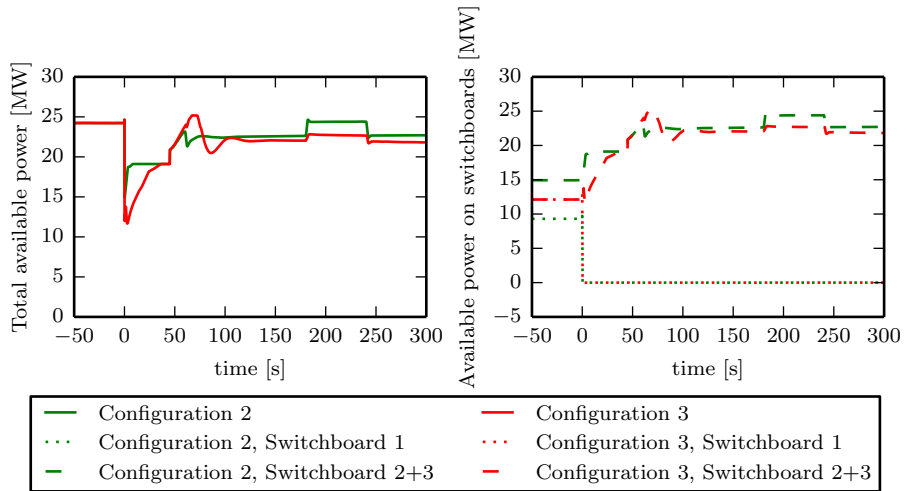
Figure 3.4: Available power after loss of switchboard for Configuration 2 and 3, Recovery A. The fault occurs at $t = 0$. Note that the available power is similar before the fault for the two configuration, while the load sharing between the switchboards differ for the configurations. After the fault, Configuration 3 has much less available power.
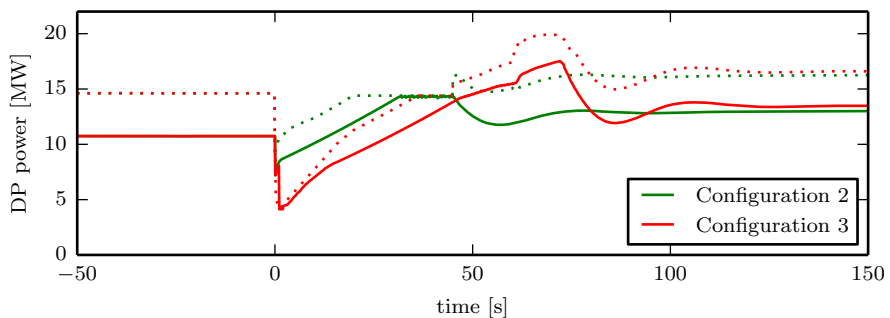
Figure 3.5: Thruster power consumption after loss of switchboard for Configuration 2 and 3, Recovery A. The fault occurs at $t = 0$. The dotted line is the available power for DP.
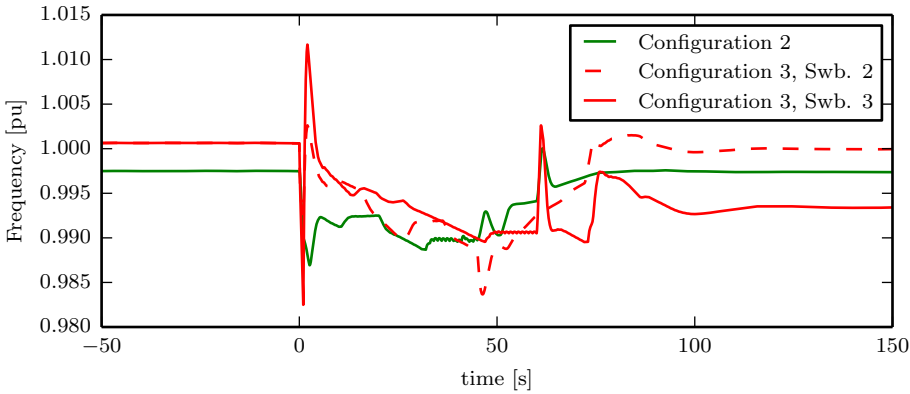
Figure 3.6: Electric frequency of switchboard after loss of switchboard for Configuration 2 and 3, Recovery A. The fault occurs at $t = 0$.

the two generators on Switchboard 1 produce the same amount as the two others, connected to Switchboards 2 and 3. Hence, the available power from Switchboard 1 is equal to the available power from Switchboards 2 and 3 combined. This is shown in Figure 3.4. The worst fault is loss of Switchboard 1, which results in the loss of half the available power. The load-sharing between the independent switchboards will typically be asymmetric during an open bus operation (Switchboard 1 is independent of 2 and 3 for Configuration 2). The worst-case is still loss of Switchboard 1; however, more power is available on Switchboards 2 and 3 after the fault with Configuration 2, which reduces the loss of position.

The electrical frequency of the switchboard is shown in Figure 3.6. The frequency drops immediately after the fault occurs. However, the fast load reduction quickly reduces the excessive load, and a large drop in frequency is avoided. The slow decrease in frequency is due to the increased power on each generator and the use of frequency droop.

Recovery B: Fast Phase Back System

The rotational energy of the generator set is utilized for emergency power when using FPBS. Results from the simulation of loss of a generator set with Configuration 1 are presented in Figures 3.7 and 3.8. This case shows another example of the need for a dynamic consequence analysis, as the vessel is not able to maintain position during the transient recovery, but arrives at a steady state afterwards. The position is plotted in Figure 3.7, where it is

seen that the vessel drifts off by 2.7 m. The reason for this loss of position is shown in Figure 3.8. When the generator is lost, the other generators take its load immediately. This results in a higher load on the generators than the diesel engines are able to produce, and the frequency decreases. The thrusters reduce their load when the frequency gets low enough, which leads to the loss of position. A new generator set is connected after 45 seconds, the frequency increases again, and the thrusters can produce the necessary thrust to maintain the position of the vessel. Note that the frequency drop with Recovery B is much larger than with Recovery A, as seen by comparing Figures 3.6 and 3.8.

Results of the consequence analysis with Recovery A and B are given in Table 3.2, which show that these two methods give significantly different results. This highlights the fact that the performance is highly dependent on the recovery-methods. Hence, the implemented recovery-methods in the simulator and the real power plant must be as similar as possible.

Nominal Operation

The choice of configuration is economically important, especially in terms of fuel consumption and maintenance. The fuel consumption is 12.4% higher in Configuration 7 than in of 2. The reason is that the diesel engine can operate close to the optimal working point. In Configuration 2, the engines on Switchboards 2 and 3 are delivering about 35–50% of their rated power, while on Switchboard 1 and all engines in Configuration 7, the engines run at 20–25%. The last operational point is very low and results in high fuel consumption; however, it is reported that this does occur within the industry. It should be noted that Configuration 2 can be optimized further by letting the thrust allocation share the load optimally between the switchboards (Realfsen; 2009).

The frequency variations are presented in Table 3.2. These are the variations during nominal operation and are therefore independent of the recovery-method. The variation in the simulations are small and mostly due to the use of frequency-droop. However, it can be noted that running more generator sets gives a stiffer grid, as expected.

Maximum wind speed

An estimated maximum wind speed is calculated and presented in Table 3.3. The calculations are performed with environmental parameters from DNV (2015, Part 6 Chapter 7 Appendix B). However, the wind velocity is cal-
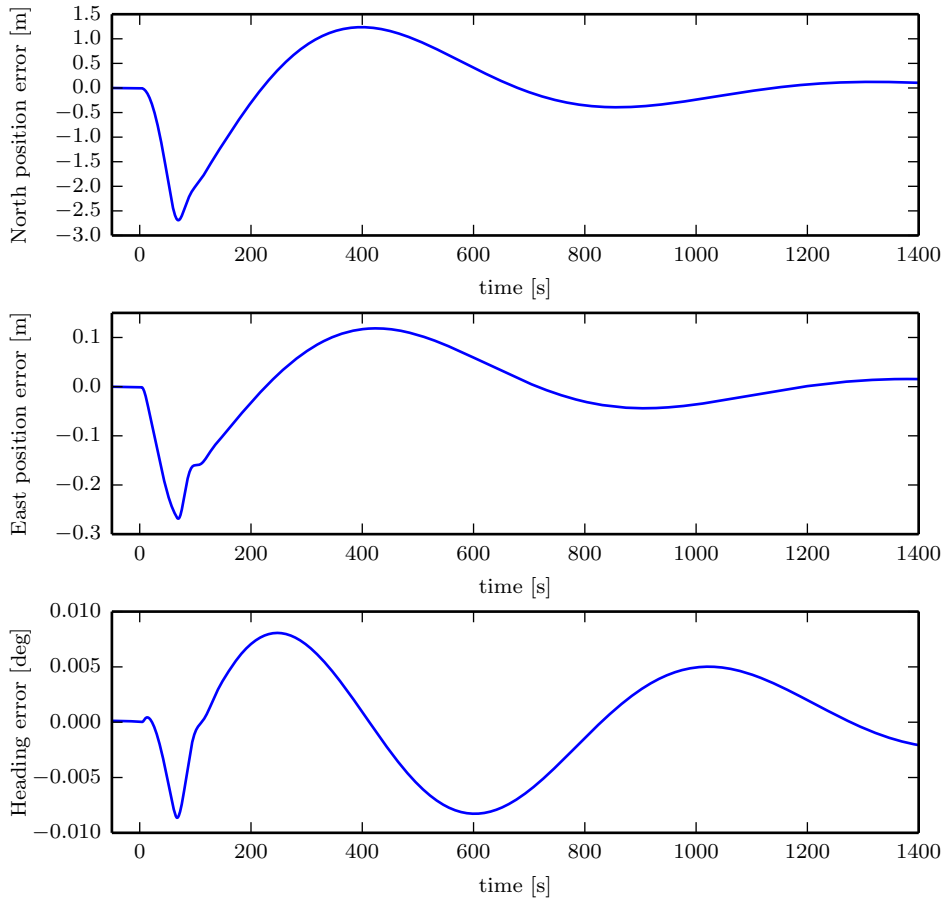
Figure 3.7: Position error after loss of generator set for Configuration 1 with Recovery B. The fault occurs at $t = 0$.
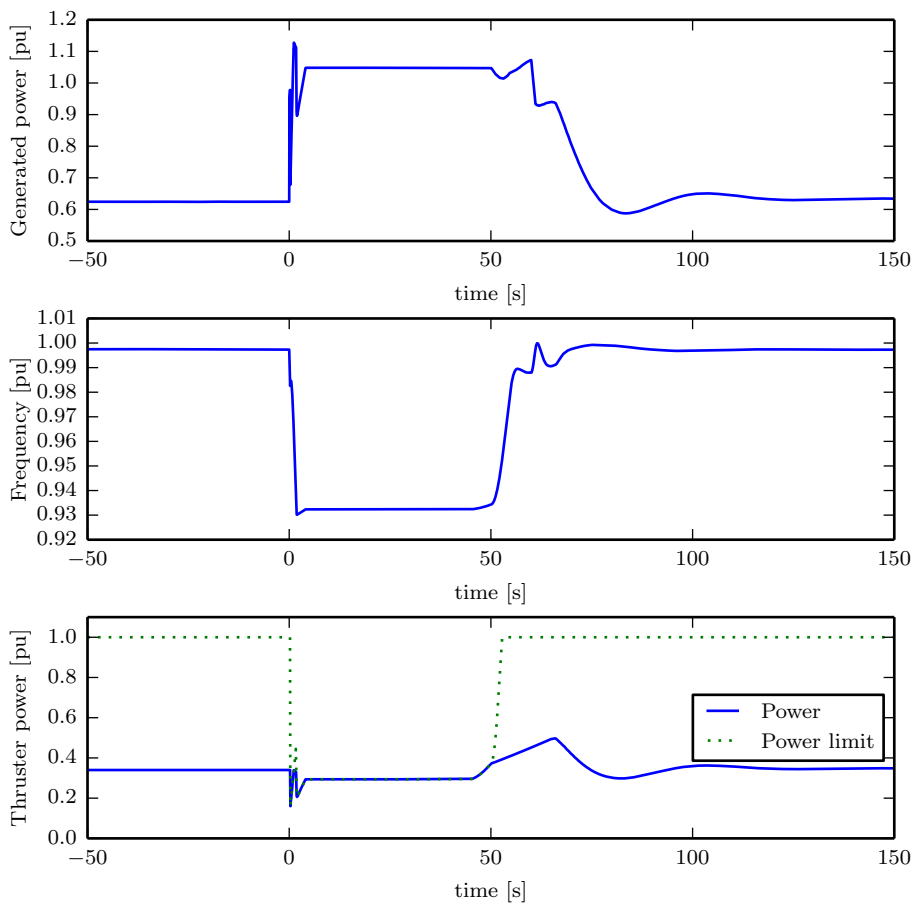
Figure 3.8: Generator power of Generator set 1, electric frequency, and consumed power and power constraints by FPBS, all in per unit, for Configuration 1 and Recovery B after a loss a generator set. Note that the FPBS in the thruster reduces the power when the frequency drops. This stabilizes the power of the generator set and the electric frequency. The fault occurs at $t = 0$.

Table 3.3: Maximum wind speed for different configurations and Recovery A.

Configuration	1	2	3	4	5	6	7
Maximum wind speed [m/s]	2.19	10.01	7.48	10.01	6.21	10.01	10.01

culated without any safety-margin and is only valid for the 10° heading. The accepted wind velocity is underestimated, since only values given from the environmental regularity-numbers in DNV (2015, Part 6 Chapter 7 Appendix B) were tested. For example, the velocities 10.01 and 11.39 m/s were tested for Configuration 2, and the fault scenarios passed for 10.01 m/s, but not for 11.39 m/s. Therefore, the configuration's maximum allowed wind velocity is between 10.01 m/s and 11.39 m/s.

DP-capability plot

A DP-capability plot is shown in Figure 3.9. It is calculated, for varying headings, both with the standard static method, see for example DNV (2015, Part 6 Chapter 7 Appendix B), and with the method presented in this chapter. In this case no safety-margins are used for either method. The presented method gives a conservative estimate compared with the static method, since it includes both the transient recovery and the power constraint.

3.2.3 Discussion

The results from this case study show that a vessel may be able to withstand the mean environmental forces after a fault, but during the transient fault recovery the vessel may temporarily lose position. It is also shown that different fault recovery-methods result in significantly different responses of the power plant and the vessel. Therefore, the consequence analysis can be used to choose the configuration of the power system and recovery functions.

The safety-factor in this simulation study is chosen as 1.1, as an example. Since the wave-drift forces are proportional to the square of the wave height, the force increased by 21% from the nominal to the fault scenario. Similar consideration can be made for both current and wind forces, as they are proportional to the square of the velocity. This approach is conservative, because it assumes that the power plant's worst fault event coincides with
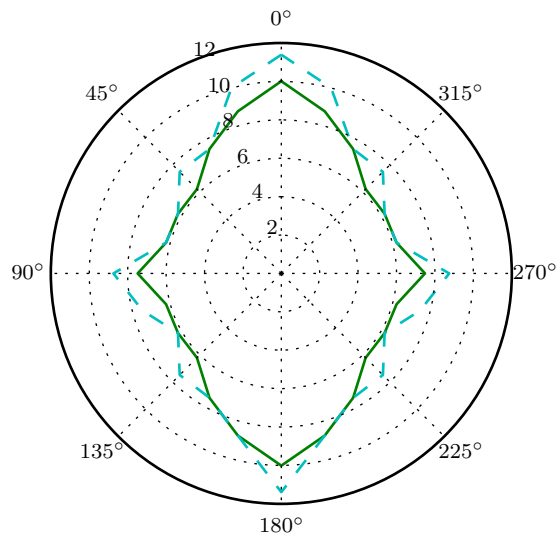
Figure 3.9: DP-capability plot, for Configuration 2, worst-case scenario and Recovery A. This shows the maximum wind speed the vessel can withstand after the single worst-case scenario. The solid green line shows the results using the method presented in this chapter. The dashed cyan line shows results using standard static analysis.

the worst-case waves, current, wind, and power consumption. Another approach may be to give a probability-threshold then calculate a safety-factor. However, this is outside the scope of this chapter. It should be noted that the safety-factor can be changed with the operation. A high factor can be used during critical operations, such as diving and drilling, while a lower factor can be used during non-critical operations, such as standby.

The simulation cases consider a vessel with AC switchboards; however, more and more vessels are now equipped with DC switchboards and batteries for emergency power (Hansen and Wendt; 2015). This consequence analysis is well suited to these types of vessel, as a dynamic model is able to verify the transient performance of such vessels. The method can also be used to check that the batteries have sufficient power and energy capacity to recover the power plant and terminate the operation, as required by DNV GL (2015b, Pt. 6 Ch. 3 Sec. 1 4.3.1). A simulation-based approach may be needed as batteries may get warm during high power demands, and in such cases the batteries may disconnect due to safety protection systems.

The switchboard voltage will be low during a short circuit of the equipment connected to the switchboard. Hence, equipment with low voltage protection may disconnect. The simulator is not able to simulate such fast transients of the electric system. Therefore, fault ride through capability of the essential equipment should be verified by other methods to avoid that equipment being disconnected or damaged during the recovery of the power plant.

Not only is the configuration of the switchboard important, the parameter settings of some functions, such as load sharing, load shedding, and thrust allocation, are also important. Optimization of these parameters is necessary to obtain optimal power plant operation. However, care should be taken when optimizing with respect to only a few scenarios. In such cases the optimum will sometimes result in changing the worst-case scenario from one scenario to another. For example, if the optimized worst-case is a blackout of Switchboard 1, the optimum may be to increase the load on the other switchboards and let Switchboard 1 produce no load. This changes the worst-case from blackout of Switchboard 1, to blackout of one of the other switchboards. Therefore, individual blackout scenarios for each switchboard must be included and not only those for the most critical switchboard. Optimizing the parameters is also a much more computationally expensive task, since many values of the continuous parameters must be checked to find the optimum.

The simulation study in Pivano et al. (2014) considers stationkeeping

performance after the transient fault recovery was complete. They did show that the vessel may not be able to maintain its position even though the vessel had sufficiently available thrust for the mean force. The method in this chapter cannot detect such performance issues as only the low-frequency motion is simulated. Therefore, a combination of the transient simulation in this chapter and the "steady-state" wave-frequency simulation in Pivano et al. (2014) is necessary.

As noted in DNV GL (2015a), more analysis is necessary to verify the integrity of a power system. Such dynamic analysis may include selectivity, short-circuits, and earth fault analysis. It is also assumed that each switchboard is independent of the others, and this must be verified (e.g., with an FMEA).

Reactive power is not considered in this simulation study; however, a generator set can trip due to reactive power overload. Consequently, load reduction and fault analysis with regard to reactive power should be considered.

During simulations, not shown in this chapter, the transient loss of position after a fault was seldom a problem for cases when the standby generator sets were not accounted for in the consequence analysis.

3.3 Conclusion

A dynamic consequence analysis tool based on time-domain simulation is shown in this study. Different configurations were simulated during multiple fault scenarios to evaluate the DP-performance during transient recovery. It is observed for the chosen cases that the transient recoveries after faults are the limiting factor when choosing a configuration, as the vessel may be able to maintain its position before and after the fault, but not during the transition. This is especially important for configurations where one or more standby generators are connected after a fault, as recently allowed by some class notations. It is seen that the result of a reconfiguration can be unpredictable as the thruster system and power plant are complex systems. This method allows the power plant to be configured depending on the required safety level, since more safety-margins can be used during critical and non-critical operations.

Chapter 4

Dynamic Safety Constraints by Scenario-Based Economic Model Predictive Control

This chapter is based on Bø and Johansen (2014, n.d.b).

4.1 Introduction

There is a need for autonomous handling of faults in many industrial control systems. These faults can be due to actuator faults, sensor faults, external faults, or internal faults. There are also often constraints on the system to make sure that the system is safe. However, it can take some time before the controller is fully reconfigured and the system recovers after a fault. Conservative safety limits are therefore sometimes used to make sure that the system is safe also during the transients after the fault.

Active redundancy is often used when downtime of a system is not acceptable. This is the case for the electrical power system on board advanced marine vessels. A typical marine power plant consists of multiple pairs of generators and diesel engines. The generators are connected to switchboards which distribute the electrical power to thrusters and other consumers. However, sudden disconnection of generators does happen, and then the load from the disconnected generator is shared among the remaining generators. The electric frequency will then decrease due to slow dynamics in the diesel engine. Therefore, a safety margin is needed to avoid under-frequency protection trip after disconnection of a generator. This is typically handled by regulating a fixed frequency and reducing the loads

when a fault occurs. However, the controller has more freedom for opti-
mization if the frequency is allowed to vary within some dynamic safety
constraints and unnecessary load reduction can be avoided. Therefore, the
plant can be safer and increase the operational performance by explicitly
including the fault scenarios in the controller. Detecting that the system
cannot recover from a fault is as important as recovering the system. We
therefore propose a method for detecting if the faults can or cannot be re-
covered from. Such information can be used for proactive reconfiguration
of the plant, or change of control objective.

Model predictive control (MPC) with scenarios will be used to establish
a fault-tolerant controller. Scenarios in MPCs are mostly used for robust
MPC. An MPC for linear systems is presented in Bernardini and Bemporad
(2009), where the system matrices can switch between a finite number of
scenarios, with a given probability for each scenario. Other combinations
of MPC and scenarios are presented in e.g., Calafiore and Fagiano (2013);
Maiworm et al. (2015); Schildbach et al. (2014). These studies use scenarios
to handle model uncertainties and disturbances. It has been proposed to
use approximate reachable sets to establish a robust MPC (Bravo et al.;
2006). However, this gives conservative estimates, since a common control
input is calculated for all possible sequences of uncertainties and distur-
bances (open-loop control). For linear systems, Scokaert and Mayne (1998)
suggest including feedback in the optimization problem. For non-linear sys-
tems this gives an infinite dimension optimization problem, it is therefore
proposed to use a semi-feedback formulation, see Limon et al. (2009) and the
references therein. Scenario-based model predictive control has also been
suggested used in optimization of hedge options (Bemporad et al.; 2014),
for scheduling of batch processes (Bonfill et al.; 2008), and scheduling of
emergency vehicles (Goodwin and Medioli; 2013).

There have been some studies on transients of the plant after reconfig-
uration of controllers due to faults. An investigation of responses due to
reconfiguration of the controller is presented in Kovâcshâzy et al. (2001),
with different method for initializing the next controller. For faults which
can be predicted, it has been suggests to use MPC to make a smooth ac-
commodation of the fault (Lao et al.; 2013). It is suggested to use back
calculation to set the initial states of the reconfigured controller and use
a progressive accommodation scheme to achieve new LQR-gains (Blanke
et al.; 2006).

Another approach to control a plant to a safe set is to use backward
reachable set to calculate the fault-tolerant set (Gillula et al.; 2011). The

backward reachable set is a set containing all initial states which can avoid an unsafe state set, under a specified set of disturbances. A method for validating that a controller can avoid unsafe sets for linear hybrid systems using reachability analysis is presented in Torrisi and Bemporad (2001). A similar study is done for nonlinear hybrid system using barrier certificates (Prajna et al.; 2007). A method for selecting switching rules for a hybrid system, such that the state variables avoid an unsafe set, is presented in Coogan and Arcak (2012).

The method presented in the present chapter is a variant of the method presented in Bernardini and Bemporad (2009). However, in the present chapter the models are nonlinear, fault-tolerance and economic objective emphasized, and a deterministic framework is used.

Control of the speed of generator sets in a marine diesel-electric power plant are one of the example cases in the present chapter. Currently generator sets are controlled in speed droop or isochronous using PID or similar algorithms for speed governors (Ådnanes; 2003). Model predictive control and nonlinear control by feedback linearization are proposed as alternative control methods (Hansen et al.; 1998; Hansen and Fossen; 1999; Veksler et al.; 2013). In Radan (2008), multiple methods for better control of engines are proposed, this includes observer design, for noise-filtering, and inertia control, to suppress frequency variations.

The present chapter presents a method for establishing dynamic safety constraints based on fault scenario. The idea of the controller was first presented in Bø and Johansen (2013), for a marine electric power plant. It was later formalized in Bø and Johansen (2014), including a linear case plant. The MPC uses multiple predictions internally for each fault scenario in addition to the nominal scenario. By using this method the safety constraints are moved from being applied to the nominal scenario to being applied to the fault scenario, and this is the main contribution of this chapter. Therefore, this method is suited when the constraints are set to avoid unsafe states, e.g., during the transients after a fault. Typically, this gives less conservative constraints and the opportunity to operate the plant safer with increased performance. The controller is applied to two example cases, a linear plant and a marine electric power plant.

4.2   Problem Statement

Consider a plant where we have safety constraints on the control input and the states. In particular, there are given some fault scenarios which the

plant must be able to handle safely. We would like to design a controller which makes sure that the plant can be recovered after any of these fault scenarios. This consists of three requirements:

Recoverability: The controller should keep the system in a state set where it is possible to recover the system if one of the fault scenarios occurs.

Robust Control: The controller should use a control input which is appropriate for the nominal system and the faulty system until the fault is detected and the fault is accommodated by the controller.

Detection of recoverability: It should be detected if the system cannot be recovered when one of the fault scenarios occurs.

The fault scenarios considered in this chapter are modeled as change of the dynamics or constraints of the system.

4.3 Model Description

The plant is described with one model for each scenario. The difference equation for the states is of the form:

$$\mathbf{x}(t_{k+1}) = \mathbf{f}(\mathbf{x}(t_k), \mathbf{u}(t_k)) \tag{4.1}$$

where $\mathbf{x} \in \mathbb{R}^n$ and $\mathbf{u} \in \mathbb{R}^m$ are the state and input vectors. The state and control input vectors for the control horizon are given by:

$$\mathbf{X}(t_i) = \begin{bmatrix} \mathbf{x}^\top(t_i) & \dots & \mathbf{x}^\top(t_{i+N-1}) \end{bmatrix}^\top \tag{4.2}$$

$$\mathbf{U}(t_i) = \begin{bmatrix} \mathbf{u}^\top(t_i) & \dots & \mathbf{u}^\top(t_{i+N-1}) \end{bmatrix}^\top \tag{4.3}$$

where t_i is the time instant at the beginning of the control horizon, and N denotes the length of the control horizon. Note that we assume no unknown disturbances, model uncertainties, or measurement noise; however, these effects can be included as additional scenarios along with faults, or by tightening the constraints. The state and control input are constrained by:

$$\begin{aligned} \mathbf{G}_{\mathrm{nr}}(\mathbf{x}, \mathbf{u}) &\leq \mathbf{0} \\ \mathbf{G}_{\mathrm{r}}(\mathbf{x}, \mathbf{u}) &\leq \mathbf{s} \\ \mathbf{0} &\leq \mathbf{s} \end{aligned} \tag{4.4}$$

where $\mathbf{G}_{\mathrm{nr}}(\mathbf{x}, \mathbf{u}) : \mathbb{R}^n \times \mathbb{R}^m \to \mathbb{R}^{n_{cn}}$ and $\mathbf{G}_{\mathrm{r}}(\mathbf{x}, \mathbf{u}) : \mathbb{R}^n \times \mathbb{R}^m \to \mathbb{R}^{n_{cr}}$. It is assumed that all non-relaxable constraints (hard constraints) are stacked in
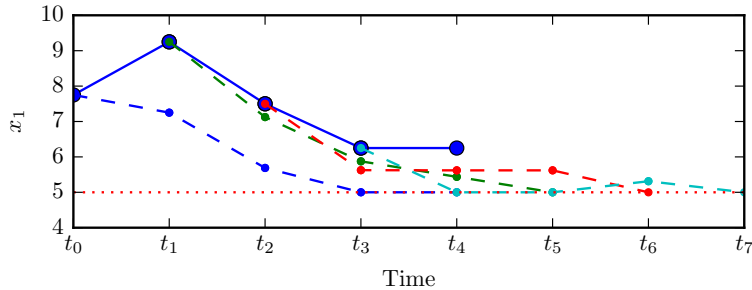
Figure 4.1: Possible future trajectories for the linear system in Section 4.7.1. The solid blue line is the predicted trajectory of the nominal scenario. The dashed lines are the predicted fault scenarios, starting at $t_f = t_0$, t_1, t_2, t_3 respectively. The dotted red line represents the lower limits which all trajectories should be above.

the first constraints, and relaxable constraints (soft constraints) are stacked in the second. The vector $\mathbf{s}$ contains slack variables, $\mathbf{s} = \mathbf{0}$ when the relaxable constraints are satisfied, and $\mathbf{s}$ has positive elements when the relaxable constraints are relaxed.

4.4 Fault-Tolerant MPC

4.4.1 Predicted Trajectories

Multiple predicted trajectories are used in the MPC to achieve the control objectives. A snapshot of some trajectories are shown in Figure 4.1. The nominal trajectory (solid blue) is the prediction for the nominal scenarios. The fault trajectories (dashed lines) are the prediction for the fault scenarios. These trajectories starts from the points on the nominal trajectory, where the fault events may occur. A fault trajectory is started at each point in the nominal trajectory, except the end point, for each fault scenario. The red dotted line is the lower constraint on all trajectories.

The optimization problem is to find the optimal control sequences such that all predicted trajectories satisfy the constraints. When this problem is feasible, the controller can recover the plant if any of the fault scenarios occurs. The controller will remove the relaxable constraints in the beginning of the trajectories when the optimization problem is infeasible. This may give some trajectories that do not satisfy all the constraints; however, after some time the controller is able to satisfy all constraints for all scenarios.

In Figure 4.2, the plant is in a state where the problem is infeasible. The constraints are then relaxed during the three first time steps, and constraints in the fault scenarios starting from these points in the nominal trajectory are also relaxed.

Superscript $^{(n)}$ and $^{(fj)}$ are used to distinguish between the different models and constraints for each scenario, where n denotes nominal scenario and fj denotes fault scenario number j. The following notation is used to distinguish the different predictions at different times for the fault: $\mathbf{x}^{(fj)}(t|t_f = t_k)$ where t_k is the time when the fault occurs. Further, we will use the word *event* for predictions starting from different times, and *scenarios* for predictions with different faults. This means that $\mathbf{x}^{(f1)}(t_3|t_f = t_2)$ is the predicted state at time instant t_3, for the *fault* scenario number 1, and corresponding to the event starting at t_2.

It is assumed that the state and input variables of the fault trajectory is set by the state and input variables of the nominal trajectory at the time of the fault:

$$
\begin{aligned}
\mathbf{x}^{(fj)}(t_f) &= E_j \mathbf{x}^{(n)}(t_f) \\
\mathbf{u}^{(fj)}(t_f) &= F_j \mathbf{u}^{(n)}(t_f)
\end{aligned}
\tag{4.5}
$$

where E_j and F_j are matrices of proper size.

The stage cost of each point in the trajectory, $l(\mathbf{x}, \mathbf{u})$, is assumed to be smooth.

4.4.2 State Constraints

The trajectories are always constrained by the non-relaxable constraints: For the nominal scenario, during $t_0 \leq t_k < t_N$:

$$
\mathbf{G}_{\mathrm{nr}}^{(n)}(\mathbf{x}^{(n)}(t_k), \mathbf{u}^{(n)}(t_k)) \leq \mathbf{0}
\tag{4.6}
$$

For the fault scenarios, during $t_0 \leq t_f < t_N$ and $t_f \leq t_k < t_{N,f}$:

$$
\mathbf{G}_{\mathrm{nr}}^{(fj)}(\mathbf{x}^{(fj)}(t_k|t_f), \mathbf{u}^{(fj)}(t_k|t_f)) \leq \mathbf{0}
\tag{4.7}
$$

where $t_{N,f} := t_f + t_N - t_0$ is the end time of the fault trajectory.

During the relaxed period, slack variables, $\mathbf{s}$, are used to relax the relaxable constraints, $t_0 \leq t_k < t_{N_{\mathrm{relaxed}}}$:

$$
\begin{aligned}
\mathbf{G}_{\mathrm{r}}^{(n)}(\mathbf{x}^{(n)}(t_k), \mathbf{u}^{(n)}(t_k)) &\leq \mathbf{s}^{(n)}(t_k) \\
\mathbf{0} &\leq \mathbf{s}^{(n)}(t_k)
\end{aligned}
\tag{4.8}
$$

Similarly for the entire fault trajectories starting within the relaxed period. That is $t_0 \leq t_f < t_{N_{\text{relaxed}}}$ and $t_f \leq t_k < t_{N,f}$:

$$
\begin{aligned}
&\mathbf{G}_{\mathrm{r}}^{(fj)}(\mathbf{x}^{(fj)}(t_k|t_f), \mathbf{u}^{(fj)}(t_k)) \leq \mathbf{s}^{(fj)}(t_k|t_f) \\
&\mathbf{0} \leq \mathbf{s}^{(fj)}(t_k|t_f)
\end{aligned}
\tag{4.9}
$$

For the rest of the trajectories, all the constraints should be satisfied for the nominal scenario, $t_{N_{\text{relaxed}}} \leq t_k < t_N$:

$$
\mathbf{G}_{\mathrm{r}}^{(n)}(\mathbf{x}^{(n)}(t_k), \mathbf{u}^{(n)}(t_k)) \leq \mathbf{0}
\tag{4.10}
$$

Similarly for the remaining fault scenarios, $t_{N_{\text{relaxed}}} \leq t_f < t_N$ and $t_f \leq t_k < t_{N,f}$:

$$
\mathbf{G}_{\mathrm{r}}^{(fj)}(\mathbf{x}^{(fj)}(t_k|t_f), \mathbf{u}^{(fj)}(t_k|t_f)) \leq \mathbf{0}
\tag{4.11}
$$

The predicted states are constrained to the dynamics of the system in the given scenario:

$$
\begin{aligned}
\mathbf{x}^{(n)}(t_{k+1}) &= \mathbf{f}^{(n)}\left(\mathbf{x}^{(n)}(t_k), \mathbf{u}^{(n)}(t_k)\right) \\
\mathbf{x}^{(fj)}(t_{k+1}|t_f) &= \mathbf{f}^{(fj)}\left(\mathbf{x}^{(fj)}(t_k|t_f), \mathbf{u}^{(fj)}(t_k|t_f)\right)
\end{aligned}
\tag{4.12}
$$

The initial condition of the nominal scenario is $\mathbf{x}(t_0)$ and the initial condition of the fault scenario is the value of the nominal scenario at the initial time of the event:

$$
\begin{aligned}
\mathbf{x}^{(n)}(t_0) &= \mathbf{x}(t_0) \\
\mathbf{x}^{(fj)}(t_k|t_f = t_k) &= E_j \mathbf{x}^{(n)}(t_k)
\end{aligned}
\tag{4.13}
$$

4.4.3 Robust Control Input

Fault detection, identification, and fault accommodation will often take some time. It is therefore important that the control input is appropriate in the time between the fault occurs and the fault is accommodated in the controller. The fault trajectories are therefore restricted to use the same control input as the nominal trajectory during the first time steps of the fault trajectory. We define τ_{robust} as the maximum number of time units between a fault occur and the controller is reconfigured. This gives the following additional constraints, for $k \leq i < \min(k + \tau_{\text{robust}}, N)$:

$$
\mathbf{u}^{(fj)}(t_i|t_f = t_k) = F_j \mathbf{u}^{(n)}
\tag{4.14}
$$

For $t_f + \tau_{\mathrm{robust}} \geq t_N$ the inputs are constrained to be equal to $\mathbf{u}^{(n)s}$, since we can prolong the nominal trajectory with the pairs $(\mathbf{x}^{(n)s}, \mathbf{u}^{(n)s})$:

$$\mathbf{u}^{(fj)}(t_i | t_f = t_k) = F_j \mathbf{u}^{(n)s} \tag{4.15}$$

where $\mathbf{x}^{(n)s}$ and $\mathbf{u}^{(n)s}$ are later defined in Definition 2.

4.4.4 Terminal Constraints

Terminal constraints are used to achieve recursive feasibility. This is done by finding the optimal equilibrium of each scenario and constraining the end of the predicted state trajectories to this state.

Remark 1 *In the MPC literature it is known that equilibrium terminal constraints often lead to numerical challenges and may suffer from small region of attraction. For this reason a terminal set constraint rather than a terminal point constraint has benefits. However, for the case plants in Section 4.7, the constraints are active and the stage cost may be non-zero on the optimal safe equilibrium (defined later in this section). For such system, the authors are only aware of results on recursive feasibility when terminal equilibrium constraint is used (Angeli et al.; 2012). One exception is Grüne (2013), but this approach requires other strong assumptions.*

The fault trajectories are constrained by the optimal equilibrium terminal constraints. It is defined as:

Definition 1 *An optimal equilibrium for fault scenario j, $(\boldsymbol{x}^{(fj)o}, \boldsymbol{u}^{(fj)o})$ is any solution to:*

$$(\boldsymbol{x}^{(fj)o}, \boldsymbol{u}^{(fj)o}) = \arg\min_{\boldsymbol{x}^{(fj)}, \boldsymbol{u}^{(fj)}} l^{(fj)}(\boldsymbol{x}^{(fj)}, \boldsymbol{u}^{(fj)})$$

such that
$$\boldsymbol{x}^{(fj)} = \boldsymbol{f}^{(fj)}(\boldsymbol{x}^{(fj)}, \boldsymbol{u}^{(fj)}) \tag{4.16}$$
$$\boldsymbol{G}_r^{(fj)}(\boldsymbol{x}^{(fj)}, \boldsymbol{u}^{(fj)}) \leq \boldsymbol{0}$$
$$\boldsymbol{G}_{nr}^{(fj)}(\boldsymbol{x}^{(fj)}, \boldsymbol{u}^{(fj)}) \leq \boldsymbol{0}$$

The optimal steady state cost is $l^{(fj)o} = l^{(fj)}(\boldsymbol{x}^{(fj)o}, \boldsymbol{u}^{(fj)o})$.

For convenience we assume an optimal equilibrium exists and is unique.

The terminal value of the non-relaxed fault trajectories is constrained to the optimal equilibrium:

$$\mathbf{x}^{(fj)}(t_{N,f} | t_f) = \mathbf{x}^{(fj)o} \tag{4.17}$$

The constraint is relaxed for $t_0 \leq t_f < t_{N_{\text{relaxed}}}$:

$$\mathbf{x}^{(fj)}(t_{N,f}|t_f) = \mathbf{x}^{(fj)o} - \mathbf{s}_N^{-(fj)}(t_f) + \mathbf{s}_N^{+(fj)}(t_f)$$
$$\mathbf{0} \leq \mathbf{s}_N^{-(fj)}(t_f) \tag{4.18}$$
$$\mathbf{0} \leq \mathbf{s}_N^{+(fj)}(t_f)$$

where $\mathbf{s}_N^-$ and $\mathbf{s}_N^+$ are slack variables and $\mathbf{x}^{(fj)o}$ is found by solving (4.16).

A terminal stability constraint is used for the nominal scenario, both to make sure that the limit of the closed loop average cost is upper bounded and to make sure that the control problem is recursively feasible. We start by defining an optimal safe equilibrium.

Definition 2 *An optimal safe equilibrium for the nominal scenario, $(\boldsymbol{x}^{(n)s}, \boldsymbol{u}^{(n)s})$, is any solution to:*

$$(\boldsymbol{x}^{(n)s}, \boldsymbol{u}^{(n)s}) = \arg\min_{\boldsymbol{x}^{(n)}, \boldsymbol{u}^{(n)}} l^{(n)}(\boldsymbol{x}^{(n)}, \boldsymbol{u}^{(n)})$$

such that
$$(\boldsymbol{x}^{(n)}, \boldsymbol{u}^{(n)}) \in \mathbb{Z}_{safe,eq}$$
$$\boldsymbol{G}_r^{(n)}(\boldsymbol{x}^{(n)}, \boldsymbol{u}^{(n)}) \leq \boldsymbol{0} \tag{4.19}$$
$$\boldsymbol{G}_{nr}^{(n)}(\boldsymbol{x}^{(n)}, \boldsymbol{u}^{(n)}) \leq \boldsymbol{0}$$

where $\mathbb{Z}_{safe,eq}$ is the set of equilibrium points satisfying $\boldsymbol{x}^{(n)} = \boldsymbol{f}^{(n)}(\boldsymbol{x}^{(n)}, \boldsymbol{u}^{(n)})$ such that for each fault scenario j there exist a feasible trajectory with the length N:

- *starting at $E_j \boldsymbol{x}^{(n)}$,*

- *the control input of the fault scenario is $F_j \boldsymbol{u}^{(n)}$ during the first τ_{robust} samples of the trajectory,*

- *the constraints (4.7) and (4.11) are satisfied at every point on the trajectory and (4.17) at the end point of the trajectory.*

The optimal safe equilibrium cost is $l^{(n)s} = l^{(n)}(\boldsymbol{x}^{(n)s}, \boldsymbol{u}^{(n)s})$.

For convenience we assume that there exists an unique optimal safe equilibrium. The terminal constraint for the nominal trajectory is:

$$\mathbf{x}^{(n)}(t_N) = \mathbf{x}^{(n)s} \tag{4.20}$$

where $\mathbf{x}^{(n)s}$ is found by solving (4.19).

4.4.5   Optimization Problem

All optimization variables can be stacked in a vector $\mathcal{U}$, containing control inputs and slack variables for all scenarios. Penalty functions $g_i(\mathbf{s})$ and $g_N(\mathbf{s}^+, \mathbf{s}^-)$ are added to the cost function to limit the violation of the constraints. The objective function is:

$$
\begin{aligned}
\phi(\mathbf{x}(t_0), \mathcal{U}) = &\sum_{i=0}^{N-1} l(\mathbf{x}^{(n)}(t_i), \mathbf{u}^{(n)}(t_i)) \\
&+ \sum_{i=0}^{N-1} g_i^{(n)}(s^{(n)}(t_i)) \\
&+ \sum_{j=1}^{M} \sum_{i=0}^{N-1} w_i^{(fj)} \left[\sum_{k=0}^{N-1} g_k^{(fj)}(\mathbf{s}^{(fj)}(t_k | t_f = t_i)) \right. \\
&\left. + g_N^{(fj)}(\mathbf{s}^{-(fj)}(t_f = t_i), \mathbf{s}^{+(fj)}(t_f = t_i)) \right]
\end{aligned}
\tag{4.21}
$$

where the first term is the sum of the stage costs of the nominal scenario, the second term is the penalty cost of the nominal trajectory, and the last term is the penalty of the fault scenarios. M is the number of fault scenarios and $w_i^{(fj)}$ are positive weights for fault scenario j. For example, the controller may optimize the input for feasibility of the most probable scenario by using the probability of each scenario as weights. Other choices can be to use the risk of each scenario or a priority of scenarios. Note that the stage costs of the fault scenarios are not included, since we often only want the fault scenarios to be feasible and it is not important that their trajectories are optimal. We assume all functions (models, cost, and constraints) are smooth, so that the optimization problem is well defined with global solutions.

A minimal time approach will be used to make sure that the plant gets safe as quickly as possible (Rawlings and Muske; 1993). This means that before solving for the optimal trajectory we solve this problem:

$$
\begin{aligned}
(N_{\text{relaxed}}^*, \tilde{\mathcal{U}}) = &\underset{N_{\text{relaxed}}, \mathcal{U}}{\arg\min} \; N_{\text{relaxed}} \\
&\text{subject to} \\
&(4.6) - (4.15), (4.17), (4.18), \text{ and } (4.20)
\end{aligned}
\tag{4.22}
$$

This is the smallest N_{relaxed} needed to make the optimization problem fea-

sible. Then, the optimal control sequence is found by solving:

$$\mathcal{U}^* = \arg\min_{\mathcal{U}} \phi(\mathbf{x}(t_0), \mathcal{U})$$

subject to

$$N_{\text{relaxed}} = N_{\text{relaxed}}^*$$

$$(4.6) - (4.15), (4.17), (4.18), \text{ and } (4.20)$$

$$(4.23)$$

The controller will then apply $\kappa(\mathbf{x}(t_0)) = \mathbf{u}^{(n)*}(t_0)$ from $\mathcal{U}^*$, and in the nominal scenario the closed loop system is:

$$\mathbf{x}^{(n)}(t_{k+1}) = \mathbf{f}^{(n)}(\mathbf{x}^{(n)}(t_k), \kappa^{(n)}(\mathbf{x}^{(n)}(t_k)))$$

$$(4.24)$$

The algorithm can be summarized in one offline step and two online steps:

Offline: Find the optimal equilibrium for the fault scenarios and the optimal safe equilibrium for the nominal scenario by solving (4.16) and (4.19).

1. **Online:** Find $N_{relaxed}^*$ by solving (4.22).

2. **Online:** Find the optimal control sequence by solving (4.23).

Challenges related to the computation of global solution of nonlinear programs in real time are well known and important. However, they are considered out of scope of this study.

Remark 2 *Vada et al. (2001) have shown that for linear systems with quadratic cost, a linear penalty function can be designed to ensure that the problem is feasible as early as possible in the prediction horizon. Hence, the online steps can be merged into one step by using such penalty function.*

4.5   Feasibility and Stability

To investigate the stability of the fault tolerant MPC we first present an equivalent optimization problem. We will utilize the fact that there exist a time-invariant set which can be used as a fixed constraint set, since the scenarios and system are time-invariant.

Definition 3 *The safe state set, $\mathbb{X}_{safe}$, is the largest forward invariant set containing all $\boldsymbol{x}(t_0)$ such that the optimization problem (4.23) is feasible with zero slack variables (i.e., $\boldsymbol{s} = \boldsymbol{0}$). Let $\mathbb{X}_N$ denote the set where there exist a solution to (4.23) with horizon length N.*

Lemma 1 *Assuming the states have converged to $\mathbb{X}_{safe}$ (i.e., $N_{relaxed} = 0$) the optimization problem (4.23) can be simplified to the following:*

$$\boldsymbol{U}^* = \arg\min_{\boldsymbol{U}} \sum_{i=0}^{N-1} l^{(n)}(\boldsymbol{x}^{(n)}(t_i), \boldsymbol{u}^{(n)}(t_i))$$

such that

$$\left.\begin{array}{l} \boldsymbol{x}^{(n)}(t_i) \in \mathbb{X}_{safe} \\ \boldsymbol{x}^{(n)}(t_{i+1}) = \boldsymbol{f}^{(n)}(\boldsymbol{x}^{(n)}(t_i), \boldsymbol{u}^{(n)}(t_i)) \end{array}\right\} t_0 \leq t_i < t_N \qquad (4.25)$$

$$\boldsymbol{x}^{(n)}(t_N) = \boldsymbol{x}^{(n)s}$$

This optimization problem gives the controller and the nominal closed loop system:

$$\kappa_l^{(n)}(\boldsymbol{x}^{(n)}(t_k)) = \boldsymbol{u}^{(n)*}(t_k) \qquad (4.26)$$

$$\boldsymbol{x}(t_{k+1})^{(n)} = \boldsymbol{f}^{(n)}(\boldsymbol{x}^{(n)}(t_k), \kappa_l^{(n)}(\boldsymbol{x}(t_k))) \qquad (4.27)$$

The optimal nominal trajectory of optimization problem (4.23) is also the optimal trajectory of (4.25).

Proof The optimization problem (4.23) can be reformulated to (4.25) by the steps below. All constraints are satisfied in $\mathbb{X}_{safe}$, including the relaxable constraints. Consequently, slack variables and penalty functions can be removed. The fault scenarios does only make sure that $\mathbf{x}^{(n)} \in \mathbb{X}_{safe}$ and does not alter the cost. Hence, they can be removed from the optimization problem when $\mathbf{x}^{(n)} \in \mathbb{X}_{safe}$ and $\mathbf{x}^{(n)}$ is constrained to be within $\mathbb{X}_{safe}$. It follows, that the optimal nominal trajectory of these equivalent optimization problems will be equal, since the optimization problems are equivalent. ■

Lemma 2 *For all closed loop trajectories starting from $\boldsymbol{x}^{(n)}(t_0) \in \mathbb{X}_{safe}$ the trajectory of the nominal system system (4.24) will not leave $\mathbb{X}_{safe}$ and the average cost,*

$$\bar{l} = \limsup_{N \to \infty} \sum_{k=0}^{N} \frac{l(x(t_k), u(t_k))}{N+1}, \qquad (4.28)$$

will be lower or equal to the optimal safe steady state cost.

Proof This results follows directly from Theorem 1 in Angeli et al. (2012) by using the equivalent optimization problem (4.25). ■

Theorem 1 *The following holds for the nominal scenario:*

1. *The optimization problem* (4.23) *will stay feasible if it is initially feasible.*

2. *It will take a maximum of N steps to reach $\mathbb{X}_{safe}$ from the time* (4.23) *is feasible, and from that time it will stay in $\mathbb{X}_{safe}$.*

3. *The closed loop system has an average cost which is less than or equal to the optimal safe steady state cost for all initial conditions in $\mathbb{X}_N$.*

Proof   The recursive feasibility can be assured by a proof similar to Mayne et al. (2000). If we have a feasible input sequence at the previous step, we can always shift this sequence one step and extended the tail with $\mathbf{u}^{(n)}(t_{N-1}) = \mathbf{u}^{(n)s}$, denote this trajectory $\mathbf{U}'$ and the corresponding state trajectory $\mathbf{X}'$. This will make $\mathbf{x}^{(n)}(t_N) = \mathbf{x}^{(n)s} \in \mathbb{X}_{safe}$, and the nominal scenario feasible. We know that the shifted part of this trajectory will make all fault scenarios feasible, since they were feasible at the previous step. For the prolonged part $\left(\mathbf{x}^{(n)}(t_{N-1}), \mathbf{u}^{(n)}(t_{N-1})\right) = \left(\mathbf{x}^{(n)s}, \mathbf{u}^{(n)s}\right)$, we know that this is not only feasible, but it does also satisfy the relaxable and non-relaxable constraints. Hence, this input sequence is feasible; therefore, the problem is recursive feasible, and part (1) is proven.

Next, we prove that the closed loop system will enter $\mathbb{X}_{safe}$ within N steps by induction. The trajectory $\mathbf{U}'$ will make sure that the relaxable constraints are feasible one time step earlier in the horizon than at the previous iteration. We know that the solution will honor the constraints as early as possible due to the minimization of $N_{relaxed}$. The prediction of $\mathbf{x}(t_N)$ ends up in $\mathbb{X}_{safe}$ if the problem is feasible at t_0. At each following step the length of the tail which honor the relaxable constraints is increased with at least one step. Therefore, it will not take longer than the length of the prediction horizon N to reach $\mathbb{X}_{safe}$. This proves result (2).

The third result follows from the fact that the states will reach $\mathbb{X}_{safe}$ in finite time. Further, from Lemma 2, we know that inside $\mathbb{X}_{safe}$ the cost is lower than or equal to $l^{(n)s}$. Let t_{k_e} be the time when the closed loop system enters $\mathbb{X}_{safe}$. The cost from t_0 to t_{k_e} is bounded, since $l(\cdot)$ is smooth

on $\mathbb{X}_N$. The average cost will then be:

$$
\begin{aligned}
& \limsup_{N\to\infty} \sum_{i=0}^{N} \frac{l(\mathbf{x}(t_i), \mathbf{u}(t_i))}{N+1} \\
& = \limsup_{N\to\infty} \sum_{i=0}^{k_e} \frac{l(\mathbf{x}(t_i), \mathbf{u}(t_i))}{N+1} + \sum_{i=k_e}^{N} \frac{l(\mathbf{x}(t_i), \mathbf{u}(t_i))}{N+1} \\
& = \limsup_{N\to\infty} \frac{C_1}{N+1} + \sum_{i=k_e}^{N} \frac{l(\mathbf{x}(t_i), \mathbf{u}(t_i))}{N+1} \\
& = \limsup_{N\to\infty} \sum_{i=k_e}^{N} \frac{l(\mathbf{x}(t_i), \mathbf{u}(t_i))}{N+1} \leq l^s
\end{aligned}
\tag{4.29}
$$

∎

Corollary 1 *From the time $\boldsymbol{x}$ enters $\mathbb{X}_{safe}$ the plant can be recovered from any of the fault scenarios, without violating the constraints.*

Proof   This result follows directly from the definition of $\mathbb{X}_{safe}$ and the fact that the state will stay in $\mathbb{X}_{safe}$ after it has entered it. ∎

4.6   Reconfigurable Control

The controller may be reconfigured in the event that one of the fault scenarios occurs. In this case, we are only interested in recovering the plant; therefore, the MPC will only consider this fault. Slack variables are used to relax the constraints, since we cannot know in advance if the system is recoverable (unless $N^*_{relaxed} = 0$). The constraints during the relaxed period, $t_0 \leq t_i < t_{N_{\text{relaxed}}}$, are:

$$
\begin{aligned}
& \mathbf{G}_{\mathrm{r}}^{(fj)}(\mathbf{x}^{(fj)}(t_i), \mathbf{u}^{(fj)}(t_i)) \leq \mathbf{s}(t_i) \\
& \mathbf{G}_{\mathrm{nr}}^{(fj)}(\mathbf{x}^{(fj)}(t_i), \mathbf{u}^{(fj)}(t_i)) \leq \mathbf{0} \\
& \mathbf{0} \leq \mathbf{s}(t_i)
\end{aligned}
\tag{4.30}
$$

and after the relaxed period, $t_{N_{\text{relaxed}}} \leq t_i < t_N$:

$$
\begin{aligned}
& \mathbf{G}_{\mathrm{r}}^{(fj)}(\mathbf{x}^{(fj)}(t_i), \mathbf{u}^{(fj)}(t_i)) \leq \mathbf{0} \\
& \mathbf{G}_{\mathrm{nr}}^{(fj)}(\mathbf{x}^{(fj)}(t_i), \mathbf{u}^{(fj)}(t_i)) \leq \mathbf{0}
\end{aligned}
\tag{4.31}
$$

The system is also constrained to the dynamics of the system:

$$\mathbf{x}^{(fj)}(t_{i+1}) = \mathbf{f}^{(fj)}(\mathbf{x}^{(fj)}(t_i), \mathbf{u}^{(fj)}(t_i)) \tag{4.32}$$

Terminal constraints are used to guarantee recursive feasibility:

$$\mathbf{x}^{(fj)}(t_N) = \mathbf{x}^{(fj)o} \tag{4.33}$$

where $\mathbf{x}^{(fj)o}$ is found by solving (4.16). To minimize the time before all constraints are feasible, a minimal time approach will be used:

$$(N^*_{\text{relaxed}}, \mathcal{U}) = \underset{N_{\text{relaxed}}, \mathcal{U}}{\arg \min} \ N_{\text{relaxed}}$$
$$\text{subject to } (4.30) - (4.33) \tag{4.34}$$

The optimal trajectory is found by solving the following optimization problem:

$$\mathcal{U}^* = \underset{\mathcal{U}}{\arg \min} \sum_{i=0}^{N-1} l^{(fj)} \left(\mathbf{x}^{(fj)}(t_k), \mathbf{u}^{(fj)}(t_k) \right)$$
$$+ \sum_{k=0}^{N-1} g^{(fj)}(\mathbf{s}^{(fj)}(t_k)) \tag{4.35}$$
$$\text{subject to } (4.30) - (4.33), \ N_{\text{relaxed}} = N^*_{\text{relaxed}}$$

which gives the control law and closed loop system:

$$\kappa^{(fj)}(\mathbf{x}^{(fj)}(t_0)) = \mathbf{u}^{(fj)*}(t_0) \tag{4.36}$$
$$\mathbf{x}^{(fj)}(t_{k+1}) = \mathbf{f}^{(fj)}(\mathbf{x}(t_k), \kappa^{(fj)}(\mathbf{x}(t_k))) \tag{4.37}$$

Theorem 2 *Assume fault scenario j occurs and the controller is switched from $\kappa^{(n)}$ to $\kappa^{(fj)}$. Then the following holds for the fault scenario:*

1. *The optimization problem (4.35) will stay feasible if it is initially feasible.*

2. *It will take a maximum of N steps to make $N^*_{relaxed} = 0$, and from that time it will be 0.*

3. *The average cost will be less than or equal to $l^{(fj)o}$.*

In addition, assume that the switch of controller is done within τ_{robust} time units after the fault occurred and $N^*_{relaxed} = 0$ at the time instant when the fault occurred. Then the following holds in addition for the fault scenario:

4. *The optimization problem (4.35) is feasible with $N^*_{relaxed} = 0$.*

The proof is omitted, since it is similar to the proof of Theorem 1.

4.7 Case Study

4.7.1 Linear Plant with Nonlinear Cost

We present simulation results from a closed loop simulation of a linear plant with nonlinear cost in this section. The discrete-time system equations are:

$$
\mathbf{x}(t_{k+1}) = \begin{bmatrix} 1 & 5 & 5 \\ 0 & 1 & 0 \\ 0 & 0 & 1 \end{bmatrix} \mathbf{x}(t_k) + \begin{bmatrix} 12.5 & 12.5 \\ 5 & 0 \\ 0 & 5 \end{bmatrix} \mathbf{u}(t_k) - \begin{bmatrix} 1 \\ 0 \\ 0 \end{bmatrix} b \tag{4.38}
$$

where $\mathbf{x} = \begin{bmatrix} x_1 & x_2 & x_3 \end{bmatrix}^\top$ is the states, $\mathbf{u} = \begin{bmatrix} u_1 & u_2 \end{bmatrix}^\top$ is the control inputs, and b is a known constant. The non-relaxable constraints (superscript is omitted as the constraints are valid for all scenarios):

$$
\begin{aligned}
0 \le x_2 \le 1 \quad -0.1 \le u_1 \le 0.1 \\
0 \le x_3 \le 1 \quad -0.1 \le u_2 \le 0.1
\end{aligned} \tag{4.39}
$$

The relaxable constraint is:

$$
5 \le x_1 \tag{4.40}
$$

This system can model a buffer tank with two slow pumps, where the pumps have both saturation limits and rate constraints.

The fault scenarios are that x_2 or x_3 is suddenly set to zero (e.g., a failure of one of two pumps). This gives:

$$
\begin{aligned}
x_1^{(f1)}(t_{k+1}) &= x_1^{(f1)}(t_k) + 5x_3^{(f1)}(t_k) + 12.5u_2^{(f1)}(t_k) - b \\
x_3^{(f1)}(t_{k+1}) &= x_3^{(f1)}(t_k) + 5u_2^{(f1)}(t_k) \\
x_1^{(f2)}(t_{k+1}) &= x_1^{(f2)}(t_k) + 5x_2^{(f2)}(t_k) + 12.5u_1^{(f2)}(t_k) - b \\
x_2^{(f2)}(t_{k+1}) &= x_2^{(f2)}(t_k) + 5u_1^{(f2)}(t_k)
\end{aligned} \tag{4.41}
$$

The stage costs are:

$$
l^{(n)}(\mathbf{x}^{(n)}) = 10^{-4} \left(x_1^{(n)} \right)^4 + \left(x_2^{(n)} \right)^2 + \left(x_3^{(n)} \right)^2 \tag{4.42}
$$

$$
l^{(f1)}(\mathbf{x}^{(f1)}) = 10^{-4} \left(x_1^{(f1)} \right)^4 + \left(x_3^{(f1)} \right)^2 \tag{4.43}
$$

$$
l^{(f2)}(\mathbf{x}^{(f2)}) = 10^{-4} \left(x_1^{(f2)} \right)^4 + \left(x_2^{(f2)} \right)^2 \tag{4.44}
$$

The penalty cost functions are (sub- and superscript is omitted as the function is used for all scenarios and slack variables):

$$g(\mathbf{s}) = (\mathbf{s} - 100 \cdot \mathbf{1})^2, \tag{4.45}$$

for appropriate dimension of the vector $\mathbf{1}$.

The controller is implemented in ACADO (Houska et al.; 2011), with $\tau_{\text{robust}} = 1$. The constant b is set to 2.5, and the initial values are $x_1 = 10$, $x_2 = 0.5$, and $x_3 = 0$. This gives the optimal safe equilibrium at $x_1 = 6.25$, $x_2 = .25$, $x_3 = .25$, with the stage cost $l^s \approx 0.2776$. The horizon length is 4, which gives 40 optimization variables and 264 constraints. The computation time is around 0.4 seconds per updating period. Results from closed-loop simulation are shown in Figure 4.3, with and without fault. The total cost of the fault free trajectory is 3.479.

A comparative controller with static constraints is designed to compare the static safety constraint with scenario-based constraints. For this case we let the safety constraints be:

$$x_1 \geq 8.75 \tag{4.46}$$

This is the least conservative state constraint which ensure that the control objectives stated in Section 4.2 are fulfilled. The optimal equilibrium of the controller is $x_1 = 8.75$ and $x_2 = x_3 = 0.25$, with the stage cost of 0.7112. In Figure 4.4, a similar simulation is shown as in Figure 4.3, but with this controller. The cost of the closed loop trajectory is 6.321 and the computation time is around 0.02 seconds per updating period. This shows the advantage of using scenario-based constraints as the cost is lower due to the less conservative safety constraints.

4.7.2 Marine Electric Power Plant

An example of the use of this controller is shown for a more complex case in this section. The task is to control three equally sized generator sets of 5 MW in a marine diesel-electric power plant. For this case it is important that a single failure should not lead to a blackout. In contrast to onshore power grids, the numbers of generator sets are few, which gives a weak power grid. One fault scenario is that one generator is suddenly disconnected. This may occur due to failure in the generator, diesel engine, or auxiliary systems. The load produced by the previously connected generator is then distributed to the remaining generators. However, rate constraints on the diesel engines' torque prohibit the diesel engine to produce the necessary
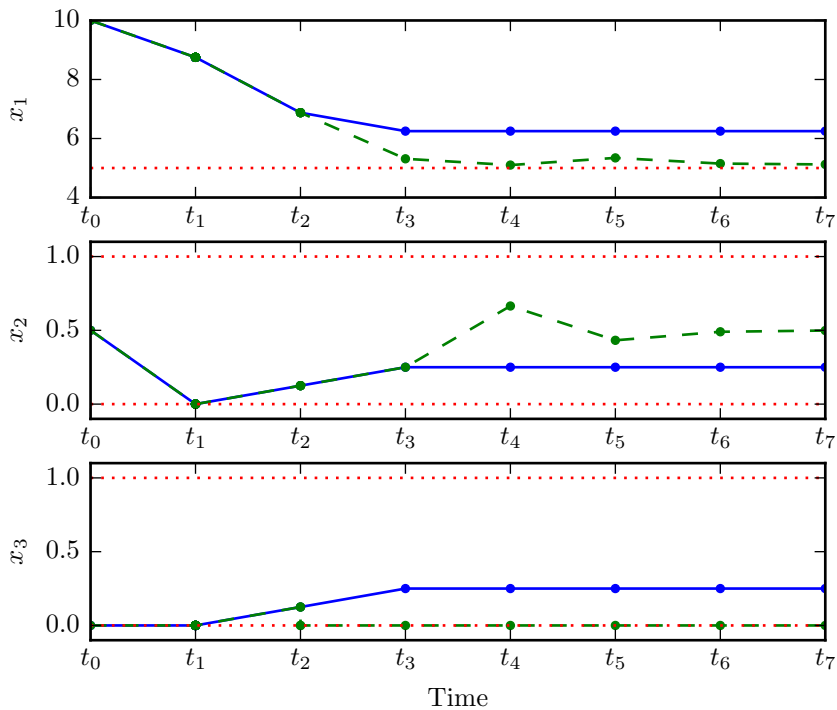
Figure 4.3: Closed loop simulation of the linear plant. Results from a fault free simulation are plotted with solid blue lines. The dashed green lines present the trajectory of a simulation where Fault 2 occurs at t_2, the controller is reconfigured at t_3. The dotted red lines are the lower constraints.
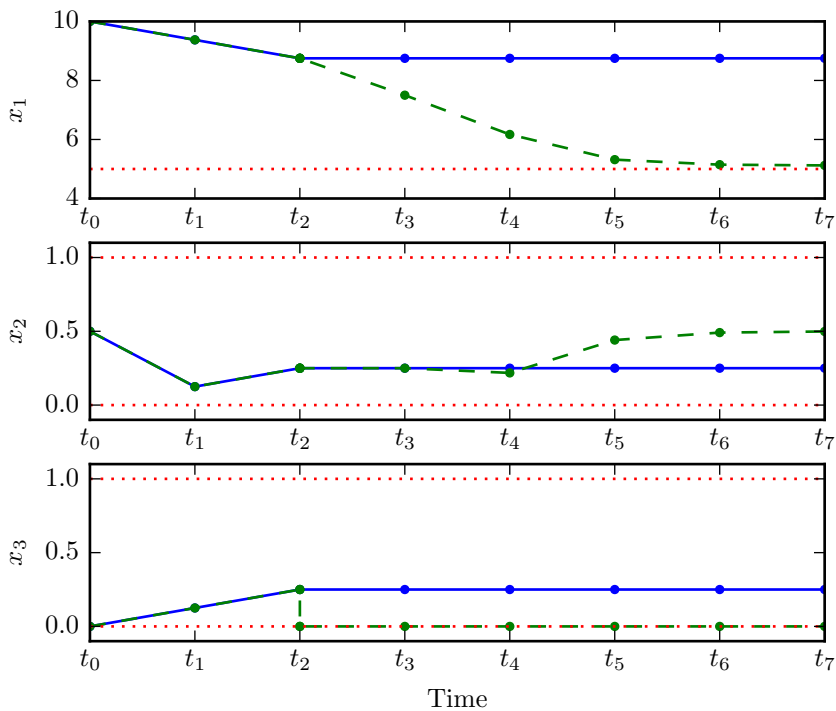
Figure 4.4: Closed loop simulation of the linear plant with the static safety constraints.

power immediately. These constraints are used to avoid incomplete combustion and large thermal stress on the diesel engine. Hence, the frequency decreases, which can lead to a blackout as protection relays can trip due to under-frequency. The electric frequency can be raised to increase the safety margin, since the frequency can be changed by up to 5% from the nominal value (DNV; 2015, Part 4, Chapter 8, Section 2-A206). The control objective for this case is to control the marine power grid's electrical frequency, by adjusting the set-points of the local controller, such that disconnection of one generator set does not lead to under-frequency.

In the power plant, governors are used to control the frequency of the generator set, which indirectly sets the electric frequency. The governor uses droop control to control the speed. A reference speed is calculated from the generated power by:

$$\omega_{\text{ref}} = \omega_{\text{NL}}(1 - \text{Droop}\, p), \tag{4.47}$$

where ω_{ref} is the reference frequency, ω_{NL} is the no-load frequency, Droop is a positive constant, and p is the per-unit active power delivered by the generator. This reference frequency is given to a PID-controller which controls the frequency of the diesel engine to the reference frequency. In this case, the no-load frequency is adjusted online by the MPC controller to obtain optimal fault-tolerant load sharing and to change the frequency of the engines, this is called compensated droop. The control hierarchy of the plant is shown in Figure 4.5.

The dynamics of a generator set can be found by the swing equation and assuming linear damping (Skjetne; 2010):

$$\dot{\omega} = \frac{1}{2H}\left[k_{\dot{m}}\dot{m} - \frac{p}{\omega} - D_{fw}\omega \right], \tag{4.48}$$

where ω is the per-unit electrical frequency, H is the inertia constant of generator set, $k_{\dot{m}}$ is the gain from fuel rate input to per unit torque, $\dot{m}$ is the fuel rate, and D_{fw} is the mechanical damping constant.

A strong synchronization torque will keep generator sets at the same frequency when multiple synchronous generators are connected together. By using an energy balance and assuming that the difference in frequency is small, the equation of the frequency can be found as a function of the total consumed power and the total amount of fuel injected:

$$\dot{\omega} = \frac{1}{2H_T}\left[\sum_i s_{b,i} k_{\dot{m},i}\dot{m}_i - \frac{p_{bus}}{\omega} - \sum_i s_{b,i} D_{fw,i}\omega \right], \tag{4.49}$$
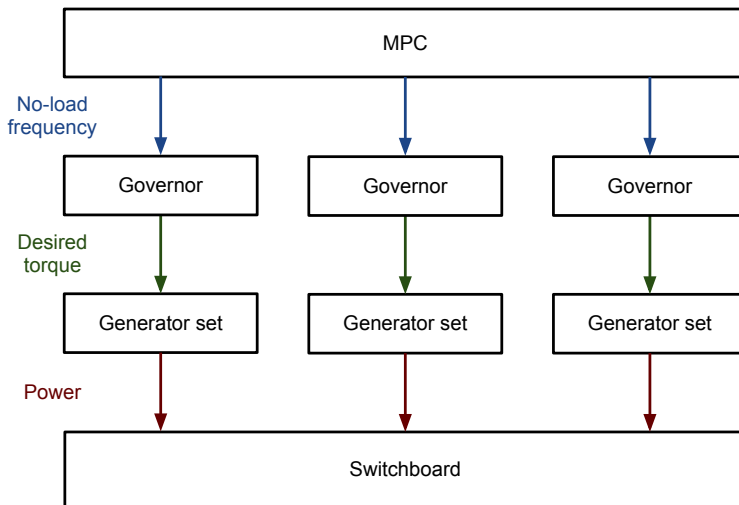
Figure 4.5: Control architecture of the power plant. The designed controller (MPC) gives a no-load frequency to the governor. The governor uses this signal to control the frequency of the generator set, by adjusting the desired torque (fuel command) to the generator set. The generator sets produces power which is fed to the switchboard.

where H_T is the combined inertia constant of all generator sets; $s_{b,i}$, is the ratio between base power of Generator set i and total base power; and p_{bus}, is the per-unit consumed power. Note that this equation cannot detect if the frequency of two generator sets oscillates in opposite phase. However, this stability issue is neglected as the governor should take care of it.

As mentioned, rate constraints are used to avoid large thermal stress and incomplete combustion. Hence, the fuel rate is constrained to 5%/s. The controller is implemented in ACADO (Houska et al.; 2011) and simulated in Simulink. The terminal constraints and relaxable constraints are relaxed by using slack variables, due to infeasibility by numerical problems. It is assumed that the fault is immediately detected, so that $\tau_{\text{robust}} = 0$. This is needed in this setup, since we are controlling the no-load frequency and have rate limitations on the fuel rate. The fuel index will increase after a fault if the no-load-frequency is kept constant. This increase may be, in this case, faster than the rate constraint. Consequently, it is not possible to find a no-load-frequency which can honor the rate constraints both for the nominal scenario and the fault scenario. In typical plants, rate constraints are implemented in the governor, these constraints will be reach both when the fault is detected and undetected. Since, the MPC will try to use the maximum power of the generator, and the governor will typically give maximum fuel-index as a reaction to the decreasing frequency. Therefore, the extra robustness is not needed as it is already inherent in the governor. Moreover, such faults are directly detected and identified using common measurements.

Results from a closed loop simulation are shown in Figure 4.6. The load is set to 40 % of connected capacity, the sampling time is 3 seconds, and the prediction horizon is 15 seconds. The sampling time and prediction horizon was chosen such that the controller is able to achieve real-time performance. The prediction horizon should be long enough to achieve a sufficiently large region of feasibility $\mathbb{X}_N$. The sampling time should be short enough to capture all dynamics. However, the computational complexity increases with the number of points in the prediction.

The plant is simulated both without a fault and with a fault occurring after 21 seconds. Note that the frequency for the closed-loop simulation with fault violate the under-frequency constraint during an inter sample. This occurs since the constraints are only checked at the discretization points. A small safety margin can be added to avoid this. In addition, the sampling time could be decreased to decrease the inter-sample constraint violation. This margin can be small compared with conventional static safety con-
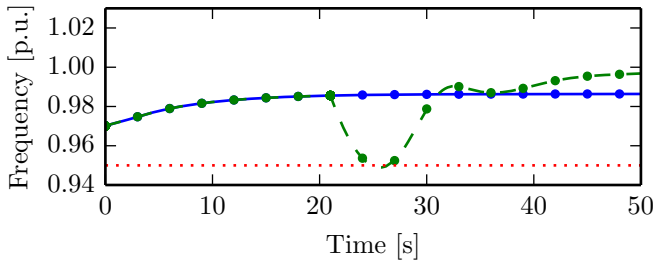
Figure 4.6: Closed-loop simulation of the case plant. The solid blue line shows the closed-loop trajectory during nominal (fault free) operation. The dashed green line shows the closed-loop trajectory when simulating that a fault occurs after 21 seconds. The dotted red line shows the under-frequency limit. Note that the frequency of the faulty system violates the under-frequency constraint during an inter sample, this occurs since the constraints are only checked at the discretization points in the trajectory (dots in the trajectory).

straints, since it should only take care of numerical and model errors, and not the fault dynamics. The frequency is often controlled close to the rated value when controlling the frequency of marine diesel-electric power plant. The electric load is normally reduced after the fault is detected to avoid under-frequency. However, in this case this is unnecessary and undesired, as the fault must be detected and the operation may be interrupted. The frequency drop can be reduced by adding more diesel engines to the grid; however, this decreases the efficiency of the power plant. The frequency after the fault settles down close to the nominal frequency, since the recoverable controller is tuned to control the frequency to the nominal frequency. This is generally considered as the safest frequency after a fault.

Since we have relaxed the constraints in this simulation, N^*_{relaxed} is equal to N, which means that N^*_{relaxed} is not a good measure for the fault-preparedness. However, the size of the slack variables will give a good indication of preparedness for fault in the plant. One method for preparedness indication could be to set a threshold on the size of the slack variables, such that the plant is considered as prepared for faults when all slack variables are less than this threshold. This threshold can be found by system knowledge and should correspond to the size of the safety margin mentioned in the previous paragraph.

The optimization problem consists of 195 optimization variables and 157 constraints. The computational time is between 0.5 and 2.5 seconds per

update period, when using ACADOs C++ interface and a 3.4 GHz Intel$^{\circledR}$ Core$^{\mathrm{TM}}$ i7 processor. Note that ACADO's C++ interface is not designed for constraints that combine constraints at different time instances, such as the initial constraint of a fault trajectory $\left(\text{e.g., } \mathbf{x}^{(n)}(t_1) = E_j\mathbf{x}^{(fj)}(t_0|t_f = t_1)\right)$. This is by-passed by adding auxiliary optimization variables. Therefore, the implemented optimization problem can be substantially condensed. It is also the authors' experience that using ACADO's c-code export function will give a significant performance improvement (typically 10 to 100 times faster).

4.8 Conclusion

This chapter proposes a method to introduce safety constraints based on fault scenarios. The controller uses the fault scenarios internally in the model predictive controller to make sure that it controls the states to a state set where the plant is recoverable if faults occur. The advantages of the controller is less conservative safety constraint, and exact safety constraints are not needed. The disadvantage is a larger and more computational expensive optimization problem, in addition to the need to identify and model the fault scenarios.

The performance of the controller was tested by closed-loop simulation of a linear plant and a marine power plant with relaxed constraints. The simulations show that the controller fulfills the control objectives as long as a safety margin is used, even when the constraints are relaxed.

Chapter 5

Battery Peak-Shaving Control in Electric Marine Power Plant using Nonlinear Model Predictive Control

This chapter is based on Bø and Johansen (n.d.a).

5.1 Introduction

On some marine vessels the power consumption fluctuates heavily in certain operational and environmental conditions. This combined with the weak power grid gives problems such as fluctuating frequencies, excessive wear and tear of power producers, and synchronization problem when connecting additional generator sets. Currently this problem is solved by connecting additional generators, which gives a stiffer grid, but reduces the efficiency of the plant, and increases the need for maintenance. Recently, it has been suggested to add batteries to the power plant. The batteries can be used for peak-shaving, while the generator sets produce slowly varying power to meet the demand.

   The batteries used for this task must be able to charge and discharge large currents. However, the storage capacity can be small, since the mean current is zero. One problem with such large charge and discharge current is the produced heat. This heat production must be controlled, else the batteries will be disconnected due to overheating. For some vessel the batteries

can be used for emergency power, this require a larger battery bank, which is less exposed to heat challenges.

The power fluctuation on a vessel may come from heave-compensators, auxiliary systems, hotel loads, and thrusters. Typically, the load periods vary from 0.1 seconds to hundreds of seconds. The diesel engines would like to have as constant load as possible, since this reduces the thermal stress due to temperature transients. Diesel engines have difficulties with compensating for loads with dynamics faster than about 10 seconds, due to the turbo-lag. On the other hand, the inertia of the generator set can compensate for some load fluctuation. Typically, the inertia can handle dynamics faster than 2 seconds. However, this increases the mechanical stress on the generator set. On a marine vessel the total produced power can be measured at the generators. This is often done every 0.1 second.

Therefore, the peak-shaving algorithm should handle fluctuations with periods from 0.1 seconds to 100 seconds, and most important, take care of loads fluctuations with periods between 2 seconds and 10 seconds.

A dynamic approach should be chosen, so that most of the load fluctuations are removed. However, only the most important load fluctuations should be removed when the battery starts to get too warm. The temperature dynamics of the batteries is slow, and it may take several hours to cool them down. We therefore suggest a hierarchy of controllers, with a high-level controller, which selects the periods of the load fluctuations to cancel out. And, a low-level controller, which takes care of the peak-shaving by removing the periods given by the high-level controller.

Alternative methods to reduce power fluctuations on marine vessels has already been proposed. It is proposed to use the thrust allocation and feedforward in the governor to reduce the power fluctuations (Mathiesen et al.; 2012; Veksler et al.; 2012b). Another approach is to use the thrusters directly for peak-shaving by generating a thruster load which counteracts other load variations (Radan et al.; 2008). Typically, thruster biasing is used on DP vessels to reduce load variations. Then, thrusters are counteracting each other to waste power, such that other load variations are canceled out (Shi et al.; 2011). The mass of the vessel can also be used to reduce the power fluctuations if a drift force is present (Johansen et al.; 2014). None of these employ batteries for energy storage.

Batteries are starting to be used in marine vessels. MS Viking Queen will soon be retrofitted with batteries (Eidsvik; 2015), while MS Ampere is in operation and is only driven by batteries (Martini; 2015). It is also suggested to use batteries on naval vessels, which can take care of pulse

loads from weapon systems (Huhman and Wetz; 2015; Kuznetsov; 2015). Batteries can also be used for emergency power, as demonstrated in Kim et al. (2015).

The problem of adapting time constants for the peak-shaving algorithm has similarities with the *power split* problem for hybrid electric vehicles, where the desired torque is generated by a combustion engine and an electric motor with a battery. Many different strategies are suggested, for the original Toyota Prius a rule based controller was used (Hermance and Sasaki; 1998). Stochastic model predictive control has been suggested (Moura et al.; 2011), as well as using dynamic programming for design of a rule based controller (Lin et al.; 2003). A controller which optimize fuel consumption and emissions is presented in Johnson et al. (2000). Battery energy storage systems (BESS) are also proposed for wind turbine plants. BESS can be used to smooth the power fluctuations due to the variations of the wind speed (Hovgaard et al.; 2013; Sebastián and Quesada; 2006; Zeng et al.; 2006). Kottick et al. (1993) demonstrated how BESS can be used in an isolated power grid to reduce frequency variations.

Model predictive control (MPC) is used in this chapter as a high-level controller. A model of the plant is used in the MPC to predict the future state of the system. A cost function is used to evaluate the future performance of the system. The MPC optimizes the cost for the prediction horizon. At every step the free variables are optimized with respect to the cost function and constraints, and only the variables for the first step is applied on the system. There already exists multiple suggestion for use of MPC in marine power plants, such as Bø and Johansen (2013); Park et al. (2015); Stone et al. (2015); Veksler et al. (2012b).

We will use probabilistic constraints in this chapter, since future load prediction is uncertain. These are constraints on the form $\text{Prob}(X < x_{\min}) < \eta$, where $\text{Prob}(\cdot)$ is the probability, $0 < \eta \ll 1$ is the probability threshold and X is a stochastic variable. For a linear system with Gaussian disturbance it is shown that the constraints can be converted to an explicit second order cone constraint (Hovgaard et al.; 2011; Oldewurtel et al.; 2010). It is also suggested to use scenarios and conditional value at risk as an approximation of the probabilistic constraint (Hanssen et al.; 2015). An approximation using scenario and mixed integer quadratic programming is presented in Matusko and Borrelli (2012).

The main contribution of this chapter is a controller which can adaptively optimize parameters based on estimates of the power spectrum density. It is applied to optimal tuning of *peak-shaving*. This is done with

batteries to smooth out the power demand of a marine vessel. The battery is controlled by a band-pass filter, so that only power variations in a given frequency band are counteracted.

5.2 Control Plant

The control architecture is shown in Figure 5.1. A load consumes the load P_{Load}, where P_{Load} is stochastic with the power spectrum $p_{pp}(\omega)$. A battery is used to smooth the fluctuations in the generated power. The goal is to keep the temperature and state of charge of the battery within the operational limits, while reducing the power fluctuations on the generator set as much as possible.

The charging and discharging power of the battery are given by a band-pass filter. The input to the band-pass filter is P_{load}, while the output is the desired charging power, P_{ref}. The MPC adjusts the time constants of the band-pass filter to avoid too high battery temperatures. This cancels out power fluctuations with frequencies between the cut-off frequencies of the band-pass filter. This will give a zero-mean charging power of the battery. However, the battery will still be discharged even with zero-mean charging power, due to losses in the battery. Consequently, the MPC gives a mean charging power, P_{MCP}, to control the mean state of charge (SoC).

It should be noted that measurements of the generated power may not be synchronized and may have measurement errors. We assume that the total consumed and generated power is measured without any measurement errors, in this study.

A first order high-pass filter and low-pass filter are put in series to implement a band-pass filter. However, any linear band-pass filter could have been chosen. The transfer function for this filter is:

$$H_f(s) = \frac{P_{\text{ref}}(s)}{P_{\text{load}}(s)} = \frac{\bar{\tau}s}{(1 + \underline{\tau}s)(1 + \bar{\tau}s)n_{\text{cells}}} \tag{5.1}$$

where $\bar{\tau}$ and $\underline{\tau}$ are the highest and lowest time constant of the band pass filter, and n_{cells} is the number of cells in the battery.

A simple model is used for the battery, as shown in Figure 5.2. The internal resistance, R_i, and open circuit voltage, V_o, are assumed to be constant. The temperature of the battery is modeled by Newtons law of cooling:

$$\frac{\mathrm{d}T}{\mathrm{d}t} = \frac{hA}{c}(T_{air} - T) + \frac{1}{c}Q_{el} \tag{5.2}$$
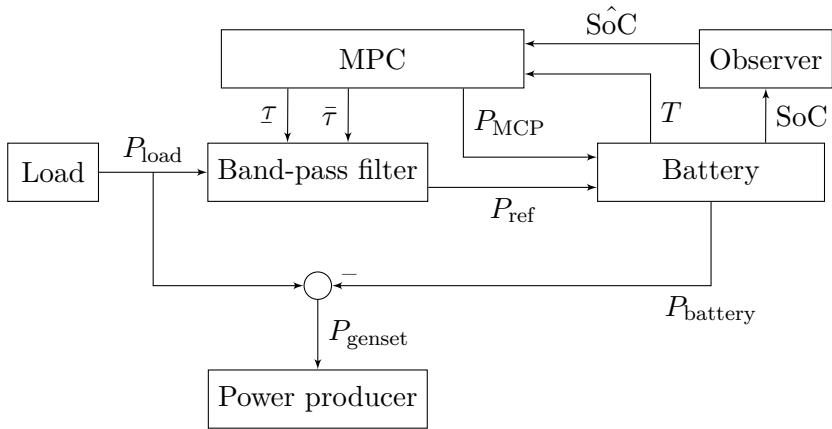
Figure 5.1: Hierarchy of the control system for the peak-shaving control.
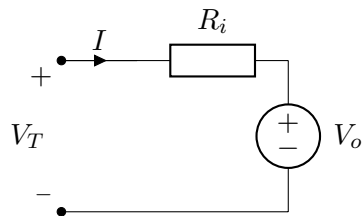
Figure 5.2: Model of battery used internally in the MPC with internal resistance, R_i, and open circuit voltage, V_o, output voltage and current v and i.

where T is the battery temperature, h heat transfer coefficient, A is the surface area of the battery, c is the heat capacity of the battery, T_{air} is the temperature of the cooling air, and Q_{el} is the heat generated in the battery. The heat is assumed to be equal to the electrical loss

$$Q_{el} = R_i I^2 \tag{5.3}$$

where I is the current through the battery.

Due to safety requirements the battery has a temperature limit for operation:

$$T \leq T_{max} \tag{5.4}$$

The battery must be disconnected when this level is reached.

The charging power is controlled by a bi-directional AC/DC converter, and it is controlled to the sum of the reference from the band-pass filter and the MPC:

$$P_{\text{battery}} = P_{ref} + P_{MPC} \tag{5.5}$$

Setting $P_{\text{battery}} = I(V_o + R_i I)$, and solving for the current, we get:

$$
\begin{aligned}
I &= \frac{-V_o + \sqrt{V_o^2 + 4R_i P_{\text{battery}}}}{2R_i} \\
&= \frac{P_{\text{battery}}}{V_o} - \frac{P_{\text{battery}}^2 R_i}{V_o^3} + O(P_{\text{battery}}^3)
\end{aligned}
\tag{5.6}
$$

The SoC of the battery is modeled as an integrator of the current (Moura et al.; 2011):

$$\frac{\mathrm{dSoC}}{\mathrm{d}t} = \frac{I}{Q_{\text{nominal}}} \tag{5.7}$$

where Q_{nominal} is the rated charge of the battery. Hence, the SoC of the battery is 0 when depleted and 1 when fully charged. It is assumed that SoC is measured or estimated, as SoC estimates from Coulomb counting will drift-off. There exists multiple methods for such estimation, e.g. Kim (2008); Piller et al. (2001); Plett (2004). The SoC is also constrained:

$$\text{SoC}_{\text{min}} \leq \text{SoC} \leq \text{SoC}_{\text{max}} \tag{5.8}$$

The minimum and maximum state of charge, can be set by an operator or a plant optimizer. SoC_{min} and SoC_{max} can be used to avoid accelerated

aging, which for lithium batteries occurs at low and high SoC. Since P_{Load} is stochastic we reformulate (5.8) to two probabilistic constraints:

$$\text{Prob}(\text{SoC}_{\min} \leq \text{SoC}) \geq 1 - \eta_{\text{SoC}}$$
$$\text{Prob}(\text{SoC} \leq \text{SoC}_{\max}) \geq 1 - \eta_{\text{SoC}} \tag{5.9}$$

where η_{SoC} is the chosen probability threshold for violation of the constraints.

The temperature of the battery depends on P_{battery}. Since P_{battery} is stochastic, T is also stochastic. However, an estimate of the expected temperature is useful for the MPC. From (5.2):

$$\frac{\text{d}}{\text{d}t} E[T] = \frac{hA}{c} (T_{air} - E[T]) + \frac{1}{c} E[Q_{el}], \tag{5.10}$$

where

$$E[Q_{el}] = E\left[\frac{P_{\text{battery}}^2 R_i}{V_o^2}\right] = R_i \frac{P_{\text{MCP}}^2 + \sigma_{p,ref}^2}{V_o^2}. \tag{5.11}$$

The variance of P_{ref} can be estimated by (5.21) and (5.22)

$$\sigma_{p,ref}^2 = \int_0^\infty p_{pp}(\omega)|H_f(j\omega)|^2 \, \text{d}\omega. \tag{5.12}$$

Note that the variance of the temperature will be small if the time-constant of the temperature, (c/hA), is large compared with the largest period in $p_{pp}(\omega)|H_f(j\omega)|^2$ with significant power. However, we assume that the filter's time-constants are small compared with the time-constant of the temperature dynamics. Therefore, the temperature will be close to the expected value estimated above, and constraining the expected value is reasonable.

5.3 Chance Constraint

An example of how to approximate chance constraints is given in this section. We would like to convert the chance constraints (5.9) to explicit constraints. Assuming P_{load} is close to normal distributed and nonlinearities of the SoC dynamics are small, SoC can be approximated to be normal distributed. Using (5.23), the chance constraints can be approximated to

$$\text{SoC}_{\min} \leq E[\text{SoC}] - F^{-1}(1 - \eta_{\text{SoC}})\sigma_{\text{SoC}}$$
$$\text{SoC}_{\max} \geq E[\text{SoC}] + F^{-1}(1 - \eta_{\text{SoC}})\sigma_{\text{SoC}} \tag{5.13}$$

where $F^{-1}(\cdot)$ is the inverse cumulative distribution function of the standard normal distribution.

An estimate of $E[\text{SoC}]$ and σ_{SoC}^2 is needed. We get:

$$
\begin{aligned}
\frac{\text{d}}{\text{d}t} E\,[\text{SoC}] &= E\left[\frac{P_{\text{battery}}}{V_o Q_{\text{nominal}}} - \frac{P_{\text{battery}}^2 R_i}{V_o^3 Q_{\text{nominal}}}\right] \\
&= \frac{P_{\text{MCP}}}{V_o Q_{\text{nominal}}} - \frac{(P_{\text{MCP}}^2 + \sigma_{p,\text{ref}}^2)R_i}{V_o^3 Q_{\text{nominal}}}
\end{aligned}
\tag{5.14}
$$

by using (5.5), (5.6), and (5.7), neglecting third and higher order terms, and utilizing $E[P_{\text{ref}}] = 0$.

The variance of SoC can be estimated by linearizing (5.6). This gives a linear system from P_{load} to SoC.

$$
\sigma_{\text{SoC}}^2 \approx \int_0^\infty p_{pp}(\omega) \frac{|H_f(j\omega)|^2}{Q_{\text{nominal}}^2 V_o^2}\,\text{d}\omega
\tag{5.15}
$$

The state of charge can be seen as a slowly varying mean, $E[\text{SoC}]$, with a superimposed noise.

$$
\text{SoC} = E[\text{SoC}] + v,
\tag{5.16}
$$

where v is the measurement noise. $E[\text{SoC}]$ is then the initial condition of (5.14). To estimate $E[\text{SoC}]$ a discrete Kalman filter is applied, where SoC is the measured state. The process is modeled as:

$$
\frac{\text{d}\hat{\text{SoC}}}{\text{d}t} = \frac{P_{\text{MCP}}}{V_o Q_{\text{nominal}}} - \frac{(P_{\text{MCP}}^2 + \sigma_{p,\text{ref}}^2)R_i}{V_o^3 Q_{\text{nominal}}} + w
\tag{5.17}
$$

$$
y = \hat{\text{SoC}} + v
\tag{5.18}
$$

where $\hat{\text{SoC}}$ is the estimated $E[\text{SoC}]$, w is the process noise, and v is the measurement noise. The variance of v is assumed to be white noise with variance σ_{SoC}^2. The variance of w is a tunning parameter for the filter, which includes model errors. More details about Kalman filters can be found in e.g., Brown and Hwang (1997, Chapter 5).

Both $E[\text{SoC}]$ and σ_{SoC} can be controlled to fulfill (5.13). It was observed during the simulation study that when both $E[\text{SoC}]$ and σ_{SoC} are controlled the optimal solution is sometime to reduce σ_{SoC} by decreasing the distance between $\underline{\tau}$ and $\bar{\tau}$. However, the desired performance is that

$\underline{\tau}$ and $\bar{\tau}$ are used to control the temperature, while P_{MCP} is used to control the SoC. Therefore, σ_{SoC} is set to $\max[\sigma_{\mathrm{SoC}}(\underline{\tau}, \bar{\tau})] = \sigma_{\mathrm{SoC}}(\underline{\tau}_{ref}, \bar{\tau}_{ref})$. This gives a conservative performance of the SoC; however, as long as $\mathrm{SoC}_{\max} - \mathrm{SoC}_{\min} \gg 2F^{-1}(1 - \eta_{\mathrm{SoC}})\sigma_{\mathrm{SoC}}(\underline{\tau}_{ref}, \bar{\tau}_{ref})$ the $E[\mathrm{SoC}]$ can move within a range.

5.4 Model Predictive Control

To achieve the control objectives mentioned in Section 5.2, a MPC is implemented. The decision variables of the controller are $\boldsymbol{\xi} = \begin{bmatrix} \underline{\tau} & \bar{\tau} & P_{\mathrm{MCP}} \end{bmatrix}^{\top}$, with reference values $\boldsymbol{\xi}_{\mathrm{ref}}$. Some slack variables will also be used, to make sure that a feasible solution is always available, $\boldsymbol{s} = \begin{bmatrix} s_{\mathrm{SoC}} & s_T \end{bmatrix}^{\top}$, with the reference $\boldsymbol{s}_{\mathrm{ref}}$. The stage cost is:

$$
\begin{aligned}
l(\boldsymbol{\xi}, \boldsymbol{s}) =& h_1 \left(\frac{\underline{\tau}}{\underline{\tau}_{ref}} - 1 \right)^2 + h_2 \left(\frac{\bar{\tau}_{ref}}{\bar{\tau}} - 1 \right)^2 + h_3 P_{\mathrm{MCP}}^2 \\
& + (\boldsymbol{s} - \boldsymbol{s}_{\mathrm{ref}})^{\top} H_2 (\boldsymbol{s} - \boldsymbol{s}_{\mathrm{ref}}),
\end{aligned}
\tag{5.19}
$$

where h_1, h_2, and h_3 are positive constants and H_2 is a positive definite weight matrix. The cost function penalize $\underline{\tau}$ and $1/\bar{\tau}$, this is chosen to penalize an increase of $\underline{\tau}$ to its double equally as reducing $\bar{\tau}$ to its half.

The optimization problem is:

$$
\begin{aligned}
\Psi^* = \underset{\Psi}{\mathrm{argmin}} \sum_{k=0}^{N-1} & l(\boldsymbol{\xi}(t_k), \boldsymbol{s}(t_k)) \\
\text{subject to } & (5.10), (5.14), \\
\mathrm{SoC}_{\min} \leq E[\mathrm{SoC}] - F^{-1}(1 - \eta_{\mathrm{SoC}})&\sigma_{\mathrm{SoC}} + s_{\mathrm{SoC}}(t_k) \\
\mathrm{SoC}_{\max} \geq E[\mathrm{SoC}] + F^{-1}(1 - \eta_{\mathrm{SoC}})&\sigma_{\mathrm{SoC}} - s_{\mathrm{SoC}}(t_k) \\
E[T(t_k)] &\leq T_{\max} + s_T(t_k) \\
0 &\leq \boldsymbol{s}(t_k) \\
E[T(t_0)] &= T(t_0) \\
E[\mathrm{SoC}(t_0)] &= \mathrm{S\hat{o}C}(t_0)
\end{aligned}
\tag{5.20}
$$

where

$$
\Psi = \begin{bmatrix} \boldsymbol{\xi}(t_0) & \boldsymbol{s}(t_0) & \dots & \boldsymbol{\xi}(t_{N-1}) & \boldsymbol{s}(t_{N-1}) \end{bmatrix}^{\top}
$$
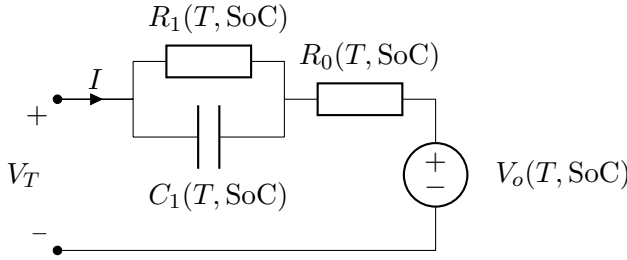
Figure 5.3: Model of battery used in process plant with internal resistances, R_0 and R_1; capacitor, C_1; and open circuit voltage, V_o, output voltage and current v and i. All parameters dependent on SoC and temperature. The model and parameters are adapted from Huria et al. (2012).

contains all the decision variables and Ψ^* is the optimal solution. The first control input $\boldsymbol{\xi}^*(t_0)$ is applied and (5.20) is re-optimized at each time instant.

5.5   Simulation Study

The simulations are done in the simulator presented in Bø et al. (2015). The vessel is a supply vessel operating in dynamic positioning. The significant wave height is 4 m. The vessel has five thrusters, two 1.5 MW, two 2.7 MW, and one 850 kW thruster. Four diesel generator set are used to produce electric power, two 2.2 MW and two 3.3 MW generators. A load proportional with the heave velocity is included to simulate a heave compensator. The battery model presented in Huria et al. (2012) is used as process plant model for the simulations (Figure 5.3). This model includes an RC-circuit in addition to the internal resistance. Additionally, the resistances, capacitance, and internal voltage are dependent on the temperature and state of charge. The parameters are given for the high power lithium cell (LiNi-CoMnO$_2$ cathode and graphite-based anode), 31Ah Kokam SLPB 78216216H. The parameters of the control model in the MPC are found by using the parameters for the process plant model at the minimum state of charge (50%) and maximum temperature (35 °C). The power spectrum density of P_{load} is estimated by using a moving window of the last 1000 seconds of the measurements. ACADO (Houska et al.; 2011) is used to implement the controller and the simulations are done in MATLAB/SIMULINK. The MPC is reoptimized every 50 seconds and the Kalman filter is updated every
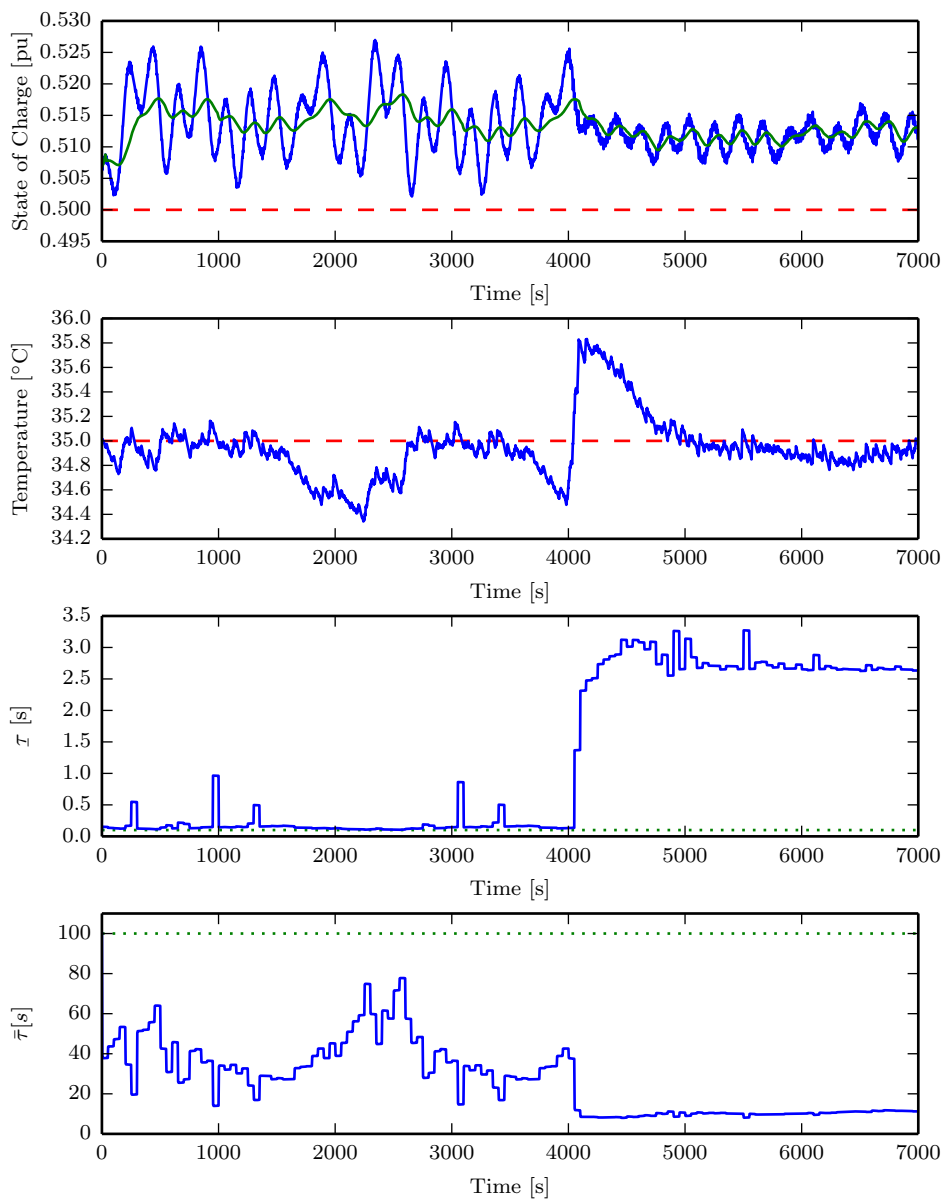
Figure 5.4: Simulation described in Section 5.5 with Case 1. The red lines are the SoC and temperature constraint. The reference value for the time constant is plotted with a green dotted line. The solid green line is the estimated E[SoC] from the Kalman filter.
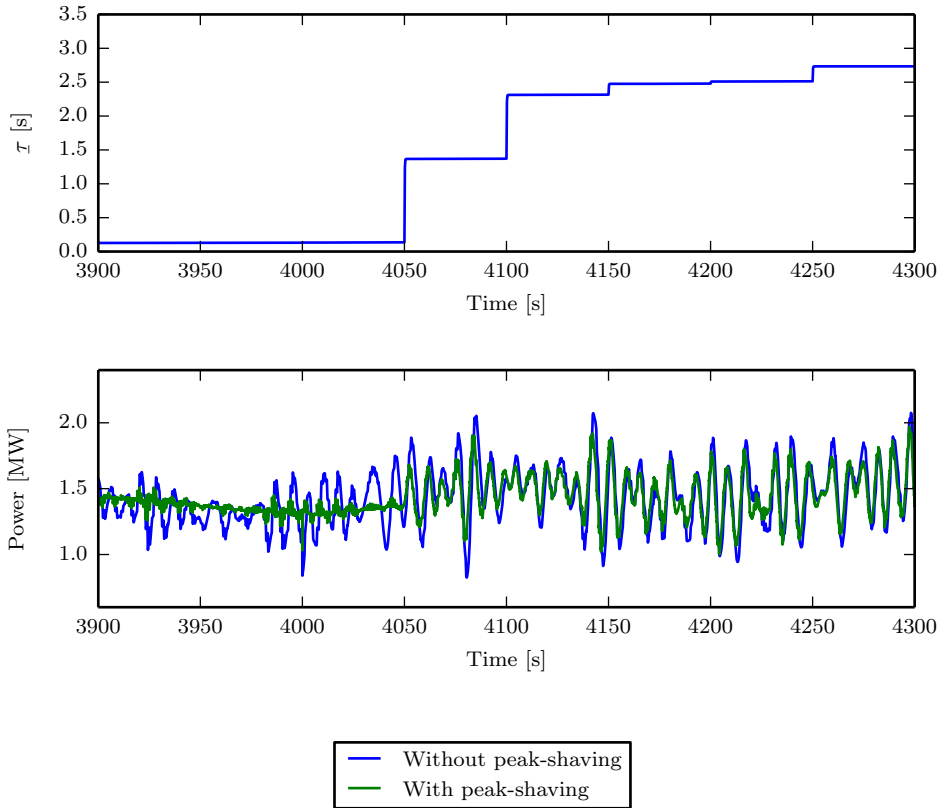
Figure 5.5: Simulation with case plant as described in Section 5.5 with Case 1. At $t = 4000$ second the load variations is increased. The time constant is changed 50 seconds after the change of the load variations, when the MPC reacts on the increased temperature of the battery.
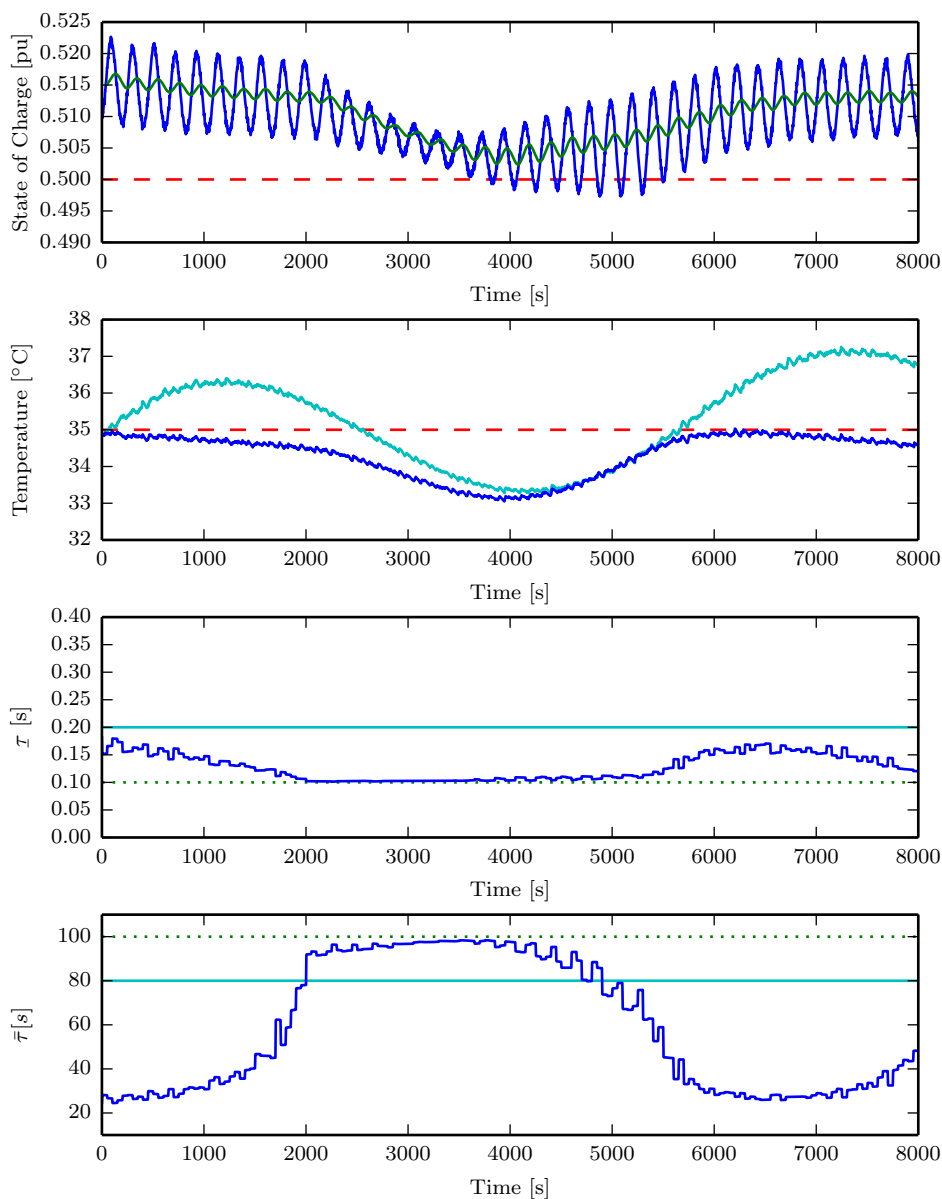
Figure 5.6: Simulation described in Section 5.5 with Case 2. The red lines are the SoC and temperature constraint. The reference value for the time constant is plotted with a green dotted line. The solid green line is the estimated E[SoC] from the Kalman filter. The results with the controller with fixed time constant are shown in cyan. The SoC is not shown for this controller, since it was not controlled.
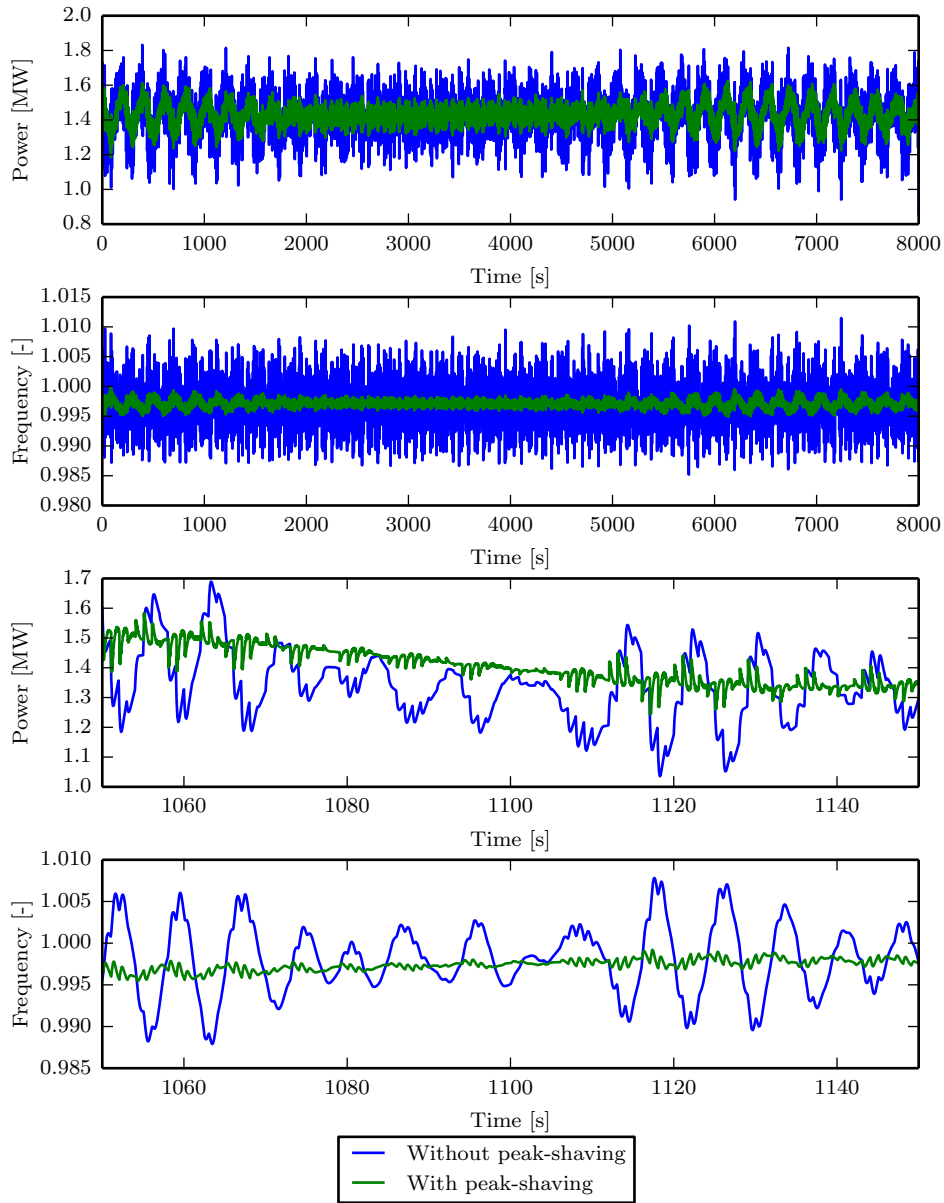
Figure 5.7: Simulation described in Section 5.5 with Case 2. The resulting electrical frequency and power generated by the generators, with (green) and without (blue) peak-shaving. The two lower plots are zoom-ins of the two upper plots.

10 second, with $\sigma_w^2 = 4 \times 10^{-8}$. The remaining parameters in the simulation are given in Table 5.1.

Two cases are simulated. In Case 1, the standard deviation of the heave compensator is 50 kW the first 4000 seconds, thereafter it is increased to 200 kW. A data series of 3000 seconds is generated and repeated three times. This is done to exemplify the steady-state performance of the controller. Results are shown in Fig 5.4 and 5.5. In Case 2 the standard deviation of heave compensator is 50 kW. However, a complete time series is used to illustrate the adaptiveness when the variance is slowly changing. The present controller is compared with a peak-shaving controller where $\underline{\tau} = 0.2$ seconds and $\bar{\tau} = 80$ seconds. Results are shown in Figure 5.6.

Results from the simulation with Case 1 are shown in Figure 5.4. It is clear that the time average of the SoC is controlled to a level above $\mathrm{SoC_{min}}$. The variance of the temperature is also small; therefore, it is reasonable to constrain the expected temperature and not necessary to use probabilistic constraints. After 4000 seconds the temperature increases rapidly due to the increase variations in the power demand. However, the controller takes action at the first update of the MPC after battery temperature starts to increase. Therefore, a safety margin on the temperature limit is needed to avoid disconnection of the battery, due to over-temperature. Details on the transition after 4000 seconds are shown in Figure 5.5. Most of the load fluctuations are canceled out until 4050 seconds. At this instant the time constants are changed to reduce the increased temperature. The band-pass filter is narrowed to time constants of 3 and 7 seconds, which is typically the most difficult time scales for the diesel engines.

Results from the simulation of Case 2 are shown in Figure 5.6 and 5.7. During this simulation the variance of P_{load} is slowly changing. The time constants of the bandpass filter are changed dynamical, such that it is wide when the battery temperature is low, and narrow when its high. It maintains the temperature below the temperature limits when the variance increases. In contrast, the fixed time constant approach gives too high temperatures, and the filter does not utilize the full potential of the peak-shaving capability when the temperature is low. This approach requires either tuning of the filter often or a very conservative tuning. Between 3500 and 4500 seconds, when the fluctuations increases again, the SoC constraint (5.8) is violated 11.5% of the time. This is mainly due to the lag of the estimation of the power spectrum density.

Simulation results with and without peak-shaving are shown in Figure 5.7, which shows the power demand on the generator sets and electrical

Table 5.1: Parameters used in simulation. Parameters for the process plant battery model can be found in Huria et al. (2012).

Parameter	Value
$\underline{\tau}_{ref}$	0.1 s
$\overline{\tau}_{ref}$	100 s
V_o	3.71 V
Q_{nominal}	27.6 Ah
R_i	0.0096 Ω
c	810 $\dfrac{J}{K}$
$\frac{hA}{c}$	1591 s
n_{cells}	1323
T_{max}	35 °C
$\mathrm{SoC}_{\mathrm{min}}$	0.50
$\mathrm{SoC}_{\mathrm{max}}$	0.90
η_{SoC}	5%
$h_1 = h_2$	1
h_3	0.1
$\boldsymbol{s}_{\mathrm{ref}}$	$\begin{bmatrix} -10 & -10 \end{bmatrix}^{\top}$
H_2	$\begin{bmatrix} 100 & 0 \\ 0 & 100 \end{bmatrix}$

frequency. It shows that the peak-shaving reduces the power and frequency variations during the entire simulations, although more variations are canceled when the band-pass filter is wide. The low-frequency variation of the electric frequency is much smaller than the power variations during the first 1000 seconds, these variations are slow enough to be handled by the diesel engine. The remaining low frequency variation of the electric frequency is a result of frequency droop in the governor for load sharing control. The lower two plots show a zoom-in of the two upper plots, it is clear that most of the remaining variations in the electrical frequency are high-frequency variations, which are handled by the inertia of the generator set. This reduced electric frequency variations makes it easier to synchronize new generator set to the grid, and reduced power variations decreases wear and tear on the generator set and possibly decreases the fuel consumption.

5.6 Conclusion

It is demonstrated in this chapter how the power spectrum density can be used to estimate expected values and variance of state of charge and expected temperatures of a battery. This is used in the optimization problem of the MPC. A peak-shaving example was used to demonstrate the control scheme. The MPC sets time constants of a band-pass filter, which controls the peak-shaving done by the battery. The controllers objective is to maintain a battery temperature below a maximum temperature and a state of charge within a desired range. It is shown that the controller achieves its control objective, by controlling the temperature and state of charge close to the constraint. However, the constraints are violated after a sudden change of the disturbance. The peak-shaving algorithm cancels out the variations that are most difficult to handle by the diesel engines, this gives less variations on the electric frequency.

5.7 Appendix: Mathematical Preliminaries

Given a linear system with stochastic input w, transfer function $H(s)$, and output x. The power spectrum density of w is $p_{ww}(\omega)$. For such a system, the power spectrum density of x is

$$p_{xx}(\omega) = p_{ww}(\omega)|H(j\omega)|^2. \tag{5.21}$$

The variance and power of the signal are given as:

$$\sigma_x^2 = \int\limits_0^\infty p_{xx}(\omega)\,\mathrm{d}\omega. \tag{5.22}$$

Given a normal distributed variable X, with the mean and variance $\bar{x}$ and σ^2. The probability constraint:

$$\mathrm{Prob}(X > x_c) \geq 1 - \eta$$

is equivalent to

$$x_c < \bar{x} - F^{-1}(1 - \eta)\sigma \tag{5.23}$$

where η is the probability threshold, and $F^{-1}(\cdot)$ is the inverse probability distribution of standard normal distribution.

Chapter 6

Dynamic Positioning System as Dynamic Energy Storage on Diesel-Electric Ships

This chapter is a reformatted version of Johansen et al. (2014).

6.1   Introduction

Dynamically positioned (DP) vessels with diesel-electric power and propulsion systems are commonly used in offshore operations in order to keep the ship position and heading at their references. While the DP system is often the main consumer of electric power on the ship, other variable power consumers are connected on the same power buses as the electric thrusters. The relatively weak electric grid on a vessel is therefore subject to significant variations in voltage and frequency caused by the dynamics of several more or less independent consumers. This causes challenges due to increased wear and tear, maintenance costs, emissions, and fuel inefficiency of diesel generators in combination with increased risk for blackout due to over- or under-frequency condition causing protection relays to trip generators. Common variable load consumers include drilling drives, heave compensators, cranes, pumps and winches whose operation are often influenced by wave-induced ship motions and other external disturbances. A further benefit of dynamic energy storage is increased operational flexibility as it allows these consumers to have higher priority than DP thrusters with respect to load reduction and load shedding, without reduced safety or operational performance, for short periods of time. Dynamic energy storage

121

is currently also much considered for power and energy management in microgrids and for integration of renewable energy sources, e.g. Levron et al. (2013); Levron and Shmilovitz (2012).

From a DP ship operator's point of view, the main goal is to maximize the operationally useful time of a DP vessel in order to maximize operational income, hence minimizing inefficient and costly downtime. At the same time, minimizing running hours on equipment such as power generators and thrusters will reduce maintenance costs. Historically, these two goals have been in conflict because the demand to maximize operational uptime has required a conservative and redundant use of power and thruster equipment, as required by the International Maritime Organization (IMO) rules for DP vessels (IMO; 1994). A new and more flexible DP notation called DYNPOS ER (Enhanced Reliability), (DNV; 2010), has recently been launched. It is "...developed to allow owners to optimize fuel usage and reduce operational costs, while maintaining high integrity towards loss of position and heading" and enables a more "...flexible, redundant and fuel-efficient way of structuring DP systems". Such a new development on the classification side, which is a result of new technological developments, opens up new possibilities for improved and integrated DP and power control functionality, thus motivating the dynamic energy storage on DP vessels.

Although large resistor banks and thrust allocation with thruster biasing are sometimes used to waste of power on DP ships in order to reduce the effects of power transients on the system, e.g. Jenssen and Realfsen (2006), it is clear that more efficiency and flexibility could be achieved with dynamic energy storage. While several concepts are currently being investigated, such as DC grids (e.g. Hansen et al. (2011)), hybrid power systems (e.g. Zahedi and Norum (2013)), battery banks, capacitive storage and increased mechanical inertia such as fly-wheels, the purpose of this chapter is to study a much simpler approach that does not require any new equipment, i.e. the use of the inertia of the vessel hull itself as dynamic energy storage controlled by the DP system.

The forces that act on a DP vessel can be assumed to be limited to the environmental forces and the thruster forces commanded by the DP controller. Further, assume that the slowly-varying components of the environmental forces are sufficiently large. The vessel hull itself is an effective dynamic energy storage due to its inertia. For example, accelerating the vessel forward by an electrical thruster will convert electric energy to mechanical energy that is at first stored as kinetic energy (due to velocity resulting from the acceleration caused by the thrust) and later as potential energy

(a change in position in the presence of the slowly-varying environmental force field) that can be converted back by returning the vessel back to the original position. Temporary energy storage can therefore be provided by the DP system by allowing the vessel to move away from the setpoint within a given position tolerance. This is not a new idea, and some power control and thrust allocation methods that exploits this mechanical energy storage capacity have been studied and implemented in various forms (Mathiesen et al.; 2012; Radan et al.; 2008; Veksler et al.; 2012a,b).

The main contribution of this chapter is derivation and verification of a new and simple analytical formula that relates the amplitude of the position deviations that need to be allowed to achieve a given capacity of the dynamic energy storage characterized by the frequency and amplitude of the stored power. This allows bounds on the dynamic energy storage capacity provided by methods such as Mathiesen et al. (2012); Radan et al. (2008); Veksler et al. (2012a,b) to be quantified using a very simple formula. Consequently, the need and benefits of new concepts for dynamic energy storage can be more easily discussed and compared in a wider perspective, as dynamic energy storage capacity can be provided within a reasonable range of frequencies and amplitudes simply through functions that can be realized in DP software without the need for any new power system hardware or other equipment.

6.2 A Conceptual Control Architecture for Dynamic Energy Storage in Dynamic Positioning

Figure 6.1 shows a control architecture that intends to illustrate the main idea. In a DP system there is a positioning controller that commands forces in surge and sway directions, as well as the yaw moment, in order to keep position and heading at their specified setpoint, (Fossen; 2011; Sørensen; 2011). Conventionally, a thrust allocation module allocates these forces to the individual thrusters in order to meet these commands whenever possible, where exceptions would be when the thrust demands cannot be met due to the static or dynamic limitations in the thruster system, machinery, or the electric power system. Those limitations are commonly managed through a power available signal from the power management system (PMS) that has the basic function of preventing overloading of the power plant due to equipment failures or protection trips due to under-frequency or under-voltage that would potentially lead to loss of position and emergency operation.

The architecture in Figure 6.1 deviates from conventional DP architec-
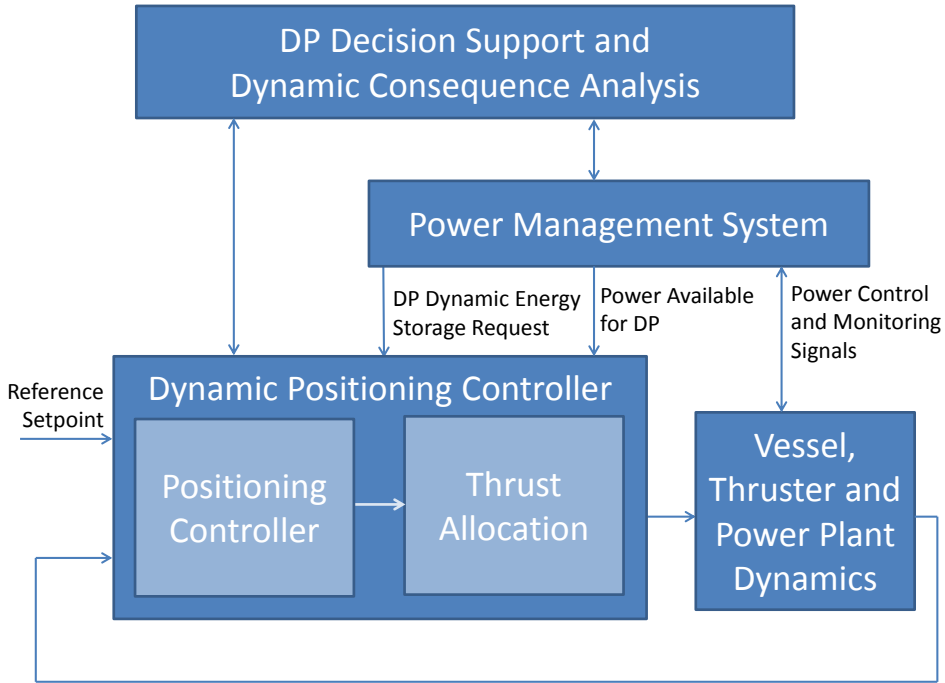
Figure 6.1: The Power Management System is allowed to request dynamic energy storage from the DP controller. A supervisory control and monitoring systems may provide advice and control in order to minimize risk for DP loss of position and other hazards due to electric power shortage resulting from equipment failure or operational issues.

tures since it allows the PMS to request dynamic energy storage to the DP controller. Such dynamic energy storage requests would typically either be issued to compensate for known or predictable load variations in other electric power consumers, e.g. heave-compensators, or in response to failures or operational issues such as loss of generator capacity or partial blackout. Some further discussion on the potential benefits of dynamic energy storage in provided in Section 6.5. The DP controller can then implement dynamic energy storage functionality in many different ways, for example

- Modify the position set-point slightly to increase or decrease the power consumption during the transient.

- Modify the thrust request to the thruster controllers, (Radan et al.; 2008), without any analysis of consequences for positioning errors.

- Modify the thrust request to the thrust allocation with an amount that corresponds to the requested dynamic energy storage rate. This is the approach that will be used in this chapter for demonstration and analysis, for simplicity.

- Modify the power available and limits to the thrust allocation in order to implement the dynamic energy storage request in a smooth and efficient way with minimum impact on the operation of the system, (Mathiesen et al.; 2012; Veksler et al.; 2012a,b).

Dynamic storage of energy as kinetic and potential energy in a DP vessel has some inherent limitations. First, the energy storage cannot change faster than the thruster dynamics. While the electric thruster power can be changed in much less time than one second using frequency converters, it should be realized that persistent fast changes will cause mechanical stress on the system and increased tear and wear. Hence, in practice we expect that energy storage dynamics faster than about 0.5 - 1 Hz cannot normally be accommodated by the DP system. Note that higher frequencies than this would be effectively handled by the mechanical inertia of the diesel-generators, and the capacitances and inductances in the electric system, (Radan; 2008). On the other hand, the DP system typically has a control bandwidth corresponding to a response time of 15-60 seconds for a typical diesel-electric vessel. This bandwidth is chosen due to the dynamics of thrusters as well as the desire to avoid to act against the first order wave induced motions, which is commonly achieved with wave filtering, (Sørensen; 2011). Hence, energy dynamics slower than about 0.05 rad/sec, or about 0.01 Hz, will be typically counteracted by the DP controller unless special functionality is implemented to allow certain position deviations. Consequently, the DP dynamic energy storage will typically be mostly effective for power variations in the range of 0.01 Hz to 0.5 Hz. Although this is a limited frequency band, it is still very useful since it captures important dynamics such as heave compensation systems, some drilling control systems, and other large consumers. Dynamic energy storage requests of lower frequency can be effectively handled by load changes on the diesel generators, as they typically will be able to follow frequencies of 0.01 Hz.

6.3 Dynamic Energy Storage Capacity Analysis

Consider a vessel with mass m that is under DP control. For simplicity of analysis, we assume the vessel is headed against the weather (i.e. against the resultant steady-state environmental force vector) and consider only the surge axis position x. Assume further that a PID controller is used (Sørensen; 2011), and wind variations and first order forces due to ocean waves are neglected. It can be simplified as $F_{DP} = -(K_p x + F_I + K_d \dot{x})$ where a slowly time-varying force F_I (due to integral action) is assumed to cancel the slowly time-varying total environmental force F_E such that $F_I + F_E = 0$. Assume further that the DP system allocates a thrust according to F_{DP} except for a component that is requested as dynamic energy storage to compensate for electric power variations outside the DP:

$$F_{alloc} = F_{DP} + K_0 P_{req} \tag{6.1}$$

where P_{req} is the requested dynamic energy storage (power), and $K_0 \, [N/W]$ is the thrust/power factor that is assumed to be constant for a given thruster configuration near some operating point. The equation of motion for the ship along the surge axis is

$$m\ddot{x} + D\dot{x} = F_{alloc} + F_E \tag{6.2}$$

where D is the hydrodynamic damping coefficient. This leads to

$$m\ddot{x} + (D + K_d)\dot{x} + K_p x = K_0 P_{req} \tag{6.3}$$

Next, consider the allocated (stored) power that is dervied directly from (6.1):

$$P_{alloc} = P_{DP} + P_{req} \tag{6.4}$$

$$= F_{DP}/K_0 + P_{req} \tag{6.5}$$

$$= -\frac{1}{K_0}(K_p x + F_I + K_d \dot{x}) + P_{req} \tag{6.6}$$

Disregarding the stationary power F_I/K_0 needed to compensate for stationary environmental forces F_E, and transforming eqs. (6.3) and (6.6) to the Laplace domain gives the following equations:

$$\frac{1}{K_0}\left(ms^2 + (K_d + D)s + K_p\right)X(s) = P_{req}(s) \tag{6.7}$$

$$P_{alloc}(s) + \frac{1}{K_0}(K_p + K_d s)X(s) = P_{req}(s) \tag{6.8}$$

Combining with (6.4) leads to the following transfer functions after some straightforward algebra:

$$\frac{X}{P_{alloc}}(s) \;=\; \frac{K_0}{ms^2 + Ds} \tag{6.9}$$

$$\frac{P_{alloc}}{P_{req}}(s) \;=\; \frac{ms^2 + Ds}{ms^2 + (K_d + D)s + K_p} \tag{6.10}$$

Simulations in Section 6.4 show that for a typical vessel and DP controller, the hydrodynamic damping force corresponds to less than 1-2 % of the power, so we get the following approximate transfer functions:

$$\frac{X}{P_{alloc}}(s) \;\approx\; \frac{K_0}{ms^2} \tag{6.11}$$

$$\frac{P_{alloc}}{P_{req}}(s) \;\approx\; \frac{ms^2}{ms^2 + K_d s + K_p} \tag{6.12}$$

Assuming the dynamic energy storage request is sinusoidal $P_{req}(t) = P_a \sin(\omega_1 t)$, we get that for $\omega_1 >> \omega_0 = \sqrt{K_p/m}$

$$P_{alloc}(t) \;\approx\; P_{req}(t) \tag{6.13}$$

$$x_a \;\approx\; \frac{K_0}{m\omega_1^2} P_a \tag{6.14}$$

where x_a is the amplitude of the resulting sinusoidal motion $x(t) = x_a \sin(\omega_1 t + \phi)$ of the ship. By also accounting for the hydrodynamic damping, a slightly more accurate approximation can be made

$$x_a \;\approx\; \frac{K_0}{\sqrt{m^2 \omega_1^4 + D^2 \omega_1^2}} P_a \tag{6.15}$$

Based on these simple formulas, some observations can be made.

- The dynamic energy storage capacity P_{alloc} decreases when the dynamic power load frequency ω_1 decreases, in particular when it becomes smaller than the bandwidth ω_0 of the DP controller. For ω_1 much larger than ω_0 we have $P_{alloc} \approx P_{req}$, i.e. full capacity is available. For ω_1 much smaller than ω_0 we get $P_{alloc}/P_{req} \approx 0$, cf. (6.12).

- The amplitude x_a of the ship motion required to accommodate the dynamic energy storage decreases rapidly as ω_1 increases, cf. (6.14). This is a natural physical interpretation since high-frequency motions

require relatively higher force and power than low-frequency motions of the same amplitude. Conversely, smaller high-frequency motion amplitudes will be generated using the same power.

- Net power savings are possible only when the environmental force $F_E \neq 0$, and full dynamic energy storage capacity is available only when $|F_E| \geq K_0 P_a$. This may not be seen as a practical limitation since large dynamic energy storage capacity may primarily be needed when there are high waves, which usually result from high winds that also lead to large $|F_E|$.

The calculations can be easily generalized for dynamic power load variations that are not sinusoidal by considering power spectra or Fourier series.

6.4 Verification – Case Study

The simulation example considers a case where a sinusoidal electric power system disturbance, corresponding to a given power amplitude and period, is added to the thrust commanded by the DP controller to implement dynamic energy storage according to (6.1). The modification to the thrust command is allocate to the surge force only, before the command is sent to the thrust allocation module.

The simulations are conducted using Matlab and the six-degrees-of-freedom Marine Systems Simulator, (Fossen; 2011). The DP vessel considered is a typical drillship, $m = 43, 7 \cdot 10^6$ kg, where the main need for dynamic energy storage comes from active heave compensation of the drill-string or riser. The simulations consider a typical situation with a steady-state (constant) environmental force resulting from mean wind and current forces. In order to accurately analyse the dynamic energy storage functionality by itself, we have not included dynamic disturbance forces due to ocean waves and wind variations in the simulations. These forces could be super-positioned on the simulated forces to give additional dynamic variations in positon, thrust and power consumption. In addition to the 6-degrees-of-freedom model of vessel motion with hydrodynamic and aerodynamic loads, the simulator contains a PID-based DP controller and a thrust allocation algorithm based on the pseudo-inverse. A simple model of the power plant dynamics is given by the diesel generators momentum balance, (Veksler et al.; 2012b), inlet air pressure restrictions, (Radan et al.; 2008) and electric system power balances, (Bø; 2012). Based on this, other variables such as voltages and currents can be computed. The DP system is designed with
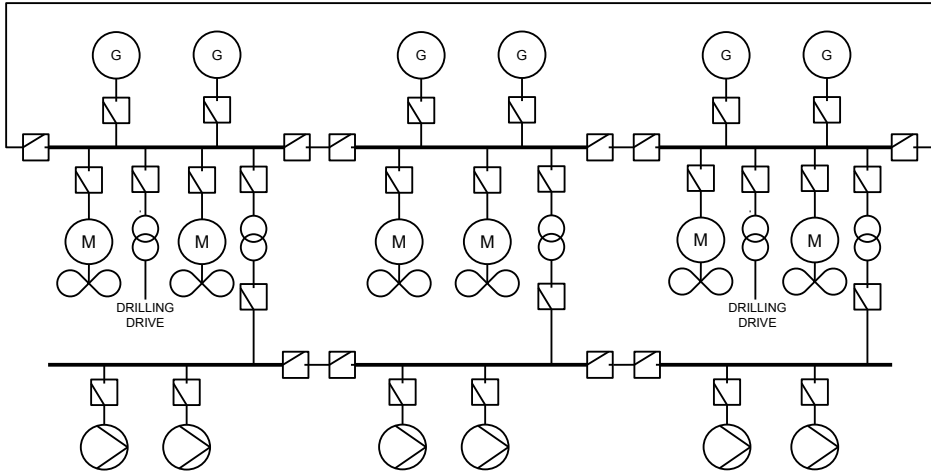
Figure 6.2: Power plant of simulated drilling vessel used in case study.

a bandwidth in surge, sway and yaw of $\omega_0 = 0.033$ rad/s and critical relative damping $\zeta = 1.0$.

The power plant with diesel generators, distribution and consumers is illustrated in Figure 6.2, and is characterized as follows

- There are three main 11 kV buses/switchboards with 2 diesel-generators having circuit breakers that allows them to be connected or disconneted. The generators operates with frequency-control by governors in droop mode.

- There is a ring bus and bus-tie breakers that allows the bus segments to be connected in as a single bus, or in 2-split or 3-split modes. In the simulations we operate with closed bus-ties.

- There are six azimuth thrusters arranged in a standard geometric layout, two for each power bus segment.

- There are several additional consumers connected through transformers or 440 V switchboards that are fed by the main switchboards. For simplicity the figure only shows some main other drilling consumers, i.e. active heave drawworks drive, mud pumps and top drive.

$P_{alloc}[MW]$	$P_{req}[MW]$	$\omega_1[rad/s]$	$x_a\ [m]$ (sim)	$x_a\ [m]$ (eq. (6.14))	$x_a\ [m]$ (eq. (6.15))
0.65	1.26	0.033	1.04	1.09	1.04
2.06	3.99	0.033	5.20	5.42	5.18
3.60	3.99	0.100	1.02	1.03	1.03
8.82	9.78	0.100	2.05	2.06	2.05
9.63	9.78	0.330	0.19	0.21	0.21
3.94	3.99	0.500	0.03	0.04	0.04
9.58	9.78	1.000	0.04	0.02	0.02

Table 6.1: Numerical results from case study.

Simulation results are shown in Table 6.1. They consider a number of cases with different power storage request amplitudes and frequencies, corresponding to different drilling loads

- Dominating wave amplitudes commonly correpond to the range 0.33 rad/s - 1.0 rad/s, e.g. Fossen (2011); Torsethaugen (1993).

- Power variations with frequencies in the range 0.033 rad/s - 0.1 rad/s correspond to low-frequent wave motions such as swells or more exceptional waves that ma occur i some regions.

- Even in rough sea states an active heave drawwork and drilling drives has power consumption variations with amplitudes of less than 5 MW. The scenarios simulated are therefore to be considered as conservative worst cases.

The table reports the simulated and analytic (using (6.14)) position deviation amplitudes as well as dynamically stored energy. The simulations confirm that several megawatts of power variations can be managed by the power management and DP system by accepting relatively small position deviations on a typical mobile offshore drilling unit. Note that typical position deviation for a DP system in normal conditions is about 1 meter. At $\omega_1 = \omega_0 = 0.033\ rad/s$ the dynamic energy storage only has about 50% effect as the allocated (stored) power is only half of the requested dynamic energy storage, due to interactions resulting from the conflict with the primary position control objectives of the DP controller.

The simulations confirm the accuracy of the simple analytic formula (6.14) with accuracy typically better than 5% error. For cases with very

small surge amplitudes, the deviation between x_a predicted by the simple model and the advanced simulation model is relatively large in percent (up to 50%) but negligible in absolute position deviations (a couple of cm). The main reason why higher relative deviations are observed in these cases is the "higher order" dynamic effects of couplings between surge/pitch (longitudinal) and sway/roll (lateral) ship motions included by variations in thruster forces and moments.

The simulations also verify that the dynamic energy storage has the benefit that it makes the variations in electric frequency very small (less than 1% for all cases) and even less variations in voltage. Moreover, the dynamic energy storage it balances out the difference between consumed and produced power that results due to the dynamics of the diesel generators.

It has been verified by simulations that the formulas (6.14)-(6.15) qualitatively are in good agreement also with more advanced implementation of DP dynamic energy storage, (Veksler et al.; 2012a,b).

6.5 DP Decision Support and Dynamic Consequence Analysis

According to established industry standard system design and operational procedures for dynamically positioned ships, (IMO; 1994), it is up to the operator to enable or disable a sufficient amount of thrusters based on the DP decision support tools such as online consequence analysis, capability analysis, and motion prediction, while the PMS ensures that a sufficient amount of generators are running at all times to serve both operational and positioning power needs. Conventionally, a redundant number of online generators and thrusters are employed to guarantee safety and operational availability. However, such a redundancy leads to equipment running at low and inefficient loads, and increases both fuel and maintenance costs as well as exhaust gas emissions.

By increasing the information exchange and actively taking advantage of the dynamic energy storage capacity offered by the DP system, a less conservative use of generators and thrusters can be achieved. In particular, the following enhancements can be envisioned within the framework presented in Figure 6.1, see Bø et al. (2013); Mathiesen et al. (2012) for further details. An online simulation-based dynamic consequence analysis can take into account information about the vessel dynamics, the weather situation (wind, waves and current), load situation, startup time of standby generators and thrusters, etc. to realistically calculate an optimal position reference for

the DP system which minimizes the chance of drift-off or drive-off while simultaneously maximizing the available operational time after generator or switchboard failure, i.e., how long it is possible to prioritize the operational drives in favor of the thruster drives before safety is compromised. This knowledge can be used to reduce the amount of online generators and thrusters while still achieving operational availability and safety in case of a failure, sending the information back to PMS system for consumer load control.

Such integrated and simulation-based power management functionality can for instance be employed by drilling vessels, which have flexibility in positioning depending on the water depth and the corresponding length of the drill string. For such vessels, the functionality will ensure that safety will not be compromised if equipment fails even if a minimum power and thrust configuration is used, because there will be enough time to remedy the failure situation by enabling/disabling relevant power/thrust equipment. Examples include:

- If a generator fails and results in insufficient power, the power consumption must be reduced to avoid a blackout. In order to continue the drilling operation, the thrust consumption must be reduced instead of the drilling consumption. Hence, the vessel will experience a drift-off. However, using a simulator-calculated position reference, e.g. Bø et al. (2013), the vessel is already located such that it can safely be allowed to drift for a certain period of time without having to reduce the drilling power consumption in favor of the positioning. During this time frame, the vessel will be able to start the necessary standby generators in order to restore sufficient power to stop the drift-off and bring the vessel back into position.

- In the worst case, if the vessel moves close to the safety limit during a drift-off, the power to the operational drives (e.g. drilling drives and mud pumps) must be reduced in favor of power to the thruster drives, in order to maintain the safety of the vessel, equipment and crew. Hence, the integrated system will automatically prioritize drilling versus positioning needs depending on the vessel drift pattern, in order to continue the drilling operation as long as safely possible.

6.6 Conclusions

Simple formulas are derived in order to related the dynamic energy storage capacity to the maximum allowed ship position deviation, as a function of the frequency of the requested dynamic energy storage. The formulas are verified using a high-fidelity vessel simulator, and show that for dynamic energy storage requests at wave frequencies (resulting e.g. from an active heave compensation system) that power variations of several megawatt will result in position deviations that are no larger than normal position deviations resulting from the dynamics of ocean waves and winds, as well as inaccuracies in sensors and position reference systems.

The main advantage of this integrated approach is to maintain operational availability and safety while minimizing power consumption, which translates into lower fuel costs and exhaust gas emissions, as well as minimizing wear and tear of generators and thrusters, which translates into lower maintenance costs. Relevant applications include marine operations with positioning flexibility such as drilling.

It could also be mentioned that the method can be directly extended to other energy storage capacities on-board ships in order to allow more low-frequency dynamic energy storage requirements, e.g. thermal storage in cooling, cargo, ventilation, air conditioning and other systems. Such functionality is enabled by integrated automation systems that allows the required software functionality to be implemented.

Chapter 7

Concluding Remarks

7.1 Conclusion

The motivation behind the thesis was to reduce the environmental footprint of diesel electric propulsion on marine vessels during dynamic positioning. The focus was to reduce the number of diesel engines needed during the operation by modeling and control. The methods presented in the thesis achieve this by either giving support for selection of the optimal configuration, or increasing the performance of a configuration to fulfill the operational requirements. This was achieved by optimizing the power and propulsion systems as one complete system, and included interaction among subsystems. This approach produces a synergistic effect, as shown in Chapters 3 and 6, where the inertia of the vessel were used as energy storage during power plant recovery and to smooth out power fluctuations.

The power plant designer must be sure that the power plant can fulfill its operational requirements. This means that any single failure on DP vessels of class 2 and 3 should not lead to loss of position. Consequently, it is important that the designer have good tools for testing and verification of the vessel's systems. Otherwise, conservative solutions may be used, which often are non-optimal. The simulator in Chapter 2 is a tool for this design process. The constraining factor when designing power plants for DP vessels is often the handling of faults. Since the vessel motion dynamics and power plant were included in the simulator, new equipment and control strategy for fault handling can be tested with the simulator. For example were fault recovery methods using batteries tested with the simulator. Power plant performance is also affected by interactions between different parts of the vessel, such as the varying power demand due to propeller-wave interactions.

These effects can be studied with the simulator, and new control methods for the plant can be established.

The operator must also be certain that the power plant is configured to fulfill its operational requirements. It is reported from the industry that the operator often chooses conservative, non-optimal configurations by overriding automatic start/stop of generators and running too many engines. One of the reasons for this choice may be lack of relevant information. A dynamic consequence analysis tool was presented in Chapter 3 to verify DP performance of the vessel during a fault, so that the operator is certain that the configuration is safe enough. The operator can check different configurations, such as the number of engines and recovery methods. The desired configuration can be selected during or before operations based on the simulations using this tool.

This thesis also focused on controllers which could make more configuration able to fulfill the operation requirements. For example the electric frequency can drop after some faults in the electric system. Additional engines can be committed to avoid a too large frequency drop, which could lead to blackout. However, this may be unnecessary because the frequency margin could be increased instead. A scenario-based MPC was presented in Chapter 4, which can be used to configure the generators for higher safety margins or to configure the system so that additional generator sets are not needed.

Electric frequency variations on the grid due to power variations in demand are another challenge that requires the number of engines to be increased. These power variations increase fuel consumption and wear and tear. They also make it difficult to synchronize and connect additional generator sets when needed. Control of peak-shaving is presented in Chapter 5, which can be used to reduce these variations in power demand. An MPC was used in combination with a power spectrum analysis to control peak shaving so that load fluctuations are canceled out as much as possible, while avoiding too high battery temperatures.

Another method to reduce power fluctuations is to vary power consumption of the thrusters, which cancels power fluctuations of other loads. The effects of varying power consumption of the thrusters on the DP position are demonstrated in Chapter 6. An analytical formula is presented, which gives the size of the position variation as a function of the power variation. The formula was verified with the results from a simulation study.

These methods were simulated using the simulator presented in Chapter 2 to verify their performance. The methods presented in this thesis

were designed to achieve better control of the vessel's systems, including performance of the DP system and the power plant. These methods can be used in combination to reduce the number of diesel generators running while maintaining the required safety level or to increase the safety level through better control and information.

7.2 Further Work

The motivation of the thesis was to lower the environmental footprint of vessels with diesel electric propulsion and DP. Performance of the controllers was tested and verified through analytical methods and simulation studies. The next step would be to perform a qualitative study on how much each of these methods can reduce emissions from these vessels. This could be accomplished using the simulator or by full-scale testing. The largest reductions in emissions are achieved when diesel engine utilization is increased.

The diesel engine model used in this study was a mean value model, which was designed considering steady-state conditions. However, transient performance was not fully modeled and exhaust gas emissions were not modeled at all. These models must be developed and validated with full-scale measurements to verify reduced emissions by quantifying the reduced fuel consumption and production of emissions.

This study did not investigate reductions in SO_X, NO_X, or particulate matter (PM) emissions. However, most of the potential for reduction of these emissions is through new equipment and control of the power producers. Lower SO_X, NO_X, and PM emissions may also be achieved by the controllers described in Chapters 5 and 6, as a smoother power demand may produce lower emissions.

Batteries were not a large focus in this study; however, the development of batteries has increased rapidly in the last few years. One particularly interesting scenario is using batteries as "running stand-by" power supply, since the stand-by cost of a battery is negligible after installation compared with diesel engines. Development of such methods would be supported by the simulator developed in Chapter 2. The dynamic consequence analysis in Chapter 3 is well fitted for operations with DP and batteries, because it can be used to estimate plant performance and the minimum battery charge state. A concept study using batteries as running stand-by should be conducted to determine the increase in performance. This study should also include other power plant changes, such as using diesel engines that are optimized for slowly varying loads.

The simulator models were tested and verified individually. The next step is to verify the simulator against full-scale or model-scale measurements. Similarly, the controllers and models for the controllers should be verified with full- or model-scale tests to get one step closer to implementation.

Bibliography

ABB (n.d.). Battery-powered ferry - transport with zero emissions, online visited 16-10-2015.
  URL: *http://new.abb.com/marine/articles-and-highlights/battery-powered-ferry—transport-with-zero-emissions*

ABS (2014). Guide for dynamic positioning systems. American Bureau of Shipping.

Altosole, M., Benvenuto, G., Figari, M. and Campora, U. (2009). Real-time simulation of a COGAG naval ship propulsion system, *Proceedings of the Institution of Mechanical Engineers, Part M: Journal of Engineering for the Maritime Environment* **223**: 47–62.

Angeli, D., Amrit, R. and Rawlings, J. B. (2012). On average performance and stability of economic model predictive control, *IEEE Trans. Automat. Contr.* **57**(7): 1615–1626.

Bazari, Z. and Longva, T. (2011). Assessment of IMO mandated energy efficiency measures for international shipping, *Technical Report MEPC 63/INF.2*, Lloyd's Register and DNV.

Bemporad, A., Bellucci, L. and Gabbriellini, T. (2014). Dynamic option hedging via stochastic model predictive control based on scenario simulation, *Quantitative Finance* pp. 1739–1751.

Benajes, J., Luján, J. M., Bermúdez, V. and Serrano, J. R. (2002). Modelling of turbocharged diesel engines in transient operation. Part 1: Insight into the relevant physical phenomena, *Proceedings of the Institution of Mechanical Engineers, Part D: Journal of Automobile Engineering* **216**(5): 431–441.

Bernardini, D. and Bemporad, A. (2009). Scenario-based model predictive control of stochastic constrained linear systems, *Decision and Control, 2009 held jointly with the 2009 28th Chinese Control Conference. CDC/CCC 2009. Proceedings of the 48th IEEE Conference on*, pp. 6333–6338.

Blanke, M., Kinnaert, M., Lunze, J. and Staroswiecki, M. (2006). Diagnosis and Fault-Tolerant Control, *Diagnosis Fault-Tolerant Control*, 2nd edn, Springer Berlin Heidelberg, pp. 10–23.

Bonfill, A., Espuña, A. and Puigjaner, L. (2008). Proactive approach to address the uncertainty in short-term scheduling, *Computers & chemical engineering* **32**(8): 1689–1706.

Bosich, D., Filippo, M., Giulivo, D., Sulligoi, G. and Tessarolo, A. (2012). Thruster motor start-up transient in an all-electric cruise-liner: Numerical simulation and experimental assessment, *Electrical Systems for Aircraft, Railway and Ship Propulsion (ESARS), 2012*, pp. 1–5.

Bravo, J. M., Alamo, T. and Camacho, E. F. (2006). Robust MPC of constrained discrete-time nonlinear systems based on approximated reachable sets, *Automatica* **42**(10): 1745–1751.

Brown, R. G. and Hwang, P. Y. (1997). *Introduction to Random Signals and Applied Kalman Filtering*, third edn, Wiley.

Bø, T. I. (2012). *Dynamic model predictive control for load sharing in electric power plants for ships*, Master's thesis, Norwegian University of Science and Technology.

Bø, T. I., Dahl, A. R., Johansen, T. A., Mathiesen, E., Miyazaki, M. R., Pedersen, E., Skjetne, R., Sørensen, A. J., Thorat, L. and Yum, K. K. (2015). Marine vessel and power plant system simulator, *IEEE Access* **3**: 2065–2079.

Bø, T. I. and Johansen, T. A. (2013). Scenario-based fault-tolerant model predictive control for diesel-electric marine power plant, *MTS/IEEE Ocean.*, Bergen, Norway.

Bø, T. I. and Johansen, T. A. (2014). Dynamic safety constraints by scenario based economic model predictive control, *Proc. IFAC World Congress, Cape Town, South Africa*, pp. 9412–9418.

Bø, T. I. and Johansen, T. A. (n.d.a). Battery peak-shaving control in electric marine power plant using nonlinear model predictive control. Submitted for publication.

Bø, T. I. and Johansen, T. A. (n.d.b). Dynamic safety constraints by scenario-based economic model predictive control. Submitted for publication.

Bø, T. I., Johansen, T. A. and Mathiesen, E. (2013). Unit Commitment of Generator Sets During Dynamic Positioning Operation Based on Consequence Simulation, *Proc. 9th IFAC Conf. Control Applications in Marine Systems*, Osaka, Japan.

Bø, T. I., Johansen, T. A., Sørensen, A. J. and Mathiesen, E. (n.d.). Dynamic consequence analysis of marine electric power plant in dynamic positioning. Submitted for publication.

Calafiore, G. C. and Fagiano, L. (2013). Robust Model Predictive Control via Scenario Optimization, *IEEE Trans. Automat. Contr.* **58**(1): 219–224.

Chase, M. W. (1998). *NIST-JANAF thermochemical tables*, Vol. no. 9, American Chemical Society and the American Institute of Physics for the National Institute of Standards and Technology, Washington, D.C.

Chen, W., Ådnanes, A., Hansen, J., Lindtjørn, J. and Tang, T. (2010). Super-capacitors based hybrid converter in marine electric propulsion system, *Electrical Machines (ICEM), 2010 XIX International Conference on*, pp. 1–6.

Chow, A. and Wyszynski, M. L. (1999). Thermodynamic modelling of complete engine systems—a review, *Proceedings of the Institution of Mechanical Engineers, Part D: Journal of Automobile Engineering* **213**(4): 403–415.

Contaxis, G. C. and Kabouris, J. (1991). Short term scheduling in a wind/diesel autonomous energy system, *IEEE Transactions on Power Systems* **6**(3): 1161–1167.

Coogan, S. and Arcak, M. (2012). Guard synthesis for safety of hybrid systems using sum of squares programming, *51st IEEE Conf. Decis. Control*, pp. 6138–6143.

Dillon, T. S., Edwin, K. W., Kochs, H. D. and Taud, R. J. (1978). Integer programming approach to the problem of optimal unit commitment with probabilistic reserve determination, *IEEE Transactions on Power Apparatus and Systems* **PAS-97**(6): 2154–2166.

DNV (2010). Dynamic positioning system - enhanced reliability DYNPOS-ER, *Technical Report Rules for classification of ships, Part 6, Chapter 26.*

DNV (2012). Failure mode and effect analysis (FMEA) of redundant systems. Det Norske Veritas.

DNV (2015). *Rules for Classification of Ships.* Det Norske Veritas, July.

DNV GL (2015a). Offshore technical guide 10, DP-classed vessels with closed bus-tie(s), *Technical report.*

DNV GL (2015b). *Rules for Classification of Ships.* DNV GL. October.

DNV GL (n.d.). Sesam marine. Viewed 17-10-2015. www.dnvgl.com/services/software-for-marine-operations-sesam-marine-2321.

Dokopoulos, P. S. and Saramourtsis, A. C. (1996). Prediction and Evaluation of the Performance of Wind-Diesel Energy Systems, *IEEE Transactions on Energy Conversion* **11**(2): 385–393.

Ehsani, M., Gao, Y. and Emadi, A. (2009). *Modern electric, hybrid electric, and fuel cell vehicles: fundamentals, theory, and design*, CRC press.

Eidsvik (2015). Viking Queen installation of energy storage system. Accessed: 2015-08-27.
URL: *www.eidesvik.no/news-archive/viking-queen-installation-of-energy-storage-system-article645-299.html*

Eriksen, P. B. and Orths, A. (2008). From 20 to 50 percent of wind energy in the danish power system, Keynote presentation at 7th international workshop of large-scale integration of wind power and on transmission networks for offshore wind farms; 26–28 May 2008. Madrid, Spain.

Faltinsen, O. M. (1990). *Sea Loads on Ships and Offshore Structures*, Cambridge University Press.

Fossen, T. I. (2002). *Marine Control Systems: Guidance, Navigation and Control of Ships, Rigs and Underwater Vehicles*, Marine Cybernetics, Trondheim, Norway.

Fossen, T. I. (2011). *Handbook of Marine Craft Hydrodynamics and Motion Control*, John Wiley and sons.

Fossen, T. I. and Strand, J. P. (1999). Passive nonlinear observer design for ships using lyapunov methods: full-scale experiments with a supply vessel, *Automatica* **35**(1): 3 – 16.

Gillula, J. H., Hoffmann, G. M., Vitus, M. P. and Tomlin, C. J. (2011). Applications of hybrid reachability analysis to robotic aerial vehicles, *The International Journal of Robotics Research* **30**(3): 335–354.

Goodwin, G. C. and Medioli, A. M. (2013). Scenario-based, closed-loop model predictive control with application to emergency vehicle scheduling, *International Journal of Control* **86**(8): 1338–1348.

Grüne, L. (2013). Economic receding horizon control without terminal constraints, *Automatica* **49**(3): 725–734.

Guzzella, L. and Onder, C. H. (2010). *Introduction to Modeling and Control of Internal Combustion Engine Systems*, second edn, Springer Berlin Heidelberg, Berlin, Heidelberg.

Hansen, J. F., Ådnanes, A. K. and Fossen, T. I. (1998). Modelling, simulation and multivariable modelbased predictive control of marine power generation system, *Proceedings of IFAC Conference: Control Applications in Marine Systems, CAMS'98*, Fukuoka, Japan, pp. 45–50.

Hansen, J. F., Ådnanes, A. K. and Fossen, T. I. (2001). Mathematical modelling of diesel-electric propulsion systems for marine vessels, *Mathematical and Computer Modelling of Dynamical Systems* **7**(3): 323–355.

Hansen, J. F. and Fossen, T. I. (1999). Nonlinear control of marine power generation systems, *Proc. of 13th Power Systems Computation Conference*, Trondheim, Norway, pp. 539–544.

Hansen, J. F., Lindtjørn, J. O. and Vänskä, K. (2011). Onboard DC grid for enhanced DP operation in ships, *Dynamic Positioning Conference*, MTS, Houston, USA.

Hansen, J. F. and Wendt, F. (2015). History and State of the Art in Commercial Electric Ship Propulsion, Integrated Power Systems, and Future Trends, *Proceedings of the IEEE* **103**(12): 2229–2242.

Hanssen, K. G., Foss, B. and Teixeira, A. (2015). Production optimization under uncertainty with constraint handling, *2nd IFAC Workshop on Automatic Control in Offshore Oil and Gas Production*, pp. 62–67.

Hasselmann, K., Barnett, T., Bouws, E., Carlson, H., Cartwright, D., Enke, K., Ewing, J., Gienapp, H., Hasselmann, D., Kruseman, P. et al. (1973). Measurements of wind-wave growth and swell decay during the joint north sea wave project (JONSWAP), *Technical report*, Deutches Hydrographisches Institut.

Hermance, D. and Sasaki, S. (1998). Hybrid electric vehicles take to the streets, *Spectrum, IEEE* **35**(11): 48–52.

Heywood, J. B. (1988). *Internal Combustion Engine Fundamentals*, McGraw Hill.

Holttinen, H., Meibom, P., Orths, A., Lange, B., O'Malley, M., Tande, J. O., Estanqueiro, A., Gomez, E., Söder, L., Strbac, G., Smith, J. C. and van Hulle, F. (2011). Impacts of large amounts of wind power on design and operation of power systems, results of IEA collaboration, *Wind Energy* **14**(2): 179–192.

Houska, B., Ferreau, H. J. and Diehl, M. (2011). ACADO toolkit — an open-source framework for automatic control and dynamic optimization, *Optimal Control Applications and Methods* **32**(3): 298–312.

Hovgaard, T. G., Larsen, L. F. S., Jørgensen, J. B. and Boyd, S. (2013). MPC for wind power gradients — utilizing forecast, rotor inertia, and central energy storage, *European Control Conference*, Zürich, Switzerland, pp. 4071–4076.

Hovgaard, T., Larsen, L. and Jørgensen, J. (2011). Robust economic mpc for a power management scenario with uncertainties, *Decision and Control and European Control Conference (CDC-ECC), 2011 50th IEEE Conference on*, pp. 1515–1520.

Huhman, B. M. and Wetz, D. A. (2015). Progress in the Development of a Battery-based Pulsed Power System, *Electric Ship Technologies Symposium (ESTS), 2015 IEEE*, pp. 441–445.

Huria, T., Ceraolo, M., Gazzarri, J. and Jackey, R. (2012). High fidelity electrical model with thermal dependence for characterization and simulation of high power lithium battery cells, *Electric Vehicle Conference (IEVC), 2012 IEEE International*, pp. 1–8.

IMCA (1995–2011). Dynamic positioning station keeping incidents, *Technical report*, International Marine Contractors Association.

IMCA (2000). Specification for DP capability plots, *Technical Report IMCA M140*, The International Marine Contractors Association. Revision 1.

IMO (1994). Guidelines for vessels with dynamic positioning systems, *Technical Report Maritime Safety Committee (MSC) Circular 645*, International Maritime Organization (IMO).

IMO (2011). International convention for the prevention of pollution from ships (MARPOL) Annex VI. International Maritime Organization (IMO).

ISO (2009). ISO 13624-1:2009 Petroleum and natural gas industries – Drilling and production equipment – Part 1: Design and operation of marine drilling riser equipment. International Organization for Standardization.

Jenssen, N. A. and Realfsen, B. (2006). Power optimal thruster allocation, *Proc. Dynamic Positioning Conference, Houston*.

Johansen, T. A., Bø, T. I., Mathiesen, E., Veksler, A. and Sørensen, A. J. (2014). Dynamic positioning system as dynamic energy storage on diesel-electric ships, *Power Systems, IEEE Transactions on* **29**(6): 3086–3091.

Johansen, T. A. and Sørensen, A. J. (2009). Experiences with hil simulator testing of power management systems, *Dynamic Positioning Conference, Marine Technology Society*, Houston, USA.

Johnson, V. H., Wipke, K. B. and Rausen, D. J. (2000). HEV control strategy for real-time optimization of fuel economy and emissions, *Technical report*, SAE Technical Paper.

Juste, K. A., Kita, H., Tanaka, E. and Hasegawa, J. (1999). An evolutionary programming solution to the unit commitment problem, *IEEE Transactions on Power Systems* **14**(4): 1452–1459.

Kim, I.-S. (2008). Nonlinear state of charge estimator for hybrid electric vehicle battery, *Power Electronics, IEEE Transactions on* **23**(4): 2027–2034.

Kim, S.-Y., Choe, S., Ko, S. and Sul, S.-K. (2015). A naval integrated power system with a battery energy storage system: Fuel efficiency, reliability, and quality of power., *Electrification Magazine, IEEE* **3**(2): 22–33.

Kongsberg Maritime (n.d.). K-POS, online, view 22-10-2015.
URL: *www.km.kongsberg.com/ks/web/nokbg0397.nsf/AllWeb/ 23EE29C2A5B1E771C12571CA004B3827/$file/k-pos-brochure.pdf?OpenElement*

Kottick, D., Blau, M. and Edelstein, D. (1993). Battery energy storage for frequency regulation in an island power system, *Energy Conversion, IEEE Transactions on* **8**(3): 455–459.

Kovâcshâzy, T., Péceli, G. and Simon, G. (2001). Transient reduction in reconfigurable control systems utilizing structure dependence, *Instrumentation and Measurement Technology Conference, 2001. IMTC 2001. Proceedings of the 18th IEEE*, pp. 1143–1147.

Krause, P. C., Wasynczuk, O. and Sudhoff, S. D. (2013). *Analysis of Electric Machinery and Drive Systems*, 3 edn, McGraw Hill Higher Education.

Kristiansen, S. (2014). *Analysis of loss of position incidents for dynamically operated vessels*, Master's thesis, Norwegian University of Science and Technology.

Kuznetsov, S. (2015). Large Scale Energy Storage Module for Surface Combatants : Transmission and System Transient Characteristics, *Electr. Sh. Technol. Symp. (ESTS), 2015 IEEE*, pp. 167–172.

Lao, L., Ellis, M. and Christofides, P. D. (2013). Proactive Fault-Tolerant Model Predictive Control, *AIChE J.* **59**(8): 2810–2820.

Lee, C.-H. (1995). *WAMIT Theory Manual*, Massachusettes Institute of Technology.
URL: *http://www.wamit.com/Publications/tmanual.pdf*

Levron, Y., Guerrero, J. and Beck, Y. (2013). Optimal power flow in microgrids with energy storage, *IEEE Transactions on Power Systems* **28**(3): 3226–3234.

Levron, Y. and Shmilovitz, D. (2012). Power systems' optimal peak-shaving applying secondary storage, *Electric Power Systems Research* **89**(0): 80 – 84.

Limon, D., Alamo, T., Raimondo, D. M., Peña, D. M. n., Bravo, J. M., Ferramosca, A. and Camacho, E. F. (2009). Input-to-state stability: a unifying framework for robust model predictive control, *in* L. Magni, D. M. Raimondo and F. Allgöwer (eds), *Nonlinear Model Predict. Control*, Vol. 384, Springer Berlin Heidelberg, pp. 1–26.

Lin, C.-C., Peng, H., Grizzle, J. W. and Kang, J.-M. (2003). Power management strategy for a parallel hybrid electric truck, *Control Systems Technology, IEEE Transactions on* **11**(6): 839–849.

Lowery, P. G. (1966). Generating unit commitment by dynamic programming, *IEEE Transactions on Power Apparatus and Systems* **PAS-85**(5): 422–426.

Maciejowski, J. M. (2002). *Predictive Control with Constraints*, Pearson Eucation.

Maiworm, M., Bäthge, T. and Findeisen, R. (2015). Scenario-based model predictive control: Recursive feasibility and stability, *Proc. of 9th IFAC Symposium on Advanced Control of Chemical Processes ADCHEM 2015*, Vol. 48, Whistler, Canada, pp. 50 – 56.

MAN Engines and Systems (2013). 32/44CR Project Guide - Marine. **URL:** *marine.man.eu/four-stroke/project-guides*

Marine Cybernetics (n.d.). Technology: Cybersea. Viewed 2014-12-12. marinecybernetics.com/technology/cybersea.

Marine Environment Protection Committee, IMO (2014). Third IMO GHG study 2014, *Technical report*, International Maritime Organization (IMO).

Martini, F. (2015). First electrical car ferry in the world in operation in Norway now, *Siemens, Pictures of the Future*.

Mathiesen, E., Realfsen, B. and Breivik, M. (2012). Methods for reducing frequency and voltage variations on DP vessels, *Dynamic Positioning Conference, Marine Technology Society*, Houston, USA.

Matusko, J. and Borrelli, F. (2012). Scenario-based approach to stochastic linear predictive control, *Decision and Control (CDC), 2012 IEEE 51st Annual Conference on*, pp. 5194–5199.

May, J. J. (2003). Improving engine utilization on DP drilling vessels, *Dynamic Positioning Conference, Marine Technology Society*, Houston, USA.

May, J. J. and Foss, H. (2000). Power Management System for the "Deepwater Horizon" a dynamically positioned all weather semisubmersible, *Dynamic Positioning Conference, Marine Technology Society*, Houston, USA.

Mayne, D. Q., Rawlings, J. B., Rao, C. V. and Scokaert, P. O. M. (2000). Constrained model predictive control: Stability and optimality, *Automatica* **36**(6): 789–814.

Miniovich, I. Y. (1960). *Investigation of Hydrodynamic Characteristics of Screw Propellers Under Conditions of Reversing and Calculation Methods for Backing of Ships.*

Moura, S. J., Fathy, H. K., Callaway, D. S. and Stein, J. L. (2011). A stochastic optimal control approach for power management in plug-in hybrid electric vehicles, *Control Systems Technology, IEEE Transactions on* **19**(3): 545–555.

MSS (2010). Marine systems simulator. marinecontrol.org.

Myklebust, T. A. and Ådnanes, A. K. (n.d.). Parallel hybrid propulsion for AHTS, online, viewed 01.10.2015.
URL: *https://library.e.abb.com/public/d4355c6a83641884c1257a8a003c5 ada/ABB%20Generations_24%20Parallel%20hybrid%20propulsion %20for%20AHTS.pdf*

Oldewurtel, F., Parisio, A., Jones, C. N., Morari, M., Gyalistras, D., Gwerder, M., Stauch, V., Lehmann, B. and Wirth, K. (2010). Energy efficient building climate control using stochastic model predictive control and weather predictions, *American Control Conference (ACC), 2010*, pp. 5100–5105.

Opsand, S. (2015). Maritime battery forum, Presentation at Electric & Hybrid Marine World Expo 2015.

Overbye, S. (1989). *Fra forskning til industri, utvikling av skipsautomatis-eringsbedriften norcontrol*, Master's thesis, University of Oslo, Norway.

Pachauri, R. K., Allen, M. R., Barros, V. R., Broome, J., Cramer, W., Christ, R., Church, J. A., Clarke, L., Dahe, Q., Dasgupta, P., Dubash, N. K., Edenhofer, O., Elgizouli, I., Field, C. B., Forster, P., Friedling-stein, P., Fuglestvedt, J., Gomez-Echeverri, L., Hallegatte, S., Hegerl, G., Howden, M., Jiang, K., Cisneroz, B. J., Kattsov, V., Lee, H., Mach, K. J., Marotzke, J., Mastrandrea, M. D., Meyer, L., Minx, J., Mulugetta, Y., O'Brien, K., Oppenheimer, M., Pereira, J. J., Pichs-Madruga, R., Plat-tner, G.-K., Pörtner, H.-O., Power, S. B., Preston, B., Ravindranath, N. H., Reisinger, A., Riahi, K., Rusticucci, M., Scholes, R., Seyboth, K., Sokona, Y., Stavins, R., Stocker, T. F., Tschakert, P., van Vuuren, D. and van Ypserle, J.-P. (2014). *Climate Change 2014: Synthesis Report. Contribution of Working Groups I, II and III to the Fifth Assessment Report of the Intergovernmental Panel on Climate Change*, IPCC, Geneva, Switzerland.

Paran, S., Vu, T., El Mezyani, T. and Edrington, C. (2015). MPC-based power management in the shipboard power system, *Electric Ship Technologies Symposium (ESTS), 2015 IEEE*, pp. 14–18.

Park, H., Sun, J., Pekarek, S., Stone, P., Opila, D., Meyer, R., Kolmanovsky, I. and DeCarlo, R. (2015). Real-time model predictive control for shipboard power management using the IPA-SQP approach, *Control Systems Technology, IEEE Transactions on* **23**(6): 2129–2143.

Pascoal, R., Guedes Soares, C. and Sørensen, A. J. (2007). Ocean wave spectral estimation using vessel wave frequency motions, *Journal of Offshore Mechanics and Arctic Engineering* **129**(2): 90–96.

Pedersen, E. and Engja, H. (2000). A Bond Graph Model Library for Modelling Diesel Engine Transient Performance, *ISME Tokyo 2000*, Vol. 2, Tokyo, pp. 447–455.

Pedersen, T. A. and Pedersen, E. (2012). Bond graph modelling of marine power systems, *Mathematical and Computer Modelling of Dynamical Systems* **18**(2): 153–173.

Perez, T. and Blanke, M. (2003). DCMV a MATLAB/Simulink toolbox for dynamics and control of marine vehicles, *6th IFAC MCMC*, Girona, Spain.

Perez, T., Smogeli, Ø. N., Fossen, T. I. and Sørensen, A. J. (2006). An Overview of the Marine Systems Simulator (MSS): A Simulink Toolbox for Marine Control Systems, *Modeling, Identification and Control* **27**(4): 259–275.

Piller, S., Perrin, M. and Jossen, A. (2001). Methods for state-of-charge determination and their applications, *Journal of Power Sources* **96**(1): 113 – 120. Proceedings of the 22nd International Power Sources Symposium.

Pivano, L., Muddusetti, S. and Ramsey, J. (2014). Better analysis - better data - better decisions - better operational risk management = delivery of incident free operations: Enabled by DynCap, *Dynamic Positioning Conference, Marine Technology Society*, Houston, USA.

Plett, G. L. (2004). Extended kalman filtering for battery management systems of LiPB-based {HEV} battery packs: Part 3. state and parameter estimation, *Journal of Power Sources* **134**(2): 277 – 292.

Prajna, S., Jadbabaie, A. and Pappas, G. J. (2007). A Framework for Worst-Case and Stochastic Safety Verification Using Barrier Certificates, *IEEE Trans. Automat. Contr.* **52**(8): 1415–1428.

Qin, S. J. and Badgwell, T. A. (2003). A survey of industrial model predictive control technology, *Control Engineering Practice* **11**(7): 733 – 764.

Radan, D. (2008). *Integrated Control of Marine Electrical Power Systems*, Doctoral thesis, monograph, Department of Marine Technology, Faculty of Engineering Science & Technology, NTNU.

Radan, D., Johansen, T. A., Sørensen, A. J. and Ådnanes, A. K. (2005). Optimization of load dependent start tables in marine power management systems with blackout prevention, *WSEAS Transactions on Circuits and Systems* **4**(12): 1861–1866.

Radan, D., Sørensen, A. J., Ådnanes, A. K. and Johansen, T. A. (2008). Reducing power load fluctuations on ships using power redistribution control, *Marine Technology* **45**(3): 162–174.

Radan, D., Sørensen, A. J., Johansen, T. A. and Ådnanes, A. K. (2006). Probability based generator commitment optimization in ship power system design., *WSEAS Transactions on Systems* **5**(8): 1901–1906.

Rawlings, J. B. and Muske, K. R. (1993). The stability of constrained receding horizon control, *IEEE Trans. Automat. Contr.* **38**(10): 1512–1516.

Realfsen, B. (2009). Reducing NOx Emission in DP2 and DP3 Operations, *Dynamic Positioning Conference, Marine Technology Society*, Houston, USA.

Ren, W., Steurer, M. and Woodruff, S. (2005). Progress and challenges in real time hardware-in-the loop simulations of integrated ship power systems, *Power Engineering Society General Meeting, 2005. IEEE*, pp. 534–537 Vol. 1.

Schildbach, G., Fagiano, L., Frei, C. and Morari, M. (2014). The scenario approach for stochastic model predictive control with bounds on closed-loop constraint violations, *Automatica* **50**(12): 3009–3018.

Scokaert, P. O. M. and Mayne, D. Q. (1998). Min-max feedback model predictive control for constrained linear systems, *IEEE Trans. Automat. Contr.* **43**(8): 1136–1142.

Sebastián, R. and Quesada, J. (2006). Distributed control system for frequency control in a isolated wind system, *Renewable Energy* **31**(3): 285 – 305.

Senjyu, T. and Shimabukuro, K. (2003). A fast technique for unit commitment problem by extended priority list, *IEEE Trans. Power Syst.* **18**(2): 882–888.

Shi, X., Wei, Y., Ning, J., Fu, M. and Zhao, D. (2011). Optimizing adaptive thrust allocation based on group biasing method for ship dynamic positioning, *Automation and Logistics (ICAL), 2011 IEEE International Conference on*, pp. 394–398.

Skjetne, R. (2010). Modeling a diesel-generator power plant. Lecture notes, Norwegian University of Science and Technology.

Skjong, E., Molinas, M. and Johansen, T. A. (2015). Optimized current reference generation for system-level harmonic mitigation in a diesel-electric ship using non-linear model predictive control, *Industrial Technology (ICIT), 2015 IEEE International Conference on*, pp. 2314–2321.

Skjong, E., Molinas, M., Johansen, T. A. and Volden, R. (2015). Shaping the current waveform of an active filter for optimized system level harmonic conditioning, *International Conference on Vehicle Technology and Intelligent Transport Systems*, Lisbon, Portugal.

Skjong, E., Ochoa-Gimenez, M., Molinas, M. and Johansen, T. A. (2015). Management of harmonic propagation in a marine vessel by use of optimization, *Proc. IEEE Transportation Electrification Conference and Expo (ITEC 2015)*, Detroit, USA.

Skjong, E., Rødskar, E., Molinas, M., Johansen, T. A. and Cunningham, J. (2015). The marine vessel's electrical power system: From its birth to present day, *Proceedings of the IEEE* **103**(12).

Smogeli, Ø. N. (2006). *Control of Marine Propellers*, PhD thesis, Department of Marine Technology, Faculty of Engineering Science & Technology, NTNU.

Steurer, M., Andrus, M., Langston, J., Qi, L., Suryanarayanan, S., Woodruff, S. and Ribeiro, P. (2007). Investigating the impact of pulsed power charging demands on shipboard power quality, *Electric Ship Technologies Symposium, 2007. ESTS '07. IEEE*, pp. 315–321.

Stone, P., Opila, D., Park, H., Sun, J., Pekarek, S., DeCarlo, R., Westervelt, E., Brooks, J. and Seenumani, G. (2015). Shipboard power management using constrained nonlinear model predictive control, *Electric Ship Technologies Symposium (ESTS), 2015 IEEE*, pp. 1–7.

Sørensen, A. J. (2011). A survey of dynamic positioning control systems, *IFAC Journal of Annual Reviews in Control* **35**(1): 123 – 136.

Sørensen, A. J. (2013). *Marine Control Systems: Propulsion and Motion Control Systems of Ships and Ocean Structures.*, second edn, Dep. of Marine Technology, NTNU.

Sørensen, A. J., Pedersen, E. and Smogeli, Ø. N. (2003). Simulation-based design and testing of dynamically positioned marine vessels, *International Conference on Marine Simulation and Ship Maneuverability (MARSIM)*, Japan.

Sørensen, A. J. and Smogeli, Ø. N. (2009). Torque and power control of electrically driven marine propellers, *Control Eng. Pract.* **17**(9): 1053–1064.

Torrisi, F. D. and Bemporad, A. (2001). Discrete-time hybrid modeling and verification, *IEEE Conf. Decis. Control*, pp. 2899–2904.

Torsethaugen, K. (1993). A two peak wave spectrum model, *Proc. 12th Int. Conf. Offshore Mechanics and Arctic Technolog*, Vol. 2, pp. 175–180.

Vada, J., Slupphaug, O. and Johansen, T. A. (2001). Optimal prioritized infeasibility handling in model predictive control: parametric preemptive multiobjective linear programming approach, *Journal of Optimization Theory and Applications* **109**(2): 385–413.

Valmot, O. R. (2014). Norske batterier kan levere 54 kWh på seks minutter, *Teknisk Ukeblad* .
URL: *http://www.tu.no/industri/2014/12/19/ norske-batterier-kan-levere-54-kwh-pa-seks-minutter*

Veksler, A., Johansen, T. A., Mathiesen, E. and Skjetne, R. (2013). Governor principles for increased safety on vessels with diesel-electric propulsion, *European Control Conference*, Zurich, Switzerland, pp. 2579–2584.

Veksler, A., Johansen, T. A. and Skjetne, R. (2012a). Thrust allocation with power management functionality on dynamically positioned vessels, *Proc. American Control Conference, Monteal*.

Veksler, A., Johansen, T. A. and Skjetne, R. (2012b). Transient power control in dynamic positioning — governor feedforward and dynamic thrust allocation, *IFAC conference on maneuvering and control of marine craft.*, Arenzano, Italy.

Weisser, D. and Garcia, R. S. (2005). Instantaneous wind energy penetration in isolated electricity grids: concepts and review, *Renewable Energy* **30**(8): 1299 – 1308.

Wirasingha, S. and Emadi, A. (2011). Classification and review of control strategies for plug-in hybrid electric vehicles, *Vehicular Technology, IEEE Transactions on* **60**(1): 111–122.

Woodward (2004). Governing Fundamentals and Power Management. Viewed 2014-12-15.
URL: *woodward.com/workarea/downloadasset.aspx?id=2147483987*

Xie, Y., Sun, J., Miz, C. and Freudenberg, J. (2009). Analysis and modeling of a DC hybrid power system testbed for power management strategy

development, *Vehicle Power and Propulsion Conference, 2009. VPPC'09. IEEE*, IEEE, pp. 926–933.

Yum, K. K. and Pedersen, E. (2013). Transient performance and emission prediction of diesel engine system using pseudo bond graph model, *The 9th Asia-Pacific Conference on Combustion*, Gyeongju, Korea.

Zacharias, F. (1967). Analytical Representation of the Thermodynamic Properties of Combustion Gases, *SAE Technical Paper* **670930**.

Zahedi, B. and Norum, L. (2013). Modeling and simulation of all-electric ships with low-voltage DC hybrid power systems, *IEEE Transactions on Power Electronics* **28**(10): 4525–4537.

Zeng, J., Zhang, B., Mao, C. and Wang, Y. (2006). Use of battery energy storage system to improve the power quality and stability of wind farms, *Power System Technology, 2006. PowerCon 2006. International Conference on*, pp. 1–6.

Ådnanes, A. K. (2003). *Maritime Electrical Installations and Diesel Electric Propulsion*, Oslo, Norway.